

**Catalytic Investigations of CO and NO Reactions
Applying Exfoliated Graphite Intercalation Compounds
of AlCl₃, CuCl₂, MoOCl₃, FeCl₃, and Ce(IV)nitrate.**

Dissertation

**zur Erlangung des Doktorgrades
im Fachbereich Chemie
der Universität Hamburg**

vorgelegt von

Sylvester Kwadwo Twumasi

aus Nkuntin (Ghana)

Hamburg 2002

Die vorliegende Arbeit wurde angefertigt am Institut für Physikalische Chemie
der Universität Hamburg im Arbeitskreis von Herrn Prof. Dr. Wolfgang Metz.

Hauptgutachter: Prof. Dr. W. Metz

Mitgutachter: Prof. Dr. H. Lechert

Contents

1 Introduction

2 Graphite Intercalation Compounds (GICs)

- 2.1 Structure of Graphite
- 2.2 Structure of Graphite Intercalation Compound
- 2.3 Reaction Mechanism of Graphite Intercalation Compounds' Formation
- 2.4 Preparation Methods of Graphite Intercalation Compounds
 - 2.4.1 Intercalation from a vapour phase
 - 2.4.2 Intercalation from a liquid phase
- 2.5 Exfoliated Graphite Intercalation Compounds

3 Experimental Methods

- 3.1 Experimental Methods of Analysis
 - 3.1.1 X-ray Diffraction
 - 3.1.2 X-ray Fluorescence
 - 3.1.3 X-ray Absorption Spectroscopy
 - 3.1.4 Density Determination
 - 3.1.5 B.E.T. Surface Area Determination
 - 3.1.6 Gas Chromatography (GC)
 - 3.1.7 Reaction Kinetics
 - 3.1.8 Theory of the Plug Flow Reactor
 - 3.1.9 Determination of Empirical Formula
- 3.2 Preparation and Characterisation of the Catalysts
 - 3.2.1 Preparation and Characterisation of the Graphite Intercalation Compounds (GICs)
 - 3.2.2 Exfoliation of GICs and characterisation of the products
- 3.3 Determination of Catalyst Activity
 - 3.3.1 Instrumentation in Determination of Catalytic Activity
 - 3.3.2 Measuring procedure

4 Results: Characterisation of Graphite Intercalation Compounds (GICs) and Exfoliated Products

- 4.1 Characterisation of the $\text{AlCl}_3/\text{CuCl}_2$ – GICs and the Exfoliated Products.
- 4.2 Characterisation of the $\text{FeCl}_3/\text{CuCl}_2$ GICs and the Exfoliated Products
- 4.3 Characterisation of the $\text{AlCl}_3 / \text{MoOCl}_3 / \text{CuCl}_2$ – GICs and the Exfoliated Products.
- 4.4 Characterisation of the Ce(IV)nitrate - GICs and the Exfoliated Products

5 Results: Catalytic Activities

- 5.1 CO Oxidation
 - 5.1.1 CO oxidation – using CuO / graphite mixture as catalyst
 - 5.1.2 CO oxidation – using AlCu graphite as catalyst
 - 5.1.3 CO oxidation – using MoCu graphite as catalyst
 - 5.1.4 CO oxidation – using AlMoCu graphite as catalyst
 - 5.1.5 CO oxidation – using FeCu graphite as catalyst
- 5.2 NO Decomposition
 - 5.2.1 NO decomposition – using CuO / graphite mixture as catalyst
 - 5.2.2 NO Decomposition – using AlCu graphite as catalyst
 - 5.2.3 NO Decomposition – using AlMoCu graphite as catalyst
 - 5.2.4 NO Decomposition – using MoCu graphite as catalyst
 - 5.2.5 NO Decomposition – using FeCu graphite as catalyst
- 5.3 Activity Tests of CeO_2 graphite
 - 5.3.1 CO – Oxidation using CeO_2 graphite and free CeO_2 .
 - 5.3.2 NO – decomposition using CeO_2 graphite and free CeO_2 .
- 5.4 CO - NO Redox Reaction
 - 5.4.1 NO - CO redox reaction – using CuO / graphite mixture as catalyst
 - 5.4.2 NO - CO redox reaction – using AlCu graphite as catalyst
 - 5.4.3 NO - CO redox reaction – using FeCu graphite as catalyst
 - 5.4.4 NO - CO redox reaction – using AlMoCu graphite as catalyst
 - 5.4.5 NO - CO redox reaction – using MoCu graphite as catalyst
 - 5.4.6 NO – CO Redox using CeO_2 graphite and free CeO_2 .

6 Discussion of the Results

6.1 CO Oxidation and NO Decomposition

6.2 NO reduction with CO

6.3 Mechanism of the Catalytic Reactions

7 Summary

8 Zusammenfassung

9 Literature

1 Introduction

Environmental pollution resulting from nitrogen oxides emission by automobiles, atomic energy plants and industrial processes causes serious ecological problems. Acid rain, which is a result of it, causes very serious health hazard to plant and animal lives, especially animals in the rivers and the sea. Concern has also been expressed that increasing levels of N_2O following denitrification may eventually impoverish the ozone layer in the stratosphere. Possible chemical reactions with the oxides of nitrogen have also been identified but the extent to which they occur and whether the effects are reversible are yet not known [86GE, DS79, Fox79].

Carbon monoxide poisoning is also very well known. Conversion of CO to CO_2 does not relieve the environment completely from pollution but to a less evil product. Treatment of CO stemming out of coal *burning silos* to CO_2 is therefore a remarkable contribution to environmental cleanliness.

To combat the above named pollutants several measures have been taken. Environmental regulations have been made to limit the extent of industrial pollution. CO_2 which has CO as its intermediate product, apart from measures being taken to limit their production through international regulations and a search for alternative energy sources, is being seriously pursued. Natural gas, and solar energy are being used as alternative energy source in heating homes and in the automobile industries. Hydrogen as fuel in the automobile industries is currently being tested. All these endeavours are being done with the hope of minimizing environmental pollution resulting from NO_x , CO and CO_2 exhaust as by product of the burning of oil fuel. CO_2 is also being got rid of, through afforestation, as being practised today in Australia. Catalytic conversion of these poisonous gases to less harmful products has drawn the attention of several scientists in this field of study. A lot has already been achieved for which numerous automobiles on our motor ways bear living witnesses. Statistics also give evidence, especially in the developed countries, to the decrease in the destruction of forest as a result of the above measures taken to protect the environment. These measures being taken to fight pollution are with a cost factor incorporated.

In the search for a suitable catalyst to combat pollution a very serious consideration is given to its funding. Alternatives not demanding large capital investment but are equally effective are being

consistently sought for. In the light of this, catalysts were prepared in this project out of simple inorganic substances, mostly transition metal chlorides, the catalytic activities of which are in one way or the other already known.

It is to be noted here that different methods have been used in preparing pure metal oxides for catalytic purposes. Different preparation methods of a given metal oxide leads to different physical properties such as particle diameter, surface area, pore radius among others. These differences also lead to differences in catalytic activity. Metal oxides have also been inserted as catalyst using aluminium oxide and zeolite among others as support.

Exfoliated graphite intercalation compounds can be thought of as metal oxides supported on graphite. The activity of such an oxide would be modified by the graphite support.

To get the metal oxides on the graphite, the metal chlorides were first incorporated in graphite layers forming the so called graphite intercalated compounds GIC. The intercalated compounds were then exfoliated [MB 64, DH 69, AC84] to provide a fine dispersion of the inorganic metal oxides, or metal cluster or both on the expanded surface area of the graphite, resulting from the exfoliation.

In the course of the exfoliation process, the intercalated inorganic metal chloride undergoes thermal decomposition in the presence of air moisture which converts the metal chloride to metallic oxides and metal cluster. According to T. Ressler [Re95] the oxidation state of the metal is dependent on the exfoliation temperature. In case of FeCl_3 and CuCl_2 both high and low oxidation numbers were obtained for their oxides. To achieve good products for catalytic use the exfoliation process must be carried out at high temperature to ensure complete conversion of the chloride to the oxide and must also be carried out quickly to avoid total de-intercalation. A successful exfoliation of graphite intercalation compounds results with the complete disintegration of the graphite structure. This occurs especially in cases where the intercalation took place in liquid phase or where the intercalated substances decompose, releasing gas products, at the exfoliation temperature. In such a case a large surface area is obtained for the exfoliated product. This was observed also in the case of the exfoliation of graphite-Ce(IV)-nitrate. Compared to the other graphite intercalation compounds prepared in this project, it is the only one prepared in the liquid phase. In course of the intercalation reaction HNO_3 molecules

were also co intercalated. The incorporated HNO_3 is set free the exfoliation causing a large destruction of the graphite lattice structure and exposing layer surfaces which are normally not accessible. Unlike the graphite intercalation compounds the structure of its exfoliated form can not be elucidated using the usual x-ray diffraction method of analysis. X-ray fluorescence and energy dispersive X-ray absorption spectroscopy are used to determine the amount of transition metal element and their oxidation states as well as their coordination numbers.

To determine the catalytic activity of each prepared sample CO oxidation, NO decomposition and CO/NO oxidation-reduction were investigated. - Generally the concentrations of the investigated gases ranged from 500ppm to 1500ppm in He, the reaction temperature between 80°C to 400°C , the flow rate of reaction gas mixture between 0.5l/hr to 4.5l/hr.

The rate of reaction and the activation energies of the above reactions using the prepared catalyst were found. The results obtained were then compared with literature values of other authors using the same catalysts in their pure form or supported on other media..

Some of the catalysts prepared for this project had formerly been applied in the oxidation of aromatic compounds[E93].

The graphite intercalation compounds , as far as their preparation and structural determination are concerned, are well known. GICs containing FeCl_3 , CuCl_2 , MoOCl_3 , AlCl_3 , $\text{CeO}_2.n\text{HNO}_3$ or mixtures of some of these intercalates were prepared, exfoliated and applied in the reactions stated above. Apart from the fundamental work done by W. Rudolf [R41, R54, RS40] and Cowley/Ibers [CI56] in the preparation methods, properties and bonding relations of the metal chloride intercalate compounds, there has been several publications in the past years by the working group of W. Metz [Spa76, Sie76, Hei76, Knö77, Hoh72, Sch75, S73 , MH75, Sch78 , Sie73, MS75, HM74, MS78, Spa78, E93, R95]. The by the team in general developed physical methods for the elucidation of the structure of the intercalation compounds including that of their oxides after exfoliation triggered the desire and need to apply the GICs as catalysts. Knowing for example the coordination of the central metal atoms may allow determination of the reaction path of the catalytic reaction.

FeCl_3 , CuCl_2 , MoOCl_3 , AlCl_3 , $\text{CeO}_2 \cdot n\text{HNO}_3$ graphite intercalates were used as bases for the catalysts because their preparation methods, physical and chemical properties and that of their exfoliated products are known. The catalytic properties of the metal oxides of the above mentioned inorganic metal chlorides in the absence of graphite are also available, making it easy to determine the influence of graphite on the catalytic activity of the intercalates.

2 Graphite Intercalation Compounds (GICs)

Graphite has a very loose layer structure. Because of this property several types of molecules and ions are able to penetrate into its interstices, setting themselves between graphite layers and forming the so called graphite interaction compounds.

2.1 Structure of Graphite

Graphite, an allotropic form of carbon, is thermodynamically the most stable form at normal temperatures and pressures. It exists in two forms with two dimensional structural arrangement. The normal occurring α - or hexagonal graphite is composed of planar hexagonal nets of carbon atoms arranged in sequence ... ABAB ... with carbon atoms in equivalent layers vertically above each other. In the case of the β - or rhombohedral form, the graphite is arranged in the sequence ... ABCABC The structure of the α - or hexagonal form is shown in Fig.2.1 below, with the courtesy of Cotton and Wilkinson [80 CN]. In this figure also the C-C distance within the layer and the interlayer spacing are shown.

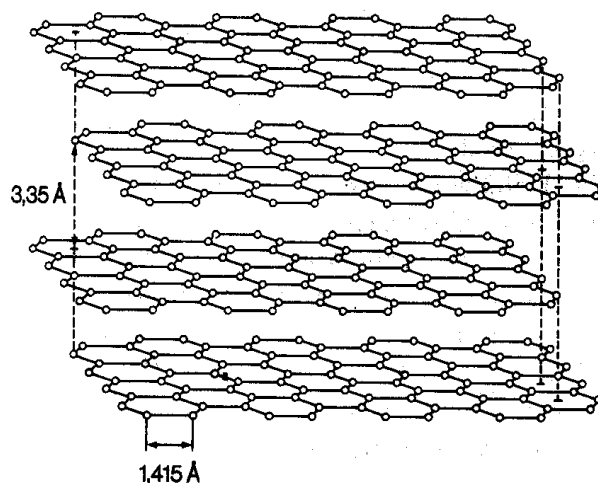
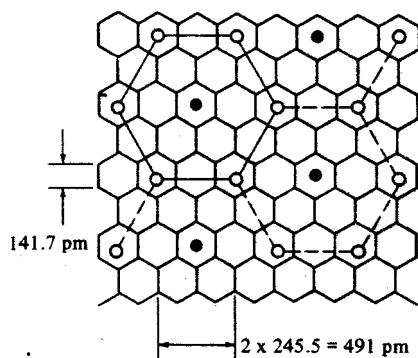


Fig.2.1: α - or hexagonal graphite. (After [80 CN])

2.2 Structure of Graphite Intercalation Compounds

In order for the intercalation to occur, the intercalate must penetrate or weave itself into the graphite inter layer spacing. By so doing the distance between the graphite layers becomes larger whereas the form of the AB-layers remains the same. The structure of the intercalated mono-molecular layer is influenced by the graphite lattice. In some cases very large differences are observed as compared to the not intercalated substances. According to N. Daumas and A. Herold [DH 69], in the case of unsaturated compounds, only partial occupation of the graphite interlayer spaces takes place. The intercalate can be arranged in such a way that a periodic sequence of n graphite layers and one intercalate layer in the direction of the c axis is formed. Then we have what is known as the n^{th} stage intercalation compound. Different ordered stages can also coexist and we have a mixed staged GIC.

Generally the small thickness of the graphene layers favours electrostatic and strain interactions along the c -axis, leading to ordered stages up to the 10^{th} . An example of the structure showing the arrangement of the host in the graphite layer is illustrated in Fig.2.2 – a 1^{st} stage potassium graphite intercalation compound with the formula C_8K . Fig.2.3 shows the stage order formation along the c -axis [93 HKK].



**Fig.2.2: K in hexagonal sites above each .
graphite layer**

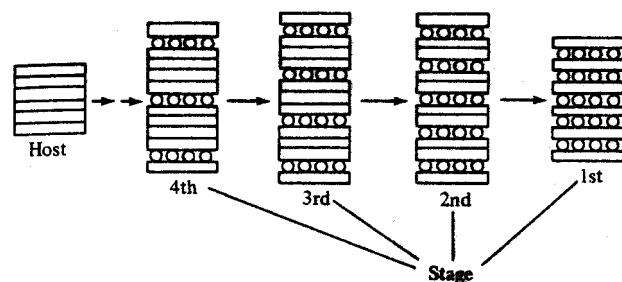


Fig.2.3: Stage order formation

According to Metz et al [SMSM 77], the ideal stage model must be refined by assuming the intercalated crystal to be divided in “domains”. Each domain has a defined stage structure

(pure or mixed), but different domains, which are separated from each other by domain walls of not-intercalated graphite, may have different stage numbers.

According to Kirczenow [Kir 84], the formation of ideal or pure stage GICs, apart from the preparation methods, depends also on the size of the domains, the extent of charge transfer, temperature and stage number. In his model, based on energy calculations, he postulated that the formation of pure GICs increases with the growth of island size. On the other hand, Siemsglüss [Sie 76] maintained that islands with small sizes are much more mobile and therefore can arrange themselves into orderly domains, meaning pure stage formation. In view of these two models we have a contradiction between thermodynamic and kinetic controlled reactions.

A difference must also be made here between a mixed stage, where various pure stages in several domains occur, and disordered stages, where in every pile sequence there is irregularity in every single domain. The idea of one dimensionally disordered stage formation has been outlined and defined by Jagodzinski [Jag 49]. According to Metz [Met 84] as well as Kirczenow [Kir84], the pure statistical distribution of intercalate layer leads to the tendency of the formation of first stage GIC.

2.3 Reaction Mechanism of Graphite Intercalation Compounds' Formation

Laminar graphite compounds (GICs) consist of plane carbon layers, the so called graphene layers and layers of intercalated substances. In addition to the intercalation compounds, made up of graphite and the corresponding reaction partners, which we term here as primary substances, are also the secondary substances. These have the primary substances as their starting material. These are formed by incorporating additional substances to the unsaturated graphite layers of the primary thereby reducing the order of the stage of the primary substance, or by partially replacing the already intercalated substances with new ones.

The reaction mechanism can be viewed in the following way:

The layers of the graphite crystals are held together by weak Van der Waals electrostatic forces resulting from the oscillation of the π -electrons in the layers. Because of the periodic vibration of the π -electrons, dipole-dipole interactions between neighbouring graphene layers take place,

which is mainly responsible for holding the layers together. The formation of the intercalation compounds results from the breaking up of these forces by the intruding compound and setting itself between the graphite layers. This can only occur when the following condition is satisfied:

The aromatic character of the graphite crystal becomes disturbed as a result of a charge transfer due to electron donation or electron uptake. The charge transfer causes changes in the distribution of the π -electrons in the layers, thus disturbing the periodic vibration of the electron gas, and consequently weakening the dipole- dipole electrostatic interactions between neighbouring layers. As a result the energy required to overcome the inter layer binding forces to enable intercalation becomes smaller than that before the charge transfer. On top of this energy is discharged as a result of the electrostatic interaction between the graphene and the intercalate layers of the GIC.

Both donor and acceptor GICs, where graphite acts as acceptor and donor respectively, are well known and have been widely prepared. The amphoteric nature of graphite enables it to act as an electron donor as well as an electron acceptor. Of all the various compounds with the ability to form graphite intercalation compounds, the metal chlorides (e.g. [RS40, RZ55, RL58, Stu77a, Stu92]) are the ones which have been mostly investigated.

Generally they are intercalated in the presence of chlorine gas. In place of chlorine other oxidizing agents such as NO_2 (intercalation of SbCl_3 ; [Stu92]), or strong Lewis acids such as BCl_3 (intercalation of BiCl_3 ; [Sch92]) have been used. According to Leong and Forsman [LF83] the intercalation of AlCl_3 in the presence of HCl has been achieved ($\text{HCl(ads)} + \text{AlCl}_3(\text{ads}) \rightarrow \text{H}^+ \dots \text{AlCl}_4^-(\text{ads})$).

Chlorine, an electrophile supporting agent with high electron affinity, initiates a charge transfer upon its adsorption on the graphite surface layer. Several metal chlorides and chlorine form, under suitable conditions, negative metal chloro complexes. These chemical entities, upon adsorption on the graphite, penetrate into the interlayer space of the graphite, serving as nucleus of reaction, where a charge transfer from graphite to chlorine takes place.

The minimum pressure of chlorine, that can initiate the formation of the complex, had been extensively investigated in our working group [MS82, MS89, Wie87, Met88] . This pressure also corresponds to the lowest limit required for intercalation.

The nucleus, between the graphene layers, grows by additional uptake of neutral metal chloride molecules. It grows, forming the so called island, which results with concentration gradients and consequently leads to its diffusion into the innermost part of the crystal.

The intercalation process or reaction can therefore be described to take the following steps: charge transfer, nucleation, and diffusion.

2.4 Preparation Methods of Graphite Intercalation Compounds

Three general methods are used in the preparation of GICs. The method employed, apart from thermodynamic factors, depends on the physical and chemical properties of the intercalating compound.

2.4.1 Intercalation from a vapour phase

This method of intercalation can be considered as a standard for the preparation of metal chloride intercalation compounds. Graphite and dry metal chloride are introduced in a dry glass tube in a reaction box filled with dry nitrogen gas. The glass tube is then evacuated to remove the nitrogen. Freshly dried chlorine gas is then introduced into the tube which is then melted off to form an ampoule. The ampoule is then tempered in an oven. At the prevailing oven temperature, the corresponding vapour pressure of the metal chloride is built up, ending up with the intercalation of the graphite in the vapour phase. This process of intercalation was employed by Stumpp and Werner [SW 66] and Stumpp [Stu60] in the preparation of several metal chlorides.

In a variant method a two-temperature oven is used, where the metal chloride and the graphite are located at the opposite ends of the tube. One temperature is the reaction temperature, the other defining the vapour pressure of the chloride. By this means different degrees of intercalation can be obtained by variation of the second temperature.

Better results are obtained when a relatively volatile metal chloride e.g. aluminium chloride, AlCl_3 , is added to the metal chloride to be intercalated. The promotion of the intercalation is due to the formation of a gas complex between AlCl_3 and the relatively less volatile metal chloride.

AlCl_3 in the solid state has a layer lattice with 6-coordinate Al, but at the mp 192.4° the structure changes to a 4-coordinate molecular dimer Al_2Cl_6 . The covalently bonded molecular dimers are the main species in the gas phase at low temperatures ($\sim 150\text{--}200^\circ$). Being very volatile at the usual reaction temperatures and having the ability to form gas complexes with the other metal chlorides (e.g. MAI_2Cl_8 with MCl_2), AlCl_3 is in the position to carry or transport the metal chlorides from solid to the vapour phase at relatively low temperatures. Instead of AlCl_3 , FeCl_3 can also serve the same purpose. Several metal chloride intercalation compounds have already been prepared with good results by employing this method [Stu77, Sc76, Sc74, Dew70].

2.4.2 Intercalation from a liquid phase

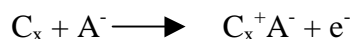
Graphite is added to a solution of the intercalate e.g. metal chloride and boiled under reflux at a fixed temperature for a period of time. Dry inert solvent is used and the temperature of the reaction is such that no reaction between solvent and the intercalate takes place.

Intercalation can also be performed in a solid solution. For instance, when graphite and certain metal chlorides are fused together in the presence of an agent such as NaCl, intercalation of the metal chlorides occurs. The function of the agent is to reduce the melting temperature of the chloride. Intercalation from a liquid phase when successful offers the possibility of getting a much more homogeneous product but also obtaining a large quantity of the product at a stretch.

W. Rüdorff and A. Boeck [BW73] employed thionylchloride solution of UCl_5 , AlCl_3 , NbCl_5 , TaCl_5 and obtained third and higher ordered stages of graphite intercalation products in reaction time of few hours to several days. A. Boeck [B 70] and J. G. Hooley [Hoo72] also reported the interaction of other chlorides including that of FeCl_3 with the help of this method. J. M. Lalancette [Lal 76] reported a successful intercalation of several metal chlorides from boiling tetrachloromethane solution saturated with chlorine gas.

Several attempts were made to prepare graphite-CuCl₂ in solutions of chloroform, tetrachloromethan, and thionylchloride. In all these cases no positive results were obtained. H. Eickhoff [E93] succeeded in intercalating Ce(IV)-nitrate from CeO₂*0.5H₂O nitric acid (65%) solution.

The graphite-Ce(IV)-nitrate intercalation compound, used for preparing the CeO₂-graphite catalyst, was prepared using Eickhoffs method [E93]. This preparation method was base on theoretical consideration of W.Rüdorff and Hoffmann [RH38]. W. Rüdorff and Hoffmann reported in 1938 that graphite can be chemically or electrochemically oxidized to form a macrocation, and that the positively charged cation can be compensated by insertion of certain anions A⁻ between the planes of the graphite lattice:



2.5 Exfoliated Graphite Intercalation Compounds

When graphite intercalation compounds are heated rapidly, the intercalated substances undergo changes in volume leading mostly to increase in pressure in the occupied graphite interspaces. The graphite layers, held together by weak van der Waals forces and further weakened by the intercalated compounds, yield to the increased pressure and breaks up to give the so called exfoliated graphite intercalation compounds. In most cases the break-up is observed at the sublimation temperature or the temperature at which the vapour pressure is extensive enough to rapture the “lattice” of the GIC. Such exfoliation temperatures have been intensively investigated for various substances in our working group by Eickhoff [E93].

The pressure increase that causes the decomposition of the GICs can also come about as a result of the decomposition of the intercalate to yield gaseous products. This is observed in the case of ferric chloride graphite intercalate at temperatures above 315°C. The pressure causing the exfoliation may also be due to a solvent that might have intercalated alongside the intercalate. This usually occurs in the cases of intercalation that takes place in the liquid phase, as has been treated under methods of intercalation. In such cases upon heating the GIC above the boiling point of the solvent can lead to its disintegration.

Exfoliated graphite intercalation compounds are characterised by their much larger specific surface. They are also associated with a much higher powder volume and, correspondingly, smaller density values. This holds also if the density is measured by gas volumetric methods, indicating the incapability of the intercalate to free itself completely of all gas pockets incorporated within the lattice. This means that complete exfoliation at a particular temperature is not easy to achieve.

Exfoliation of metal chloride GICs in air, that is in the presence of oxygen, results with the oxidation of the inherent metal - especially in the case of transition metals. The metal oxides, usually finely distributed on the enlarged graphite surface area, and often existing in various oxidation states, have a potential to serve as catalysts in various reactions.

Changes in mass, density and specific surface area

Exfoliation is an irreversible process characterised by loss in mass of the GIC, changes in its density and specific surface area. The change in mass of the exfoliated products, which is mainly dependent on the experimental conditions such as temperature, and the length of time taken for the exfoliation, is a characteristic measure of an exfoliation product. Materials are lost in the course of exfoliation as a result of de-intercalation, in which intercalated substances leave the graphite layer, resulting in GICs with higher stage numbers and in extreme cases with a total separation of the intercalated substances from the graphite layers. The change in mass can also be a consequence of a chemical transformation, in which the intercalated substances are converted from one form to another. In the case of the transition metal chlorides, conversion of the chlorides to their oxides and in that of the Ce (IV) nitrate, its conversion to CeO_2 . Conversion of the intercalated substances to their pure metals with the expulsion of the non-metals from the GICs is also a factor in the change of mass resulting from exfoliation. Depending upon the temperature and the length of exfoliation process, the graphite can also oxidise to graphite oxide with eventual decomposition to carbon monoxide and dioxide. The changes in mass, density, and specific surface area in the course of exfoliation as a function of temperature has been fully treated by H. P. Eickhoff [E93] in our working group. In his investigation of the exfoliation of several graphite intercalation compounds, he reported that high exfoliation temperature is a necessary prerequisite for obtaining exfoliation products with large surface area. In his work on

the exfoliation of acceptor GICs, namely cerium(IV) nitrate-, iron(III) chloride-, and sulphuric acid – GICs, he was able to relate the pattern taken by the density, loss in mass and surface area of the GICs at various reaction temperature. The results of his work, which he reported in a diagrammatic form is shown in Fig.2.4.

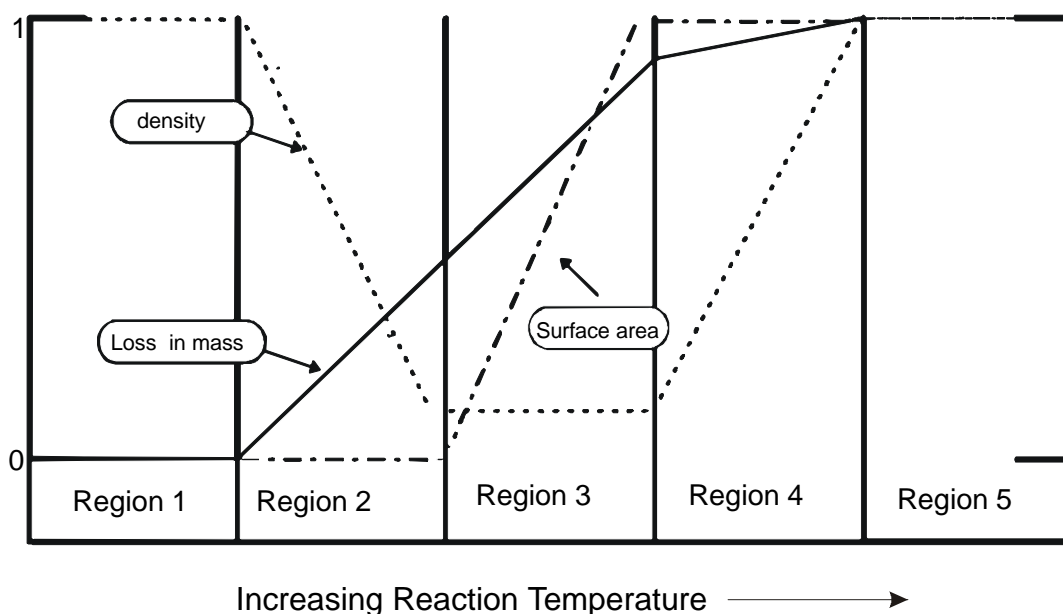


Fig.2.4 : A schematic diagram of the exfoliation process showing five different sections of the dependency of density, surface area, and loss of mass on the reaction temperature (after E93).

The maximum density of an exfoliated product is taken to be equal to that of graphite 2.26g/cm^3 and is normalised to 1. With the specific surface area of an exfoliated product far exceeding that of the GIC, its specific surface area at the stable temperature is considered negligible. The specific surface area 1 corresponds to the maximum surface area obtained in the course of the exfoliation process as shown in region 5.

In region 1, where there is no change in mass, density and specific surface area, the GICs are considered stable at the measured reaction temperatures.

In region 2 the decomposition or evaporation of the GICs takes place resulting in decrease in density and mass, and without any changes in specific surface area. The exit of vaporised intercalate or its decomposition products leaves the partially exfoliated product with sealed

cavities, which account for the decrease in density. These cavities are not accessible to the nitrogen gas used in measuring the surface area and therefore do not contribute to the measured surface area.

In region 3 a continuous loss of mass reaching about 95% of its maximum is reported. We also observe a rise in the surface area and constant density. Continuous departure of decomposition or vaporised intercalated products leads to this loss in mass. Sealed cavities open up with rise in temperature in this region, resulting in rise in the surface area. Increase in density resulting from these cavity open-ups are compensated by the built up of new cavities thus keeping the density constant in this region.

The density begins to rise at the beginning of region 4 and continues to rise till it reaches its maximum at the beginning of region 5. The increasing density at the start of region indicates the completion of the exfoliation process at the end of region 3. At the end of region 3, all vaporisable intercalate and gaseous decomposition products have left the GICs. We then have exfoliated products embodying partly sealed cavities, transition metal oxides derived from the metal chloride and the remnant of the metal chloride, about 5%, in its gaseous form, or its gaseous decomposition products. At the beginning of region 4 the sealed cavities begin to open up, resulting in increasing density. This trend continues with increase in reaction temperature till all sealed cavities are open. At the end of region 4, where the density is at its maximum, all the sealed cavities are open and the residual undecomposed intercalate still present at the end of region 3 has been converted into its oxide form. A change in specific surface area is not observed in this region, even though the sealed cavities continue to open. Instead of the cavities opening up and exposing larger surface area, they collapse into themselves, thus again making the previously sealed off graphene interlayer cavity not available for its surface area to be determined.

In region 5, the three parameters, namely loss of mass, density and specific surface area remain constant with rising reaction temperature. In this region the exfoliation is complete, and a rise in temperature above the highest temperature leads to decomposition of the graphite substrate.

3 Experimental Methods

In this chapter the theories and the experimental methods used for the characterisation of the substances prepared for the catalyst research will be outlined; the preparation of the substances as well as their characterisation will also be discussed.

3.1 Experimental Methods of Analysis

Due to the nature of the graphite intercalation compounds and their exfoliated products not all experimental methods e.g. IR are applicable in their investigation. Mainly X-ray analyses of the substances, for the structural and composition evaluation, were performed, counting on several years' experience in this field of our working group. In the catalytic investigation undertaken in this project, the qualitative as well as the quantitative evaluation of the gases inserted and their reaction products was done by means of the gas chromatography.

3.1.1 X-ray Diffraction

The aim of the X-ray diffraction investigation was not to deliver a detailed structural information of the GICs but to obtain information to help us know the content of the intercalate in the GICs. It was to serve as a supplement to gravimetric and x-ray fluorescence methods in delivering information for finding the amount of intercalate in the prepared GICs. Knowing this was necessary in providing us a guide, in finding the amount of active material (metal and metal oxides) in the prepared catalysts, derived from the exfoliated GICs. A knowledge of the stage number of the GICs was therefore enough in providing us practically all the necessary information needed.

To treat X-ray diffraction of GICs let us take once more a look at the structure of graphite intercalation compound along the crystallographic c-axis. The structure along the c-axis, which is also the structure perpendicular to the graphene layers, is characterised by stage formation; that is the formation of domains, which under ideal conditions, are stacked up in piles that are separated from each other by graphite layers, ordered in sequence, and coherent in their X-ray diffraction.

To investigate the periodicity or the disorder in the c axis of the graphite, i.e. the axis perpendicular to the base area, one falls on X-ray diffraction of the GICs.

The one dimensional stage disorder, with mainly the disarrangement in the layer sequence resulting from the various sorts of layers, reflects highly on the (00l) X-ray profile. The quantitative analysis of the intensities of the (00l) reflections of a pure stage substance can deliver in principle the projection of the structure on the c-axis, but it is to be noted that deviation from pure stage is also reflected in the position and intensities of the reflections.

The relationship between the wavelength of the X-ray beam, the glancing angle θ , and the distance between each set of planes of the crystal lattice d , is governed by the well known Bragg law:

$$m\lambda = 2d \sin\theta$$

where m is order of diffraction.

3.1.2 X-ray Fluorescence

Characteristic X-ray spectra are emitted through excitation when a specimen is irradiated with an X-ray beam with sufficiently short-wavelength. This phenomenon is similar to that of the electron probe analysis, where a specimen is bombarded with electron beam resulting in the excitation of characteristic X-ray spectra. X-ray excitation can be done in air or weak vacuum, whereas electron excitation requires high vacuum.

The general arrangement for exciting, dispersing and detecting fluorescent X-rays with a plane-crystal spectrometer is shown in Fig.3.1 below. The specimen in the sample holder is irradiated with an unfiltered beam of primary X-rays, which causes the elements present to emit their characteristic fluorescent lines. A portion of the scattered fluorescence beam is collimated by the entrance slit of the goniometer and directed onto the plane surface of the analysing crystal. The

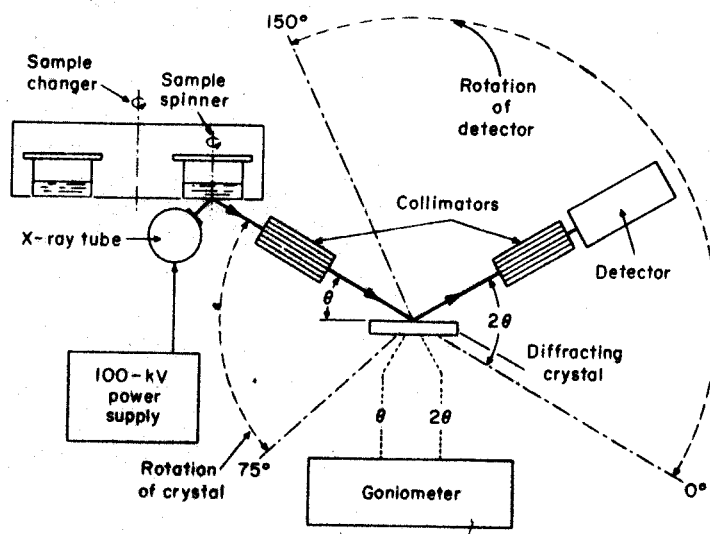


Fig.3.1 Plane crystal X-ray fluorescence spectrometer [65 WMD]

secondary beam, reflected according to the Bragg condition, pass through an auxiliary collimator(exit slit) to the detector, where the energy of the X-ray quanta is converted into electrical impulses, or counts.

The primary slit, the analyser crystal, and the secondary slit are placed on the focal circle so that Bragg's law will always be satisfied as the goniometer is rotated – the detector being rotated twice the angular change in the crystal setting. The analyser crystal is a flat single – crystal plate. The specimen holder is often an aluminium cylinder, although plastic material is used for the examination of acid or alkaline solutions. Losses in intensity as a result of absorption of long wavelength X-rays by air and window materials can be reduced by evacuating the goniometer chamber or the radiation path can be enclosed in a special boat which extends from the sample surface to the detector window and the air displaced by helium, which has a low absorption coefficient.

In order to excite fluorescence the primary radiation must obviously have a wavelength shorter than the absorption edge of the element to be detected. Continuous as well as characteristic radiation of the primary target can serve the purpose. To get a continuous spectrum of short enough wavelength and of sufficient intensity, one may calculate the voltage of the X-ray tube from the Duane-Hunt equation $\lambda_0 V = h c / e = 1234 \text{ [pm V]}.$

For qualitative analysis, the angle θ between the surface of the crystal and the incident fluorescence beam is gradually increased; at certain well-defined angles the appropriate fluorescence lines are reflected. In automatic operation the intensity as a function of the diffraction angle 2θ is recorded on an x-t-recorder as a series of peaks, corresponding to fluorescence lines, above a background which arises principally from general scattering. Additional evidence of identification may be obtained from relative peak heights, the critical excitation potential, and pulse height analysis.

In the case of quantitative analysis, the intensity of a characteristic line of the element to be analysed is measured. The goniometer is set at the 2θ angle of the peak and counts are collected for a fixed period of time, or the time is measured for the period required to collect a specified number of counts. The goniometer is then set at a nearby position of the spectrum where a scan has shown only the background to contribute. For major elements, 200,000 counts can be accumulated in 1 or 2 min. The net line intensity – peak minus background, in counts per second, is then related to the concentration of the element via calibration curve or simple proportions of concentrations and intensities.

Particle size and shape are important and determine the degree to which the incident beam is absorbed or scattered. Standards and samples should be ground to roughly the same mesh size. Errors from differences in packing density are usually handled by addition of an internal standard to the sample. Powders are pressed into a wafer in a metallurgical specimen press or converted into a solid solution by fusion with borax.

Corrections are usually made for matrix effects, before relating the intensity of the fluorescent emission to concentration of emitting element. Matrix dilution avoids serious absorption effects. The samples are heavily loaded or diluted with a material having a low absorption, such as powdered starch, lithium carbonate, lampblack or borax (applied in fusions). The concentration, and therefore the effect, of the disturbing matrix elements is reduced, along with a reduction of the measured fluorescence also. The most practical way to apply a systematic correction is by the use of the internal standard. Even so, the internal standard technique is valid only if the matrix elements affect the reference line and analytical line in exactly the same way. The choice of a reference element depends on the relative positions of the characteristic lines and the absorption

edges of the element to be determined, the reference element, and the disturbing elements responsible for the matrix effects. If either the reference line or the analytical line is selectively absorbed or enhanced by a matrix element, the internal standard line and analytical line ratio is not true measure of the concentration of the element to be determined. Preferential absorption of a line would occur if a disturbing element had an absorption edge between the comparison elements.

3.1.3 X-ray Absorption Spectroscopy

X-ray absorption spectroscopy (XAS), employed in the analysis of the exfoliated graphite intercalation compounds, is a powerful tool highly applied in the field of physics, chemistry, biology and material science in the study of structural determination. It can be considered as a supplementary tool to X-ray diffraction method in providing additional useful information in structural elucidation.

In general it offers the following information for structural determination:

- a) Bond lengths to the next bonding neighbours up to a distance of about 500 pm.
- b) Numbers of next bonding neighbours in a coordination shell.
- c) A measure of thermal and statistical disorder.
- d) Oxidation state of the examined atom.
- e) Coordination geometry.
- f) Electronic state of the investigated atom.

Since each element has its own characteristic set of K, L, M, etc., absorption edges, the wavelength at which a sudden change in absorption occurs can be used to identify an element present in a sample, and the magnitude of the change can be used to determine the amount of the particular element present.

In XAS the absorption is defined as the natural logarithmus of the quotient of the intensity of the X-ray before entering and after emerging from the sample of material under investigation, $\ln I_0/I$,

measured as a function of energy or wavelength of the incoming rays. According to the well known absorption law for electromagnetic radiation, this expression is given by $\ln I_0/I = \mu x$. The quantity μ , which is dependent upon the physical and chemical state of the absorber, is known as the linear absorption coefficient. Upon dividing μ by the density ρ we get the mass absorption coefficient, which is an atomic property.

X-ray absorption spectrum may well be illustrated by using that of palladium (Fig.3.2) in its simplified form [70LT].

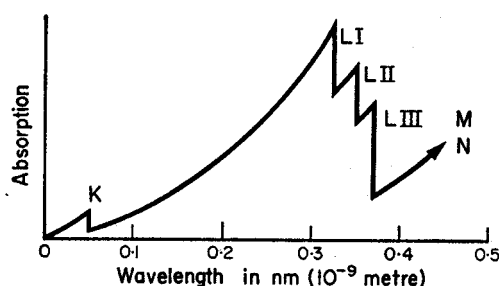


Fig.3.2: X-ray absorption spectrum (Pd., Z =46)

XAS spectra are recorded nowadays only by using synchrotron radiation. The spectrum of the incident, continuous x-rays is monochromatised with a Bragg X-ray spectrometer. A narrow beam of X-rays is made to pass through the material in the form of a thin layer. Readings with and without the absorber in position at each wavelength are made and a graph of absorption and wavelength plotted.

The spectrum is characterised by the occurrence of the so called absorption edges. At these wavelengths the ionisation energies of the corresponding shell (K,L,M...) are present. Of course, the absorption edges do not coincide with any of the lines in the corresponding emission series. Rather the edges are defined by the upper limits of the respective series. Consequently, the wavelengths at which the absorption edges are observed, are dependent upon the atomic numbers and therefore are specific elemental characteristics.

We term the range roughly 20eV before the absorption edge up to 50eV after the absorption edge as X-Ray Absorption Near Edge Structure (XANES) and the area extending beyond the edge as the Extended X-Ray Absorption Fine Structure (EXAFS).

In the XANES area, which is not well understood as that of the EXAFS, two phenomena can be considered to contribute to the modulation of μ_x . It is to be noted here that the position of the absorption edge is marred by the superposition of other absorption lines, making it difficult visually accurately to determine. Under and possibly above the absorption edge, because the exciting X-ray radiation does not possess enough energy to completely eject the electron from the atom, the absorption can be attributed to electron transition in unoccupied orbitals or bands. The modulation is also due to the so called multiple scattering. An excited electron, with kinetic energy E_{kin} corresponding to the energy difference between that of the exciting X-ray radiation and the bond energy E_0 , leaves the atom and gets scattered by electrons of neighbouring atoms. For small E_{kin} , as in the case of the XANES region, the scattering takes place in various directions. Before a scattered electron returns to its atom of origin it has undergone multiple scattering – scattering resulting from electronic interactions of neighbouring atoms. Upon its return to its original atom, the absorber atom, the scattered electron interferes with the outgoing excited electrons and depending upon the wavelength or kinetic energy of the photoelectrons, it leads to maxima and minima. Moreover, often strong peaks are observed as “white radiation lines” superimposed on the spectrogram in the XANES region. The origin of these strong absorption lines cannot with absolute certainty be attributed to inner atomic transitions or multiple scattering.

The EXAFS region lies from 50eV to 1000eV and in extreme cases 1500eV above the absorption edge. It lies in a zone of shorter wavelength in comparison to that of XANES and the dislodged electron is therefore associated with higher kinetic energy. Because of its high kinetic energy its scattering at the neighbouring atoms is one dimensional – it takes place along the line of motion of the electron, in both forward and backward direction. In contrast to the XANES region, where electrons with small kinetic energy lead to multiple scattering, here the probability of multiple scattering occurring is small because of the high kinetic energy of the electrons favouring forward scattering. Similarly to that of the XANES, upon its return to the absorber atom after a one dimensional scattering, the dislodged electron interacts with the electrons at the

absorber atom to form constructive and destructive interference. This expresses itself as a modulation of the transition probability of the electrons that is observed as a variation in the pattern taken by the adsorption-energy spectrogram in the EXAFS region. Teo [Teo86] and Koningsberg and Prins [KP 88] offer detailed information on this topic.

Mathematically, EXAFS (E) is defined as the periodic change of μ relative to the non-modulated absorption coefficient μ_0 (i.e. the absorption coefficient of an isolated atom of the same kind).

$$\chi(E) = [\mu(E) - \mu_0(E)] / \mu_0(E)$$

χ is also usually expressed as a function of the wave vector $k = 2\pi/\lambda$:

$$\chi(k) = [\mu(k) - \mu_0(k)] / \mu_0(k) \quad \text{Equation (3.1)}$$

At energy values above the absorption edge, $\mu(k)$ shows fluctuations, like a sine function, as a result of scattering from each shell of atoms at R_j , the average radial distance from absorber atom to the j th atoms. This phenomenon, EXAFS, or the oscillatory characteristics of the X-ray absorption coefficients in matter, is very useful in its application in obtaining structural information, and is given by [LP 75]:

$$\chi(k) = (-1)^1 \frac{1}{k} \sum_j \frac{N_j}{(R_j)^2} |F_j(k)| e^{-2(\sigma_j)^2 k^2} \cdot e^{-\frac{2R_j}{\lambda_j(k)}} \cdot \sin[2kR_j + \phi_{ij}(k)] \quad \text{Equation (3.2)}$$

where:

k : photoelectron wave number, defined as $k = [2m_e E(k) - E_0(k)(2\pi/h)^2]^{1/2}$, $E(k)$ is the kinetic energy of the ejected photoelectron measured from the absorption edge, $E_0(k)$ is the null point energy of the 1s electron, caused by atomic potentials and taken to be equal to the Fermi energy at low energies ($\leq 30\text{eV}$) and $E(k) - E_0(k) = h\nu - E_k - E_0(k)$, where E_k is the binding energy of the 1s electron before absorption.

l : Angular momentum quantum number

N_j : Number of neighbouring atoms, i.e. backscattering atoms in the j th coordination shell.

R_j : Average radial distance of the j th shell backscattering atoms from absorber atom

$|F_j(k)|$ Backscattering amplitude of neighbouring atoms in j th coordination shell.

In addition to k , it is also dependent on the scattering angle β .

$e^{-2(\sigma_j)^2 k^2}$: Debye Waller factor, accounts for thermal vibration or atomic position disorder; σ_j is the root mean square fluctuation of the j th shell atoms about R_j

$e^{-\frac{2R_j}{\lambda_j(k)}}$: Accounts for decay of photoelectron with mean free-path λ as a result of electron – electron scattering [Ste 74]

$\phi_{ij}(k)$: Phase shift experienced by the photoelectron in the potential field of the absorber and of the backscattering atoms. That the photoelectron experiences twice the potential field effect of the absorber atom i (outgoing and entering) and once that of the backscattering we have:

$$\phi_{ij}(k) = 2\phi_i + \phi_j(k)$$

$2kR_j$: period of a seemingly sine function attributed to atoms in the j th coordination shell at distance R_j from the absorber atom.

The EXAFS function, $\chi(k)$, is valid for only isotropic compounds. For orientated samples, such as single crystals and surface adsorbate, one has to consider polarisation effects when employing radiation of high degree of linear polarisation, such as the synchrotron radiation.

In applying this formula, a small – atom approximation is employed, implying that the atomic radius is small enough for the curvature of the incident wave to be neglected. The incident wave impinging on the neighbouring atom is then represented by a plane wave.

In the description of the EXAFS function, the dependency of the backscattering amplitude on k as well as on the scattering angle β , the angle between the incoming and the scattered photoelectron wave was stated. Maximum values are obtained for β at 0° and 180° , that is for forward and backward scattering, with a higher value for the forward (0°) scattering [Teo 81]. For simple scattering, with backscattering angle 180° , consideration of multiple scattering is not necessary and for that reason, the EXAFS function neglects it. Reference can be made to the work of Kuzmin et al [KP 93] as well as Rehr et al [RAZ 92] for the treatment of EXAFS in connection with multiple scattering.

The basic experimental determinant of the data processing technique is the measurement of X-ray absorption coefficient in the vicinity of characteristic absorption edges. In course of recording the X-ray absorption spectra of the samples, that of a reference sample, with absorption edge lying in the measuring region is also recorded. $\text{AlCl}_3/\text{CuCl}_2$ - GIC and $\text{FeCl}_3/\text{CuCl}_2$ - GIC were measured at the Cu K edge ($E = 8.979 \text{ keV}$) and Fe K edge ($E = 7.112 \text{ keV}$) respectively. The position of a characteristic feature in the reference spectrum (i.e. inflection point or white line position) is determined. The deviation of the experimental position from tabulated values is assumed to be linear over the measured spectral range and the characteristic feature, the absorption edge, is corrected accordingly.

Background corrections are made to separate absorption contributions resulting from other electrons in the absorber atom, from elements, which may be present as impurities in the sample, as well as from the support of the sample. By this undertaking, the K-shell absorption contribution for the atomic species in question is separated from all other absorption contributions resulting from other electrons in the same atom, from elements, which may be present as impurities in the sample, as well as from the support of the sample. These contributions are manifest as monotonically decreasing absorption coefficients in the low energy region before the adsorption edge and are adequately represented by the VICTOREEN formula:

$$\mu(E) = A + BE^{-3} + CE^{-4}$$

The parameters A, B, and C are found by fitting the formula to the measured absorption curve over the energy range E below the K adsorption edge of the element in question. The resulting function is extrapolated to encompass the whole region of measurement and then subtracted from the experimental curve. After the deduction, the result is the K-shell contribution to the absorption and the EXAFS – sine like function resulting from backscattering atoms in the jth coordination shell at distance R_j from absorber atom.

To evaluate the EXAFS function, it must be *normalised* and then *Fourier transformed*. After the Victoreen fit to remove the background correction, the monotonously decreasing absorption μ_0 (K-shell contribution) of the absorber atom above the absorption edge, as measured in the absence of EXAFS oscillation, is also determined. This is done by means of a polynomial fitting. By subtracting $\mu_0(k)$ from the really measured values $\mu(k)$ and dividing the result by $\mu_0(k)$ we get evaluated values of the EXAFS function in accordance with equation 3.1. The function shall practicably uniformly oscillate about a zero line. To normalise the function, a region before the absorption edge is chosen. A function of value 1, independent of photoelectron energy variation, is fitted. It is then extrapolated over the whole energy range and measured values of $\chi(k)$ are made to conform it as standard. The normalisation enables the comparison of various absorption spectra obtained from samples of different thickness.

Fourier transform of the normalised EXAFS $\chi(k)$, the oscillatory part of the X-ray absorption coefficient after separation from the smoothly varying K-shell absorption coefficient, enables us to determine the spatial variation of a scattering matrix. In other words it enables the separation of EXAFS-oscillations $\chi(k)$ with distinguishable frequencies (resulting from various distances R_j of the various jth coordination shells from the absorber atom). This technique, the application of Fourier transform algorithm on the raw data, is presented as:

$$FT(R) = \frac{1}{\sqrt{2\pi}} \int_{k_{\min}}^{k_{\max}} w(k) \cdot k^n \cdot \chi(k) \cdot e^{i2kR} d(2k) \quad \text{Equation (3.3)}$$

The weighing of the EXAFS with k^n and the use of a window function $w(k)$ ensure continuously falling, else uniform frequency of oscillation at the borders (k_{\min} and k_{\max}). k_{\min} and k_{\max} are the minimum and maximum k values of the useable experimental data. Kaiser-Bessel – and Gauß – window functions are used in this work. After the Fourier transformation (FT) a modified radial distribution function $FT(R)$ is obtained. The real distance R differs from that obtained from the peak maximum R in the FT by α , where α is half of the slope of the phase shift $\Phi_{ij} = 2\alpha k + \gamma$ (e) taking it as a linear function of k , and $R + \alpha = R$. This means that the shift in the peak's position is proportional to the slope of the phase shift function. Generally observed value of α is ca. – 50pm. In ideal situation, every maximum of the FT corresponds to a coordination shell. It is generally reasonable to coordinate the coordination shells up to a distance of about 500pm. It is to be noted that, coordination shells differing marginally in distance, can overlap in the FT. Inaccurate $\mu_0(k)$ determination as a result of experimental error may lead to misinterpretation of the Fourier transformed $\chi(k)$. The range of the experimental data chosen – this is the spectral range, that is to be evaluated – may deliver a shoulder beside a main peak, which can falsely be interpreted as an additional coordination shell. Unusual phase shift function exhibiting falling and rising regions may lead to double maxima belonging to the same coordination shell, also misleading the interpretation of the results. In order to distinguish between such misleading effects and real peaks, the amplitude and phase corrected Fourier transform can be determined [ZKBS 85, LGMSVS 85, BHLRS 94].

$$FT(R) = \frac{1}{\sqrt{2\pi}} \int_{k_{\min}}^{k_{\max}} w(k) \cdot k^n \cdot \chi(k) \cdot e^{i2kR} \cdot \frac{e^{-i\phi_j(k)}}{F_j(k)} d(2k) \quad \text{Equation (3.4)}$$

With this corrected version, for one type of atoms as nearest neighbours in a coordination shell, we get a Gaussian distribution, showing symmetric peaks at the real atomic distances that coincide with the imaginary part of the Fourier transform.

To separate the peaks corresponding to the coordination shells $j - \chi_j(k)$ in FT- from one another, the FT function must be *back transformed*. The back transformation, also termed Fourier filtering, is given by the following equation:

$$BT = FT^{-1} = \chi_j(k) = \frac{1}{\sqrt{2\pi}} \cdot \frac{2}{w(k) k^n} \int_{R_{\min}}^{R_{\max}} (FT(R) \cdot w'(R)) \cdot e^{-i2kR} dR \quad \text{Equation(3.5)}$$

$w'(R)$ is the rectangular window function, with limits R_{\min} and R_{\max} , covering the region of a coordination shell in the $FT(R)$ function. It effects the Fourier filtering.

By back transforming, we obtain a complex function $\chi_j(k)$ with a real component embodying the fine structure (in ideal case) of a coordination sphere j . The argument of the sinus function or the total phase in the EXAFS formula (eq3.2) can be obtained from the following relation:

$$\text{Arg}(k) = 2kR_j + \phi_{ij}(k) = \arctan \frac{\text{Re}[\chi_j(k)]}{\text{Im}[\chi_j(k)]}$$

where

$\text{Re}[C(k)]$ and $\text{Im}[C_f(k)]$ are the real and imaginary part of $C_f(k)$ respectively.

The amplitude function A_j , is formed by the values of $C_j(k)$ and is represented as the envelope or covering of the EXAFS oscillation.

$$A_j(k) = k \cdot \sqrt{\text{Re}^2[\chi_j(k)] + \text{Im}^2[\chi_j(k)]}$$

From the magnitude of $A_j(k)$ and with a knowledge of the coordination number N_j and the distance R_j of the j th coordination shell, the backscattering amplitude can be calculated

The final stage of the EXAFS data treatment is to obtain the structural parameters (R_j , N_j , $\Delta\sigma_j^2$ and ΔE_{0j}) by least squares fit method. To achieve this, one needs to get the necessary phase and amplitude functions of suitable reference compounds with known structural configuration. Apart from this, the differences in the coordination distances R_j of the reference specimen must not

differ very much from that of the sample under investigation. This is necessary, in order not to obtain a reduced coordination number in EXAFS-fit [V 93]. The number of independent parameters P_{free} , which can be refined, is restricted by the following relation [LSS 89]

$$P_{\text{free}} = (2/\pi) * \Delta k * \Delta R$$

where, Δk and ΔR are the Fourier transformed (FT) and back transformed (BT) regions respectively.

In our work, XAS measurements were carried out at the EXAFS II and the DEXAFS beamlines at Hamburger Synchrotron Laboratory (HASYLAB). The components of the dispersive spectrometer and their characteristics, have been outlined, in detail, by Hagelstein and Ressler [Hag 91, HCFNR 89].

The spectrometer embodies a Θ - and 2Θ -goniometers, holding the monochromator on the Θ -axis, and an optical bench on the 2Θ -axis. The detector, mirror and the sample are mounted on the optical bench. For details of double crystal see Tolentino et al [TBDFLT 90]

Synchrotron radiation coming from a bent magnet or an insertion device (Wiggler or Undulator) is monochromatized by a silicon crystal [Si(111), Si(400)] monochromator. The wavelengths or energies of the photons impinging on the sample, are defined by the Bragg's angle and the lattice distance of the monochromator. By changing the Bragg's angle by means of rotation of the monochromator in case of normal XAS or by using a bent crystal in case of dispersive XAS a series of adsorption μx and photoelectron energy measurements is made. Accompanying higher harmonics realised at the measured Bragg's angle lead to a significant distortion of the ensuing adsorption spectrum. According to Bragg's law ($n\lambda = 2d_{\text{hkl}}\sin \Theta$), X-rays with wavelengths corresponding to $n = 2, 3, 4, \dots$ (higher harmonics) are reflected by the monochromator at the same angle. A pronounced contribution of higher harmonics results in the reduction of the edge jump and a significant damping of the EXAFS amplitude. These harmonics are usually eliminated by slightly detuning the monochromator crystals. Recent modification of the EXAFS technology, as used for the analysis of our samples, has made it possible, to concentrate as many

photons as possible on the sample, by using a focusing optic of simple slits and mirror instead of detuning the monochromator crystals for the elimination of higher harmonics.

Generally X-ray absorption of the photoelectron energy without (I_1) and with (I_2) sample are measured with ionisation chamber or photo diodes, and is quantitatively presented as given in equation (3.3) :

$$\mu_{X_{\text{sample}}} = \ln(I_1/I_2)$$

Where reference substances are measured we also have:

$$\mu_{X_{\text{reference}}} = \ln(I_1/I_3)$$

I_1 and I_3 without and with reference respectively.

In our work, a photo diode array, comprising 1024 photo diode entities, capable of registering an expected count rate of 10^9 photons/s mm^2 at the DEXAFS beam line is employed. The quantum efficiency of the detector is 50% at 9keV. Because of the large energy exerted on the detector, its framework is subject to gradual deterioration, which is reflected in the form of *dark current*.

The acquisition and storage of data are carried out by means of a personal computer, connected to the detector (photo diode array) via a 100kH AD converter. The signal entering the computer is analysed by using a program WINXAS, developed by T. Ressler, a former co-worker in our group [Re 95], whose help in the instrumental measurements of the samples and data evaluation I am highly grateful. The program enhances the X-ray adsorption data analysis, delivering 100 adsorption spectra per second and the required parameters for the structuring analysis of our samples. Based on 10^9 photons/s delivered by the spectrometer, the adsorption spectra output can be considered remarkable.

X – ray absorption measurements were carried on the exfoliated products of AlCl_3 / CuCl_2 and FeCl_3 / CuCl_2 GICs. The measurements were performed at the Cu and Fe K-edges ($E = 8.979$ and

7.112 keV. respectively). CuCl_2 was made to react with air at the exfoliation temperature and used as standard for the absorption measurements.

3.1.4 Density Determination

The density of the exfoliated GIC, apart from being a physical characteristic of the catalyst, is also a prerequisite for the evaluation of the catalyst's specific surface area – a parameter essential for assessing the activity of the catalyst. The theoretical bases of the experimental determination is the assumption of ideal gas behaviour of air molecules at room temperature and pressure up to 1000mbar.

As shown in Fig.3.3, the volume of gas (air) of initial pressure p_i in a closed system of volume v_e is altered at a constant temperature by an amount of Δv to $(v_e + \Delta v)$. The pressure changes to p_f , fulfilling the ideal gas condition.

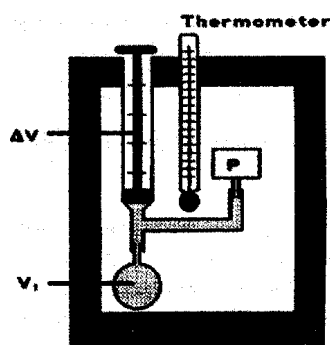


Fig 3.3: Volumetric density measurement.

p_i and p_f are determined with a manometer, Δv with a measuring cylinder. v_e , the volume of the empty round bottom flask and the connecting tube, is then evaluated by using the following relation based on the ideal gas law:

$$v_e = \frac{p_f}{p_i - p_f} \cdot \Delta v$$

Analogously, after inserting a known mass of the exfoliated GIC in the flask, we obtain the relation:

$$p_i, (v_e - v_{\text{sample}}) = p_f, (v_e - v_{\text{sample}} + \Delta v)$$

$$v_{\text{sample}} = v_e - \frac{p_f}{p_i - p_f} \cdot \Delta v$$

p_i , p_f , are initial and final pressures measured before and after altering the empty volume by Δv , but now with the sample inside. v_{sample} is the volume occupied by the sample of a known mass. The density of the sample is calculated from its measured mass and an average value of 10 measurements of the sample volume.

3.1.5 BET Surface Area Determination

The specific surface areas of the exfoliated GICs were determined through surface adsorption measurement by applying the adsorption isotherm based on BET considerations [BET 38]. Brunauer, Emmett and Teller (BET) first succeeded in developing a suitable adsorption isotherm, with practical application, for the multi layer adsorption. BET adsorption isotherm is a generalization of the ideal, localized mono layer adsorption developed by Langmuir, and describes the adsorption of gases in monomolecular layers on solid surfaces. In the development a homogeneous surface area of the adsorbent and zero interaction among the adsorbed molecules with adsorption enthalpy ΔH_A were assumed.

In developing their adsorption equation for multi molecular layer adsorption, Brunauer et al. assumed that every molecule in the first adsorbed layer serves as a possible adsorption site for a molecule in the second layer and so on. It was also assumed that an adsorption on an already adsorbed layer to be a condensation process with an enthalpy ΔH_L , which is also equal to the enthalpy of vaporisation.

The BET equation can be derived from kinetic or statistical considerations just as the Langmuir's equation. It is mostly presented in the following way:

$$\frac{p}{v_a (p^0 - p)} = \frac{1}{v_m \cdot c} + \frac{c - 1}{v_m \cdot c} \cdot \frac{p}{p^0}$$

whereby

$$c = e^{\left(\frac{\Delta H_A - \Delta H_L}{R \cdot T} \right)}$$

v_a : Volume of adsorbed gases(adsorbate) per unit mass of adsorbent.

v_m : Mono layer volume per unit of mass of adsorbent.

p : measured pressure in space where the adsorbent(sample) is.

p^0 : current air pressure.

c : a constant, which indicates the bonding relationship between the adsorbent and the adsorbate

ΔH_A : Enthalpy of adsorption. It corresponds to the activation energy of adsorption of gas molecules directly on the surface of the solid.

ΔH_L : Enthalpy of vaporisation. It corresponds to the activation energy of adsorption of gas molecules on the layers of already adsorbed gas molecules.

R and T are universal gas constant ($8.314 \text{ JK}^{-1}\text{mol}^{-1}$) and temperature of sample in (K).

The collection of data for the determination of the specific surface area was made with an equipment, trade name - sorptomatic 1900, of the firm Carlo Erba. A computer program, known as Milestone 100, provided by the firm was used for the evaluation of the data. N_2 was used to run the adsorption –desorption cycles, while always maintaining the sample temperature at 77.4°K , the boiling temperature of nitrogen. The equipment parameters – the volume of the flask for the gas dosage, v_k , the temperature of the flask, T_k , and the gas pressure in the in the dosage flask, p_k , as well as the burette constant B (determined with the empty burette), the mass of sample m_{sample} and its density ρ_{sample} are used for the calculation of v_a .

The burette constant is given by the following relation:

$$N \cdot v_k = p \cdot B$$

whereby

n: number of piston strokes

p: the pressure measured in the burette after n piston strokes.

v_a , after making room for the volume occupied by the sample, is given by the relation:

$$v_a = \frac{n \cdot v_k - p \cdot B_{\text{sample}}}{m_{\text{sample}}}$$

According to the above given BET equation, a plot of $p/v_a(p^0 - p)$ against the relative pressure p/p^0 , the so called BET plot, gives a straight line. c and v_m can be calculated and from its gradient, $(c-1)/v_m c$, and coordinate intercept, $1/v_m c$.

The relation between the specific surface area, s , and v_m is given by

$$s = (a \cdot v_m \cdot N_A) / V$$

Whereby a : area occupied by a molecule of the adsorbing gas; in this case by nitrogen molecule, which a is $16.2 \cdot 10^{-20} \text{ m}^2$.

N_A : Avogadro's number

V : volume of a mole of adsorbate

With a knowledge of c obtained from the BET plot, and of the enthalpy of condensation, ΔH_L (which is also equal in magnitude to the enthalpy of vaporisation, ΔH_v and equals 5.53 kJ mol^{-1} for nitrogen at 77.4 K), the enthalpy of adsorption, ΔH_A can be calculated. With the value of v_m obtained from the BET plot the specific surface area, s , can also be calculated.

3.1.6 Gas Chromatography

Chromatography is a physical or physical-chemical method for separating components in a mixture. The basis of the method lies within the separation column, which normally is a tube with

a small diameter, packed with a stationary bed of large surface area. A mobile phase percolates through the stationary bed. In the case where the moving phase is a gas the term or name *gas chromatography* is used. Specific terms, gas-solid chromatography and gas-liquid partition chromatography are used to apply to processes where the stationary phases are an active solid adsorbent and a liquid distributed over the surface of a solid support respectively.

The basic processes governing the gas-solid and gas-liquid chromatography are adsorption and partition, respectively. The separation process in the case of the gas-solid chromatography is based on differences in the multiple forces by which the column materials tend to retain each of the components. Notwithstanding the nature of retention, may it be adsorption, solubility, chemical bonding, polarity, or molecular filtration, the column retains some components longer than others. Components in a gas phase moving towards a column outlet are selectively retarded by the stationary phase. As a result, all the components pass through the column at different speeds and leave the column in a manner which is inversely proportional to the extent of their retention by the column material. The outline of the separation process is shown in Fig. 3.4 below.

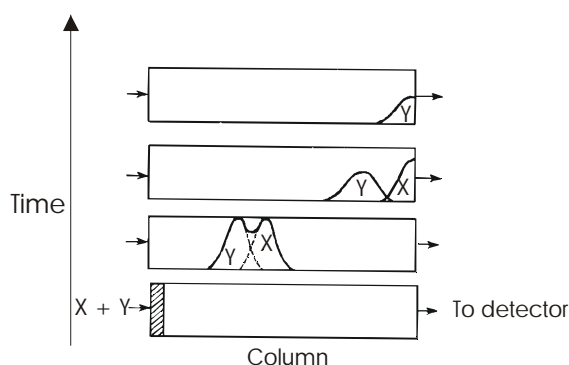


Fig. 3.4: Schematic diagram depicting the separation process of gas chromatography.

Immediately after emerging from the column, the components enter a detector, the order of their arrival at the detector depending upon their speeds through the column as explained above. Each component that gets to the detector registers a signal which appears as a peak above a base line on a recorded curve or chromatogram. A good separation, the achievement of which is dependent on the physical and chemical properties of the gas mixture, the choice of the column material, column temperature and the rate of carrier gas flow, is depicted as a succession of distinct peaks on the chromatogram. The area under each peak is a quantitative measure of the component

corresponding to it. A particular component is identified by the time lapse between the time of injection and the time of emergence of its corresponding peak, the so called “retention time”.

Gas Chromatograph, the apparatus used in gas chromatography, generally consists of the following parts:

- a) A separation column – this is the heart of the chromatograph. It is either a packed or capillary column. The packed column is commonly stainless steel, copper, cupronickel, or glass tube, either bent in U-shape or coiled. Its diameter is commonly 4mm and its length generally ranges from 1.2m to 150m. Connections are made generally with Swagelok fittings, making it easy to install the proper column for each separation desired. Various solid supports under various trade names such as Chromosorb P and W, GC-22 Super Support, and Sil-O-Cell C-22 Firebrick. Adsorbents such as silica gel, molecular sieves, alumina and activated charcoal are also used as stationary phase in gas-solid chromatography.
- b) Carrier gas and its pressure regulator and flow meter – maintenance of a highly constant carrier gas flow is a prerequisite for the efficient operation of a chromatograph. Carrier gases are generally operated between 0 and 4 bar and in the case, where a thermal conductivity cell is used as a detector, the flow rate lies between 0 and 1.2 l/h. Contaminants in the carrier gas must be prevented since it impairs the column performance and detector response when ionisation detectors are employed.
- c) The detector system – the type of detector used depends, to some extent, upon the type of column employed. Thermal conductivity cell is generally very suitable for systems where packed column is used and ionisation gauge such as flame ionisation detector is employed for capillary columns. Comparisons of detectors are very difficult since no single parameter describes their performance equally. A lot of factors such as applicability, response time, linear dynamic range, sensitivity and background signal among others must be considered.

The standard method of detection is achieved with thermal conductivity detector. Filaments within the cell form a Wheatstone bridge that detects the

difference in thermal conductivity between the sample components and reference stream of the pure carrier gas. The difference in thermal conductivity produces a signal that is amplified and recorded on a chart or recorded by means of a computer. An attenuator with a multi range selector switch is used to keep the components, whether large or small, on scale.

- d) Thermal compartment – monitoring the column temperature is very essential, whether it is intended to maintain an invariant temperature or to provide a programmed temperature. Usually an air bath chamber surrounds the column and air is circulated by means of a blower through the thermal compartment. Independent temperature controllers are desirable for the vaporiser block and the detector oven.
- e) The injection system – the most problematic aspect of the gas chromatography analysis is the sample injection system. This seemingly simple little device must introduce the sample in a reproducible manner and, if a liquid, vaporise it instantaneously. Even though large amounts of heats are required, the sample must not be decomposed nor pressure surges created. Exact amount of sample must be metered and transferred to the column without fractionation, condensation, or adsorption of components. Gas samples are injected by a gas-tight syringe or gas-sampling valve, known as *stream splitter*. In its simplest form it is merely a system of three stopcocks, between two of which there is a standard volume in which gas is trapped. Gas from this bypass capillary loop is introduced into the column by sliding or rotating a valve to connect the loop with the stream of the carrier gas.

Theory of the Gas Chromatography

The gas chromatography theory is discussed here with a view of providing a treatment of the basic parameters to help in understanding the technique.

Retention time and volume

The distance from the point of sample injection on the time axis to the peak of an eluted component registered at the detector is known as the uncorrected or gross retention time, t_{gr} , for the particular component. It is a function of column temperature, carrier flow rate, F , the affinity between the sample component and the material in the column that effects the separation. The product of the carrier flow rate and the gross retention time is the gross experimental retention volume, V_{gr} , and is given by,

$$V_{gr} = t_{gr}F$$

Unlike the gross retention time, which changes as a result of unexpected changes in the flow rate, is a good measuring unit or index because it is not affected by changes in the flow rate resulting from external influences. The gross retention volume, measured at equal time intervals, rules out error causes by unexpected changes in the flow rate.

Analogous to the eluted component, letting “gr” represent the gross retention time for unretained substances such as the rare gases – mostly used as carrier gas – and F the flow rate of the carrier gas we can formulate the gross retention volume, well known in this case as the dead volume, V_d as

$$V_d = t_dF$$

V_d represents the interstitial volume of gaseous phase in the column, plus any dead volume in the injection port and detector. In the case where a spread splitter is used, a dead volume in the tubing leading to the column must be considered.

The difference between the gross retention volume of a sample component, V_{dr} , and the dead volume, V_d , is known as the adjusted retention volume, V_r , and is given as

$$V_r = V_{gr} - V_d = t_{gr}F - t_dF$$

Retention volumes, V_r , are measured from the carrier gas peak as shown in Fig. 3.7 below. In Fig. 3.6 (a) A, B and C indicate the starting of the analysis, the inert gas peak and the substance peak respectively; Fig.3.5 (b) shows the separation of substances with the passage of time.

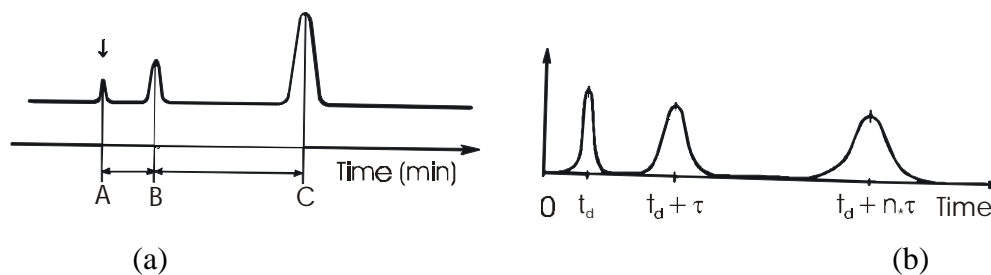


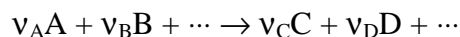
Fig. 3.5: Illustration of the separation process

Given the retention time in minutes [min], the flow rate in millilitre per minute [ml/min], the units of the retention volume is expressed as millilitre [ml].

3.1.7 Reaction Kinetics

Reaction rates.

Consider the following general chemical reaction.



where the ν_i s are the stoichiometric factors. The number of moles n_i of the consumed reactants (A and B) and the formed products (C and D) are related in the same way as the stoichiometric factors. The relationship is as follows.

$$n_A/n_B = \nu_A/\nu_B ; \quad n_C/n_A = \nu_C/\nu_A$$

Noting that the stoichiometric factors for the reactants are negative and that of the products are positive, we can formulate the differential turnover as :

$$dn_A/\nu_A = dn_B/\nu_B = dn_C/\nu_C = dn_D/\nu_D$$

Following the reaction process with the help of the changes in the number of moles of A, B, C, or D i.e. with dn_A , dn_B etc., one arrives at , according to the stoichiometric factors, different numerical results.

To avoid this discrepancy one defines the extent of reaction as :

$$d\xi = dn_i/\nu_i.$$

which permits a clear description of the reaction process. For the above chemical reaction we have

$$d\xi = dn_A/\nu_A = dn_B/\nu_B = dn_C/\nu_C = dn_D/\nu_D = \dots$$

The rate of reaction r , defined as the extent of reaction with time, is then given by the relation

$$r = d\xi/dt = dn_i/\nu_i dt.$$

Since $d\xi$ is independent of both the component chosen and the reaction conditions so also is the rate not dependent on these factors. This implies that the rate is also valid where the volume changes with time.

Assuming a constant volume or that the volume of component i as independent of time, we have after dividing preceding equation by the volume, V

$$d\xi/Vdt = dn_i/\nu_i Vdt = dc_i/\nu_i dt$$

where c_i denotes the concentration of the component i .

As stated above the rate of reaction based on a component A in a reaction mixture is given as

$$r = d\xi/dt = dn_A/\nu_A dt$$

In a homogeneous fluid, based on unit volume of fluid V_f , we define

$$r^1 = 1/V_f [dn_A/v_A dt]$$

Based on unit mass W of solid in fluid – solid systems, we define

$$r^{11} = 1/W [dn_A/v_A dt]$$

Using a unit surface area S of solid as in gas – solid systems, we define

$$r^{111} = 1/S [dn_A/v_A dt]$$

Based on unit volume V_s of solid in gas – solid systems, we define

$$r^{1V} = 1/V_s [dn_A/v_A dt]$$

One can also base the evaluation of the rate on a unit volume V of reactor, if this happens to be different from unit volume of fluid then we have the following relation:

$$r^V = 1/V [dn_A/v_A dt]$$

In heterogeneous systems all the above definitions of reaction rate are encountered; the one used being only a matter of convenience.

$dn_A/v_A dt$ being the same in all the above cases, we have

$$V_f . r^1 = W . r^{11} = S . r^{111} = V_s . r^{1V} = V r^V.$$

Heterogenous catalysis

Chemical reactions taking place on specific surface areas, in contrast to reactions of homogeneous gas mixtures, are termed heterogeneous catalysis. The solid medium on which the reaction takes place can be homogeneous or heterogeneous in nature. Generally it is made up of a

supporting material with high specific surface area on which a catalytically active substance is finely distributed. Depending upon the aim and nature of the catalytic investigation, two or more different active substances can be embodied placed on the supporting material. The terminology – catalyst – as used in this work is considered applicable to the whole entity of the support material and the active substance(s).

Catalysts are in a position to influence the reaction rate, in certain instances dictate the path of a reaction leading to selective realisation of a specified reaction product. There are also reactions, which practically would not take place without the application of catalysts. The effect of these substances lies in their ability to lower the apparent activation energy. Upon applying the catalysts, we get the reactants, partly or wholly, adsorbed on the finely distributed active component on the surface. This leads to the formation of activation complexes with low activation energies. These complexes are mostly related to electron charge transfer in one direction or the other. The adsorbed species can then react with their neighbours or with reactants in the gas phase after diffusing onto the catalyst surface. The ensuing reaction product desorbs from the active surface area.

Catalyst activity, a stuff specific property, is determined by comparing such relevant reaction parameters as reaction rate and turnover based on unit mass, unit volume or specific surface area with that measured without the use of catalyst. In contrast to catalyst activity, the effectiveness of a catalyst is non-specific material property. It is determined by such parameters as specific surface area, package density, pore volume, and particle size of the active substance.

For the characterisation of a catalyst, taking both the activity and the effectiveness into consideration, the reaction rate r is defined in terms of mole mass (or volume) of the substance consumed or formed per unit volume, mass, or specific surface area of the catalyst per unit time. The equations relating the rate and all these parameters are give in section 3.7. Assuming a homogeneous surface area for the catalyst, the specific surface area can be used as a base for measuring the rate of catalysed reaction.

Large quantities of catalyst materials may be needed, when large material conversions or turnover are required. This is especially the case as in the automobile industry for the conversion of the toxic gases CO and NO into the less harmful CO₂ and N₂. In such instances the quantitative proportions of the active substance to the support material is of great interest. The catalyst does not get consumed, in stoichiometric sense, as a result of the reaction that it catalyses. However, if even to a small extent, the possibility of catalyst material loss owing to its slight dissolution in the reaction medium or through frictional interactions with the reactants and products cannot be ruled. This leads to pollution of the products and consequently of the environment. A search for suitable catalyst must not lose sight of such factors. In the light of this, not only the duration period – time for complete exhaustion of catalyst material - in catalysis tests needs to be taken into account in catalyst assessment, but also the nature of material given up to the reaction medium in the course of the tests.

The heterogeneous catalytic oxidation and oxidation-reduction, because of their applications in removing hazardous environmental poisons such as CO and NO, have found large publicity in international media.

Metal and metal oxide catalysts are mainly used in the conversion of CO and NO into the relatively environmentally friendly products CO₂ and N₂. Should CO oxidation be undertaken upon addition of oxygen, then the relative inert O₂ must undergo an activation process. This generally takes the following steps: Adsorption, electron transfer, dissociation and eventually the incorporation in the oxide lattice. For most oxidation reactions, adsorbed oxygen results with total oxidation and oxygen with greater portion fixed in the lattice delivers partially oxidised products. By the choice of the appropriate reaction conditions, the oxidation can be geared towards obtaining the required end products. According to Sokolovskii [Sok 87] the catalytic oxidation embodies the formation of highly reactive adsorbed oxygen (O_(ads, act.) e.g. O⁻ or O₂⁻) and the fixing of the active oxygen in the oxide lattice (O_(lattice)). In his investigation of the oxidation of hydrocarbons he showed that a higher composition of adsorbed oxygen O_(ads, act.) favours total oxidation, i.e. a complete conversion to CO₂ end products. A schematic representation of the reaction mechanism as given by Sokolovskii is modified and shown in Fig.3.6.

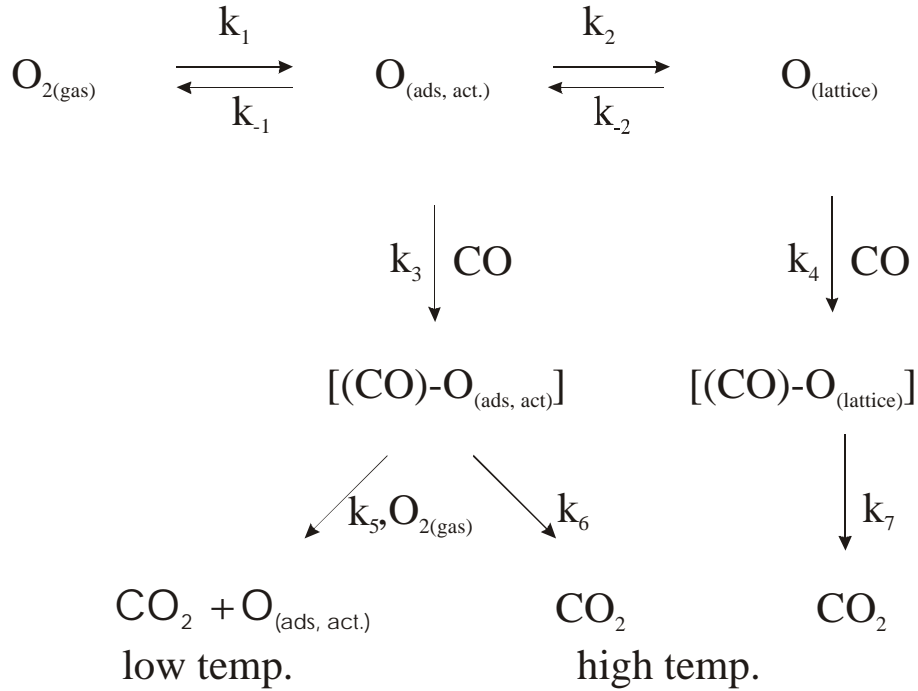


Fig.3.6 : Modified mechanism of catalysed oxidation reaction (according to Sokolovskii).

In Fig.3.6 k_1 and k_{-1} indicate the forwards and backwards rate constants of adsorption and activation of oxygen on the catalyst's surface respectively. $\text{O}_{(\text{ads, act.})}$ can form a surface complex $[(\text{CO})\text{-O}_{(\text{ads, act.})}]$ with the reacting CO (rate constant k_3). The complex can further react with oxygen in the gas phase at low temperature to yield CO_2 (rate constant k_5), leaving the catalyst's surface still adsorbed with oxygen atoms. At high temperatures desorption of CO_2 can take place without additional oxygen. The reaction rate constant is represented by k_6 . $\text{O}_{(\text{ads, act.})}$ can also be embedded in the oxide lattice ($\text{O}_{(\text{lattice})}$), when free interstitial places are available. The forward and backward rate constants of this reaction are represented with k_2 and k_{-2} respectively. The best reaction conditions for obtaining free lattice or interstitial places are high reaction temperatures. ($\text{O}_{(\text{lattice})}$) can also react with CO (rate constant k_4). The lattice complex $[(\text{CO})\text{-O}_{(\text{lattice})}]$ is formed at the maximal stoichiometric relations of the embedded oxygen and carbon monoxide. The (CO)-O lattice complex desorbs at high temperatures with rate constant k_7 to yield CO_2 .

Fig. 3.6 describes the reaction paths taken in the course of catalytic oxidation reaction. In order to obtain CO conversion to follow the path with rate constant k_3 , rate the reaction rate for adsorption and activation of oxygen (r_1) must be high, the bond energy must be possibly low [Sok 90]. The

diffusion rate of the adsorbed and at the same time activated oxygen in the interstitial places of the oxide lattice should be slow in comparison to the adsorption rate on the surface of the catalyst. Two deductions can be made from this:

1. For large k_3 (see Fig. 3.6) we have a situation where the adsorbed oxygen is consumed at a fast rate - implying very small amount of active oxygen on the catalyst's surface. The rate-determining step is the oxygen adsorption on the catalyst's surface. We then have the following relations:

$$r_1, r_{-1} \gg r_2, r_{-2} \text{ and } k_3[\text{CO}] \gg k_1[\text{O}_2] .$$

2. For small k_3 , $O_{(\text{ads}, \text{act.})}$ is large. The rate-determining step of the whole reaction is then k_3 . This is also the case for reactions with large proportion of oxygen to carbon monoxide. For such conditions we have:

$$r_1, r_{-1} \gg r_2, r_{-2} \text{ and } k_1[\text{O}_2] \gg k_3[\text{CO}].$$

It can be argued that small bond energy contradicts the demand for a high adsorption rate. Efficient catalysts have large number of free adsorption sites for the oxygen adsorption per unit surface area. Adsorption rate is dependent on the degree of absorption. By small adsorption, as in **1**, we still have enough absorption sites and therefore a high absorption rate. Such small surface area adsorption with oxygen leads, according to the conditions given in **1**, to the overall reaction rate R :

$$R = r_1 \cong n_y k_1 [\text{O}_2] \quad \text{Equation (3.6)}$$

n_y is the number of sites available for oxygen absorption per unit surface area of the catalyst.

After reacting with the adsorbed oxygen, the CO is converted into the aforementioned surface complex. It desorbs as CO_2 in the presence of molecular oxygen at low temperatures – around 200°C . At high temperatures CO_2 desorption takes place without oxygen. Taking for granted that the formation of carbonate surface complex comprises the breaking of the oxygen-catalyst bond and its desorption, (the reaction steps with rate constants k_3 and k_5) and also that k_3 , as according to **2**, the rate determining step of the reaction, the demand for weak bond between the activated oxygen and the catalyst can be justified. The smaller the bonding energy is the larger k_3 and also

the reaction rate of the overall reaction. The overall reaction rate R , given the conditions under 2, can be represented as:

$$R = r_3 \equiv n_y k_3 [\text{CO}]. \quad \text{Equation (3.7)}$$

To investigate the reaction steps 1 – 3 – 5 (or 6) the following reaction conditions were chosen:

- a) Tests of CO and O₂ gas mixtures and measurements of CO₂ produced or CO consumed per unit volume (or surface area) of the applied catalyst were carried out.
- b) Both components were alternatively passed onto the catalyst. The catalyst activity was determined by measuring the CO₂ produced or CO consumed.

The reaction path 1 – 3 – 6 requires high temperature and underlies the step by steps reaction mechanism. In contrast to concerted reaction mechanism whereby the desorption of the oxidised surface area complex occurs only in the presence of molecular oxygen and the reaction rate also depends on oxygen concentration [O₂], the step by steps reaction mechanism indicates clearly the course taken by the reaction – adsorption and activation of oxygen, oxidation of CO and desorption of CO₂. At high desorption rate (k_6) the overall reaction rate can be represented by equation (3.6) or (3.7)

The reaction rate for the reaction path 1 – 2 – 4 – 7 also underlies the step by steps reaction mechanism. It is determined by the formation of the oxidised surface area complex [Sok90] [(CO)-O_(lattice)]]. The overall reaction rate can be represented as :

$$R = k_4 [[(\text{CO})-\text{O}_{(\text{lattice})})]].$$

This can be verified by employing isotope (¹⁸O₂) exchange reaction. At high temperatures the desorption of CO₂ takes place.

The influence of CO on the reaction rate was examined by varying the CO concentration at constant oxygen concentration.

Having discussed the conditions for the heterogeneous catalytic oxidation reaction, we consider substances which are catalytically active. Two main groups of substances are worth mentioning:

- 1) Metals such as W, Au, Rh, Pd, and Pt. These metals are catalytic active and are presented in the order of increasing activity.
- 2) Metal oxides, especially of the d – group elements. Comparison of catalytic activities of various metal oxides based on oxidation of ethylene is presented by Dmuchovsky et al. [DFZ 65]. Increasing order of catalytic activity were observed for the oxides of the following elements Zn, Ti, W, Mo, Fe, Cd, V, Ni, Cu, Mn, Ag, Cr, and Co. CeO₂ has also been found by other authors to be highly catalytic active [SFTSHA 60]. Also mixed oxides such as cobalt-manganese spinel have been used as effective oxidation catalyst [LM 62]. Application of molybdate, in catalytic oxidation reactions, has been reported by Sokolovskii [Sok 90]. Numerous combined metal oxides with catalytic activity can be listed.

The behaviour of metal oxides as semiconductors is used in judging their catalytic properties [Fen 57, DL 60]. n – conductors with the exception of V₂O₅ are poor oxidation agents and p – conductors such as Cu₂O, NiO, CuO and FeO are good ones. In their judgement of the qualities of good catalysts, Voge and Adams [VA 67] concluded that the desorption energy of activated oxygen a better means of measuring catalyst properties as their semiconductor properties or their d – electron configuration.

Metal catalysts are constructed in such a form that the active substances, the metals in the form of particles, are finely distributed on a support material. The particle size does matter when considering how large the practicably active surface area is. The particle size should be small. On the other hand, the electronic properties of metals change when the cluster size falls below a certain level. With regards to the relation

$$\delta \propto \epsilon_F / N$$

the distance δ between neighbouring energy levels given the atomic number N can be determined. ϵ_F represents the Fermi energy level. Decreasing atomic number leads ultimately to δ being larger than kT (kT : the thermal energy) and consequently to the loss of the conducting properties of the metal. Investigation of the influence of particle-size and form on the catalytic properties of metals has been carried out by Che and Bennet and published in the literature

[CB89]. Particle size measurements were not carried out in this work. A hint on this topic is only to indicate the important role particle size plays in heterogeneous catalysis research and also how problematic it is.

Non stoichiometry plays an extraordinary role in metal oxide catalysis. Metal oxide catalysts are often used without support material. In course of the catalysis reaction oxygen can be removed from the lattice, creating defect sites. These defect sites are not only found on the crystal surface; oxygen exchange takes place in the interior layers of the crystal. The catalyst activity of the metal oxide turns out to be essentially influenced by these defect sites. A summary of this topic is given by Gai-Boyes [Gai 92].

Catalytic capabilities are attributed to transition metal oxides whilst their central atoms possess unoccupied d-energy levels and as a result have the possibility to promote adsorbed molecules by means of electron transfer into reactive transition state. Rare earth elements also have high energy levels, which allow uptake and donation of electrons. It is therefore not surprising that CeO_2 , a representative of the rare earth elements exhibits good catalytic properties in relation to CO oxidation. Dowden et al. describe the CeO_2 catalytic activity in CO oxidation reaction between 150 and 400°C [DMT 57]. CeO_2 serves also as a good catalyst for the oxidation of olefines [SFTSHA 60].

In combination with Pt, Rh, and $\gamma\text{-Al}_2\text{O}_3$ – in the so-called three-way catalyst – CeO_2 is used in the detoxification of exhaust gas [e.g. GPSD 76, LPK 85, NRCB 92]. It serves as storage for oxygen. In the event of oxygen deficiency, when the three-way catalyst is in operation, CeO_2 provides ‘lattice oxygen’ [YY 84]. It can also build up very reactive surface area radicals (O^\cdot , O_2^\cdot , etc.) [TPSK 88, YY 84]. It reduces considerably the activation energy for the CO oxidation [Y 84, OE 88] and thus speeds up the CO oxidation in contrast to a catalyst that does not have this property. The CeO_2 component (wash coat) in the catalyst amounts to 25 %. Apart from the roughly 1 % noble metal component, the rest is made up of $\gamma\text{-Al}_2\text{O}_3$. The peculiar interactions between the noble metals and free oxygen lattice sites leads to the enhancement of the reaction rate of the mutual oxidation and or reduction of CO and NO [LKAF 91].

3.1.8 Theory of the Plug Flow Reactor

Plug flow reactor is, among other names, also known as ideal tubular and unmixed flow reactor. As an ideal steady-state flow reactor the flow of fluid through the reactor is orderly with no element of fluid overtaking or mixing with any other element ahead or behind. In its ideal state there could be lateral mixing of fluid in a plug flow reactor but no mixing of fluid in longitudinal direction. Constant residence or contact time for all elements of fluid is the measure of an ideal flow reactor.

In a batch reactor, where reactants are charged into a container and left to react for a period of time and the resultant mixture discharged and analysed, the reaction time is the natural measure of processing rate. In the case of plug flow reactor the residence time, also known as contact time or space time is used as the measure of performance. The reciprocal of space, known as space velocity, can also be used instead of space time.

Contact time is the time required to process one reactor volume of feed measured at specified conditions. It is to be noted here that contact can also have dimensions other than “time” depending upon the definition or how the reaction rate is formulated. The contact-time or space-velocity depends on the experimental conditions such as temperature and pressure at which we choose to measure the volume of material being fed to the reactor.

Consider reactant A entering an element of reactor volume as shown Fig. 3.7 below. The equation for the material balance can generally be presented in the following way.:

rate of reactant accumulation flow into element in element of volume	=	rate of reactant flow out of element of volume	+	rate of reactant loss due to chemical reaction within the element of volume	+	rate of of reactant of volume
--	---	--	---	---	---	-------------------------------------

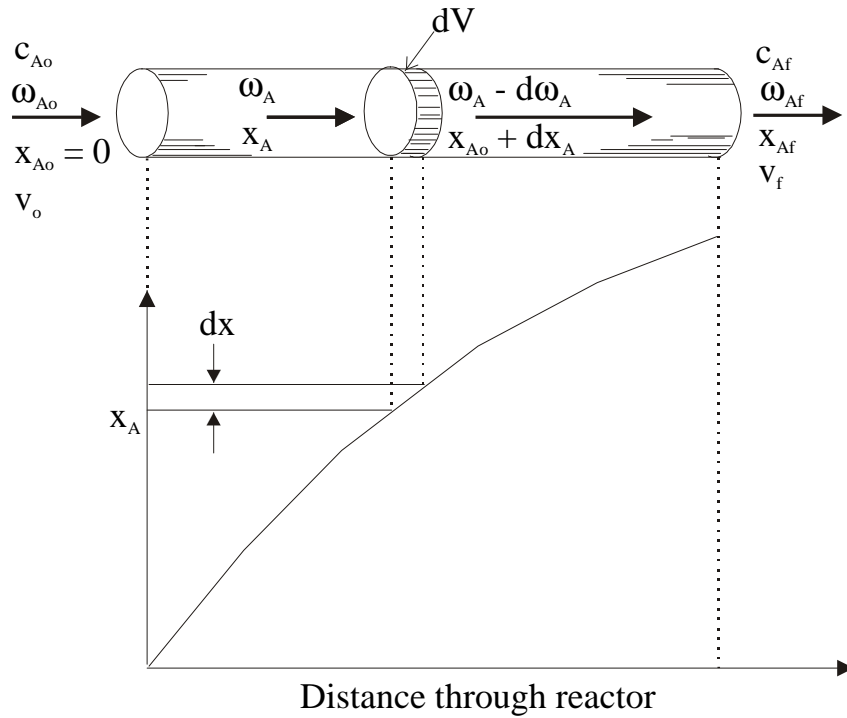


Fig. 3.7: Plug flow reactor, schematically.

In a steady-state flow reactor the fourth term is zero. As the composition of the fluid in the reactor varies from point to point along a flow path the material balance for a reaction component must be based on a differential element of volume dV .

For a component A of a reaction gas mixture the following definitions are valid:

c_{A0} = initial concentration of A

v_o = constant volumetric feed or flow rate of the gas mixture

ω_{A0} = $c_{A0} * v_o$ = the molar feed rate of component A on entering the reactor chamber assuming conversion before entry.

ω_A = $c_{A0}(1 - x_A) * v_o$ = the molar feed rate of A at time t when the conversion is x_A .

c_A = concentration of A at at time t and feed rate ω_A .

r = Reaction rate based on component A

From the above box, the material balance for a reactant A in volume dV can be expressed in the following way:

Molar feed rate of A (ω_A) at the entrance of volume element dV – feed rate of A ($\omega_A - d\omega_A$) at the exit of volume element dV = rate of consumption of reactant A, $r dV$.

It follows:

$$d\omega_A = -r dV \quad \text{Equation (3.8)}$$

The change in the feed rate of component A is

$$d\omega_A = v_0 dc_A,$$

ω_A decreasing as c_A decreases.

In order to express the feed rate in terms of concentration we define the fraction of A converted,

$$x_A = 1 - c_A/c_{A0}, \quad dx_A = -dc_A/c_{A0}.$$

Because of the great excess of helium gas in the reaction gas mixture we have a constant density system. Taking into account that

$$d\omega_A = -\omega_{A0} dx_A$$

we obtain by means of replacement of $d\omega_A$ in equation (3.8):

$$\omega_{A0} dx_A = -r dV$$

For the integral flow reactor, where the conversion x_A can be high, the following equation, obtained after grouping the terms, is used for the calculation of the reaction rate:

$$\int dV/\omega_{A0} = -\int dx_A/r$$

Testing for a first order reaction and assuming a constant density reaction, where

$$r = kc_A \text{ and } c_A = c_{A0} (1 - x_A),$$

one gets after substitution and rearrangement

$$k c_{A0} \int dV / \omega_{A0} = - \int dx_A / (1 - x_A)$$

Replacing ω_{A0} by $c_{A0} \cdot v_0$ and with integration limits of conversion from 0 to x_A , we get

$$k \int dV / v_0 = \ln 1 / (1 - x_A)$$

By varying the reactor volume or the flow rate and measuring the conversion x_A values of V / v_0 and their corresponding values of $\ln 1 / (1 - x_A)$ can be obtained.

A plot of the values of V / v_0 against $1 / \ln (1 - x_A)$ gives a straight line with gradient k .

Instead of V the volume of reactor, the mass, or the surface area of the catalyst can be used. In the case of CO oxidation the volume of the reactor as well as the surface area of the catalyst were used as a measure of the rate of reaction.

For a differential flow reactor, where the conversion x_A is kept low, the following equation is used for the evaluation of the rate:

$$\omega_{A0} dx_A = r dV, \quad r = (x_A - x_{A0}) / (V_a / \omega_{A0})$$

where x_{A0} is the conversion of A before entering the reactor and V_a the volume corresponding to x_A . This generally applies to compounds which by one means or the other decompose before arriving at the reactor or decompose as a result of reaction with the reaction vessel.

By varying the volume of reactor, the rate of flow of reactant or the initial concentration of the feed various values of x_A and x_{A0} can be measured giving way to the evaluation of the rate of reaction.

Similarly, where V_r , W , or S , the reactor volume, the mass, or the surface area of the catalyst is used as basis for the calculation, the rate is formulated as follows:

$$r = (x_A - x_{A0}) / (V_r, W, \text{ or } S / \omega_{A0})$$

3.1.9 Determination of Empirical Formula

Theoretically, the empirical formula of an intercalation compound can be evaluated from the relation between the weight portions of intercalate and graphite, i.e. the stoichiometry, and the stage number of the GIC. The weight proportion of intercalate in GIC can be determined by X-ray fluorescence and gravimetric measurements, and the stage number from X-ray diffraction. After finding these parameters the empirical formula can be calculated as follows:

Defining G_{MeCl_2} as the weight percent of the intercalate in the GIC we have:

$$G_{\text{MeCl}_2} = \frac{n_{\text{MeCl}_2} \cdot M_{\text{MeCl}_2} \cdot 100}{n_{\text{MeCl}_2} \cdot M_{\text{MeCl}_2} + n_{\text{C}} \cdot M_{\text{C}}} \%$$

In this equation n_{MeCl_2} , n_{C} are mole numbers of metal chloride and carbon resp,

M_{MeCl_2} , M_{C} are mole masses of metal chloride and carbon resp.

$$G_{\text{MeCl}_2} = \frac{M_{\text{MeCl}_2} \cdot 100}{\frac{n_{\text{C}}}{n_{\text{MeCl}_2}} \cdot M_{\text{C}} + M_{\text{MeCl}_2}} \% \quad \text{Equation (3.9)}$$

By calculating the number of Carbon atoms per the surface area occupied by a unit cell of the intercalated metal chloride, the relation of the mole number of carbon to that of the metal chloride as stated in equation (3.9) can be evaluated.

Taking the number of formula weights per unit cell and the stage number into consideration we get equation (3.10) :

$$\frac{n_C}{n_{\text{MeCl}_2}} = \left(\frac{Z_C}{F_C} : \frac{Z_{\text{MeCl}_2}}{F_{\text{MeCl}_2}} \right) \cdot S \quad \text{Equation (3.10)}$$

Z_C, Z_{MeCl_2} number of formula weights per unit cell per unit surface area.

F_C, F_{MeCl_2} area of the two dimensional unit cell.

S stage number.

Replacing in equation (3.9) we obtain:

$$G_{\text{MeCl}_2} = \frac{M_{\text{MeCl}_2} \cdot 100}{S \cdot \frac{Z_C}{Z_{\text{MeCl}_2}} \cdot M_C \cdot \frac{F_{\text{MeCl}_2}}{F_C} + M_{\text{MeCl}_2}} \cdot \% \quad \text{Equation (3.11)}$$

Let us define x as $\frac{Z_C}{Z_{\text{MeCl}_2}} \cdot \frac{F_{\text{MeCl}_2}}{F_C}$, then the composition of the graphite metal chloride

intercalation compound can be represented empirically as $\text{C}_{Sx}\text{MeCl}_2$. Substituting x in equation (3.11) we get:

$$G_{\text{MeCl}_2} = \frac{M_{\text{MeCl}_2} \cdot 100}{S \cdot M_C \cdot x + M_{\text{MeCl}_2}} \cdot \%$$

Knowing G_{MeCl_2} , the percentage composition of the metal chloride in the graphite intercalation compound, and S , the stage order, x , defined above, can be evaluated.

3.2 Preparation and Characterisation of the Catalysts

3.2.1 Preparation and Characterisation of the Graphite Intercalation Compounds (GICs)

The graphite CuCl_2 intercalation compounds, used for preparing the catalysts investigated in this project, were prepared by employing standard methods already discussed in section (2.4), using both AlCl_3 and FeCl_3 as supporting agents.

In the preparation of $\text{AlCl}_3/\text{CuCl}_2$ intercalation compound, which was later on exfoliated to give $\text{Al}_2\text{O}_3/\text{Cu}_a\text{O}_b$ (the catalyst), both aluminium and copper chlorides were first dried in an exsiccator over P_4O_{10} . The aluminium chloride was then sublimated in conjunction with a piece of aluminium foil to yield a very pure product. The relatively dried copper chloride was added gradually and under constant stirring, with great care to avoid violent gas evolution, to a round bottom flask containing freshly distilled thionylchloride at room temperature. After no more gas evolution was observed it was heated to the boiling point and refluxed for a period of 15 hours, measures being taken to avoid water from entering the system. After the reaction most of the thionylchloride was distilled off. The rest was removed under vacuum at a temperature of 150°C . The graphite used was of particle size ranging from 300 to 600 μm . Before being used for the intercalation reaction it was boiled in nitric acid, washed with distilled water, rinsed with acetone and then dried in oven at 150°C . The aluminium chloride and the copper chloride were then filled in a nitrogen atmosphere into a dried, one-sidedly sealed glass tube filled with the graphite. The copper chloride and the graphite were inserted in weight proportions of 2g CuCl_2 to 300 mg of graphite. The tube, upon application of a mild heat with the help of an electric dryer, was evacuated and finally dosed with dry chlorine to a pressure of 500 mbar. It was completely sealed off by melting into an ampoule. The ampoule was then tempered in an oven at 200°C for a period of 3 to 5 days. At the end of the reaction it was cooled down quickly with compressed air. The obtained product was thoroughly washed with distilled water and rinsed with acetone, care being taken to avoid adsorption of large quantities of the chlorides on the surface of the sample. Surface impurities cause errors in the gravimetric measurement of the intercalate content and also in the X-ray fluorescence analysis of the sample. This usually calls for leaving the sample overnight in distilled water before it is filtered and dried. Graphite CuCl_2 intercalation compounds of the first

and second stage were obtained, depending upon the reaction period or the CuCl_2 and graphite weight proportions in the reaction mixture.

Similar procedure was used for the preparation of $\text{FeCl}_3/\text{CuCl}_2$ intercalation compounds. In this case the tempering temperature was set at 350°C . First and second stage products were also obtained.

Graphite intercalation compounds containing MoOCl_3 and both MoOCl_3 and CuCl_2 were also prepared by means of AlCl_3 . MoO_3 was treated as shown above for CuCl_2 using H. Hecht's method [Hec 47]. Mainly MoOCl_3 and small amount of MoCl_5 and other molybdenumoxy-chlorides were obtained as product after refluxing in freshly distilled SOCl_2 and distilling off the SOCl_2 . After drying the obtained product completely of thionylchloride it was sublimated and pure MoOCl_3 , brownish green crystals with sublimation temperature at 190°C , were obtained.

In the preparation of $\text{AlCl}_3/\text{MoOCl}_3$ intercalation compounds, mixtures of AlCl_3 , MoOCl_3 and graphite, with the weight of molybdenumoxychloride to that of graphite in proportion of 2g to 300 mg, were inserted in a glass tube at reaction temperature of 190°C . The chlorine gas pressure was 500 mbar and the reaction period was 3 days.

The $\text{AlCl}_3/\text{MoOCl}_3/\text{CuCl}_2$ -graphite was prepared by inserting the compounds and the graphite in molar proportions of $\text{MoOCl}_3 : \text{CuCl}_2 : \text{graphite}$ (2g : 1g : 0.6g).The reaction temperature was 200°C and the time of reaction was 3 days.

In all the preparations the amount of AlCl_3 or FeCl_3 inserted for every 300mg of graphite was 200mg and the quantity of reaction mixture in an ampoule was made not to exceed 6g.

Ce(IV) nitrate-graphite was prepared by intercalation from liquid phase. Firstly, a concentrated solution of $\text{CeO}_2 \cdot 0.5\text{H}_2\text{O}$ in conc. HNO_3 (65%) was prepared. Concentrated water solution of KOH was added to a solution of $\text{Ce}(\text{SO}_4)_2 \cdot 4\text{H}_2\text{O}$ in water. $\text{Ce}(\text{OH})_4$ precipitates were filtered, washed thoroughly with water to get rid of remanent sulphate and dried at a temperature of 110°C in an oven. At this temperature and after several hours' drying process the Ce(IV) -hydroxide changes to $\text{CeO}_2 \cdot 0.5\text{H}_2\text{O}$. Compared to the CeO_2 , completely free from water, which

was obtained at drying temperatures above 325°C, the $\text{CeO}_2 \cdot 0.5\text{H}_2\text{O}$ was soluble in conc. HNO_3 (65%).

The concentrated cerium oxide solution in conc. HNO_3 (65%) was obtained by dissolving $\text{CeO}_2 \cdot 0.5\text{H}_2\text{O}$ in conc. HNO_3 (65%) till a saturated solution resulted. It was then distilled to reduce its water content. The distillation was carried on till an azeotropic mixture of water and nitric acid was obtained in the vapour phase. The solution was filtered after cooling to room temperature to get rid of precipitated substances which were mainly hydrated Ce(IV)nitrates with orange-reddish colour. The concentration of Ce(IV) in the solution was not determined experimentally but has been reported by Eickhoff [E 93] to lie generally above 200mg per millilitre.

For the preparation of cerium (IV)nitrate - graphite intercalation compound, 2g of graphite were inserted in a 250ml round bottom flask, equipped with reflux cooler, and containing 100ml of the cerium(IV)-nitric acid solution. The reaction mixture, under constant stirring at a slow rate, was refluxed on oil bath at a temperature of 110°C for a period of 2 hours. The reaction product was filtered, washed very fast with diluted nitric acid solution and rinsed with acetone. The structure of the prepared intercalation compound was investigated using both X-ray diffraction and fluorescence methods of analysis.

Characterisation

X – ray diffraction measurement

The registration of (00l) diagrams was made with a counter diffractometer (Philips PW 1050) using monochromatic Cu-K α radiation (35kV, 36mA & $\lambda = 154.2$ pm). Between 8 and 10 flocks were placed on aluminium holder and adjusted in such a manner that their rotation axis as set out by the goniometer was always perpendicular to the c-axis. There was always a fixed relation of $\theta:2\theta$ (1:2) where θ and 2θ are the angles at which the flock rotates and the glancing angle as defined by the Bragg's equation. This geometric arrangement ensures only the measurement of the 00l reflections of the intercalate and the underlying graphite layers.

In order to interpret the obtained x-ray diffraction diagrams reference is made to the works done by Metz and Hohlwein [Hoh 72,MH 75] on the effect of disorder as observed in the investigation of FeCl_3 intercalation compounds.

Stumpp [Stu 60,Stu 67] also provides literature values for *repeat distances*, c_n , along the c-axis which allow one to calculate the position of the 00l reflections for a pure stage intercalation compound. The repeat distance, c_n , of an n^{th} stage intercalation compound is defined as the distance between two intercalated layers, assuming a pure stage formation.

Fig. 3.8 offers a few examples of c_n s which are just the lengths of layer packages measured along the c-axis.

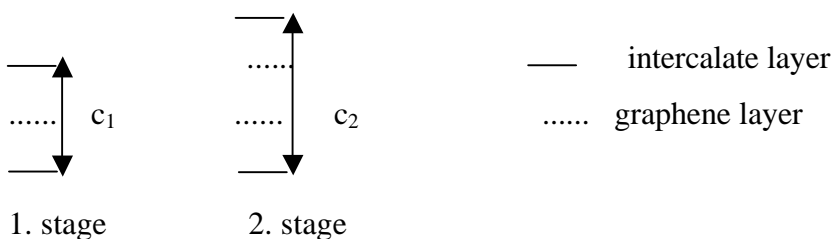


Fig. 3.8: 1st and 2nd stage graphite intercalation compounds.

Knowing c_1 one can evaluate the positions of the 00l reflections of the n^{th} stage compounds using the following equation:

$$d_{00l} = 1/l ((c_1 + (n-1) \cdot 335 \text{ pm}))$$

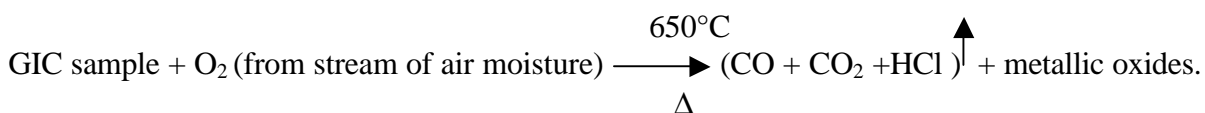
d_{00l} indicates the interplanar distance as used in Bragg's equation. l is the Bragg's order of reflection and takes the values of 1, 2 ... , n is the stage number of the compound. The distance requirement for one graphene layer is 335pm.

Gravimetric measurements to determine the contents of intercalates in the GICs.

The compositions of the intercalated substances in the GICs were obtained by completely burning out the GIC samples to obtain the intercalates in form of their metallic oxides. From the

amount of oxides obtained as residue after burning, the quantity of the converted intercalated substances in the samples can be evaluated.

A schematic diagram for the conversion of GIC to its metallic oxides can be presented as following:



In the case of cerium (IV) nitrate - graphite intercalation compounds CeO_2 is obtained as residue and carbonated as well as nitrogenous products as exhaust.

Generally 100 to 120 mg of the GIC samples were weighed and placed in a porcelain bowl of a known weight, the weight of the porcelain bowl taken after being heated in an oven at the reaction temperature for one hour and letting it cool down to room temperature.

The porcelain bowl with its contents was placed in an oven and heated to 650°C . A gently stream of air moisture was passed through the sample while being heated. Depending upon the chemical constituents of the GIC the complete conversion to the metallic oxides was over within a period of 30 minutes to one hour. The end of reaction is indicated when a colourless air moisture emerges out of the reaction chamber. In the case of the metal chloride GICs, the outgoing air moisture stream is marred by the yellowish colour of the Cl_2 and HCl reaction products. The characteristic colours of the residue corresponding to the metallic oxides also give indication of the end of the reaction.

3.2.2 Exfoliation of GICs and characterisation of the products

As already mentioned in section (2.5) the exfoliation follows the sublimation or vaporisation of the intercalate. This has been observed in the thermal treatment of Br_2 -GICs [Thi 32, MB 64, AC84, Chu 87]. The decomposition of intercalate into gaseous products of larger volume can also result in exfoliation. For instance, in the case of FeCl_3 -GIC, the decomposition of FeCl_3 into FeCl_2 and Cl_2 takes place above 315°C . The pressure exerted by the evolving gaseous metal

chloride and chlorine causes the exfoliation of the GIC. With this background, the exfoliation of the prepared graphite intercalation compounds was carried out in the following way :

A porcelain vessel is weighed and placed in a cylindrical quartz glass tube, which is then inserted in an oven as shown in Fig. 3.9.

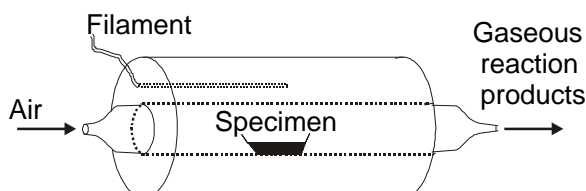


Fig . 3.9: Exfoliation apparatus

Air current (5l/h) is directed through the quartz glass tube to get rid of the gaseous dissociation products and also to convert the chlorides into oxides as in the case of the metal chloride intercalation compounds. The oven is then heated to 700°C, the temperature set for the exfoliation. At the exfoliation temperature the air current is interrupted, the quartz glass tube containing the porcelain vessel quickly removed from the oven and a weighed amount of the graphite intercalation compound is placed in the porcelain vessel. The quartz glass tube with its contents is placed in the oven and the air current is reconnected. Generally it takes two to three minutes for the exfoliation temperature to be established again. The system is then held at this temperature for about three minutes when no visible discharge of the gaseous products is observed. In the case of graphite $\text{FeCl}_3/\text{CuCl}_2$ intercalation compound, tens minutes' time was allocated for the exfoliation because of its resistance to disintegration.

The quartz glass tube with its contents is then taken out and quickly cooled down to room temperature by means of compressed air and the porcelain vessel with its content is weighed to determine the loss in weight of the product. The product is then analysed using X-ray diffraction, fluorescence and gravimetric methods. Some of the products were also analysed using x-ray absorption spectroscopy .

3.3 Determination of Catalyst Activity

3.3.1 Instrumentation in Determination of Catalytic Activity

The catalytic properties of the prepared samples were verified not only by carrying out CO oxidation, but also NO decomposition and CO – NO oxidation-reduction catalytic reactions on each of them. The GC analyses of the reactants as well as the products of these chemical reactions were made in all cases of the prepared catalysts investigated. The concentrations of the reactants and products, at the set experimental conditions, were measured and the reaction rates, reaction orders and the activation energies of the various reactions, under the experimental or reaction conditions were then evaluated.

The temperature of a catalyst, at which maximum turnover is observed, is generally dependent on the preparation methods of the catalyst, the composition of the catalytically active substances in the catalyst and the manner the reaction is carried out.

Keeping the chemical composition of a particular catalyst system constant, one can obtain the maximum turnover at a specific temperature by varying the following parameters or factors:

- the catalyst supporting material (e.g. Al_2O_3 , graphite, zeolite etc.)
- the amount of load or its compositional relations
- the manner the catalyst is prepared (e.g. preparation temperature)
- the reaction parameters such as composition of reaction gas mixture, the flow rate and the concentration of the individual gas components, etc.

In our investigation, great emphasis was laid on the catalytic effect of the metal oxide or mixture of metal oxides on graphite support as compared with that in a free state (unsupported), or rather as a mixture with graphite. Various samples were tested, and mainly the reaction parameters were varied

The main components of the apparatus used in the determination of the catalytic activity were the gas cylinders containing the reaction gas or gas mixture serving as the test gas, the fixed bed reactor – a cylindrical glass vessel containing the catalyst sample to be investigated, a gas

chromatograph equipped with a CTRI column from firm ALLTECH, a thermal conductivity detector (TCD) and an analogue-digital converter connected to a computer (Fig. 3.10).

A CTR 1 column supplied by ALLTECH was used in the separation of the reaction gas mixtures. CTR is an indication by ALLTECH for a series of columns, with several benefits, used in solving difficult analytical problems. It consists essentially of one column in another. This enables the use of two different column packages or materials in the analysis of samples. For example, using molecular sieve alone in the separation of CO, O₂, N₂ and CO₂ gas mixture is not possible. Carbon monoxide, oxygen and nitrogen can be separated but the carbon dioxide gets adsorbed irreversibly. On the other hand porous polymer and silica gel, which are used in the separation of carbon dioxide from the other components, are not in a position to isolate the carbon monoxide at room temperature from the overall air peak. To separate this gas mixture, CTR 1 column, embodying molecular sieve and porous polymer mixture in its outer and inner concentric columns respectively, is employed. This column enables the separation to be achieved in one working operation and within ten minutes time.

In the gas chromatographic analyses of the reactants or products in the CO oxidation reactions, calibration gas mixture composed of 15% CO₂, 7% CO, 7% O₂, 4.5% CH₄ and 66.5% N₂ was used as standard. After separation of reactants (bypass) or products (test) the peak areas corresponding to all the components in the reaction mixture in the registered gas chromatogram were recorded. Four gas chromatographic analyses of different amounts of the calibration gas mixture were also run. From the amount of calibration gas analysed the concentrations of the various gas components were determined. The concentration per unit peak area was calculated for each component. The concentration of each gas component in the reactants or products was evaluated by converting its peak area units into concentration units, using its corresponding concentration per unit area as found in the calibration gas measurements.

A mixture of NO, O₂ and CO could also be separated using the CTR 1 column. To determine the concentration of nitric oxide in the reaction mixture, different composition mixtures of nitric oxide and oxygen – always keeping the composition of O₂ above that of NO – were separated on the column and the constituent gases were analysed by means of gas chromatographic methods as outlined under the CO oxidation. With excess oxygen in the gas mixture, a complete conversion

of nitric oxide into other nitrogenous products was achieved. The subsequent decomposition of these products into nitrogen was achieved. This was observed as nitrogen in the gas chromatographic diagram. The peak area of the nitrogen formed was converted into concentration units. The converted nitric oxide could be deduced from the nitrogen formed in the reaction.

Three different types of reactions, namely CO oxidation, NO decomposition, and CO/NO redox reactions were investigated in each case of a prepared catalyst sample. A slight modification in the experimental set up was made, where it was found necessary. For example, in the case of CO oxidation, where a mixture of CO in He gas and synthetic air, (N_2 and O_2) in He were brought together to react on the catalyst sample at a preset reaction temperature, the CO and He and the synthetic air & He gas mixtures stored previously in separate gas cylinders, were directed independently through fine valves and the rates of gas flow were measured with flow meters F_1 and F_2 connected directly to the valves. After leaving the flow meters, the gas mixtures were brought together. The ensuing reaction gas mixture was then made to split into two parts, each taking a separate course, one via a pinhole valve connected to flow meter F_3 and the other via another pinhole valve connected to flow meter F_4 . After leaving these two flow meters, the gas mixtures, which have been regulated to have the same concentrations of the constituent gases, are then directed to the two reaction chambers embedded in the oven as shown in Fig. 3.10.

A known amount of catalyst sample is placed in the fixed bed reactor, designated in the figure as the test reactor. In the other (bypass) is the so-called blank sample. The blank was either a known amount of raw graphite or a mixture of graphite and CuO equal in weight and in the same proportion as that in the test reactor. The blank sample served only as a base for the measurement of the catalytic activity. The equilibrium temperature of the two reactor chambers was taken as that of the oven temperature. After passing through the reactor chambers at the preset reaction temperature, the reaction gas mixture from the test reactor is made to pass through a bottle for a collection of any eventual shed-outs from the test reactor. The test gas and the blank are then alternately directed by means of a switch to a loop for eventual GC analyses or to the gas chimney. The alternate switching of the Test and Blank gas mixture to the loop enables an independent analysis of the two gas mixtures at the same reaction conditions.

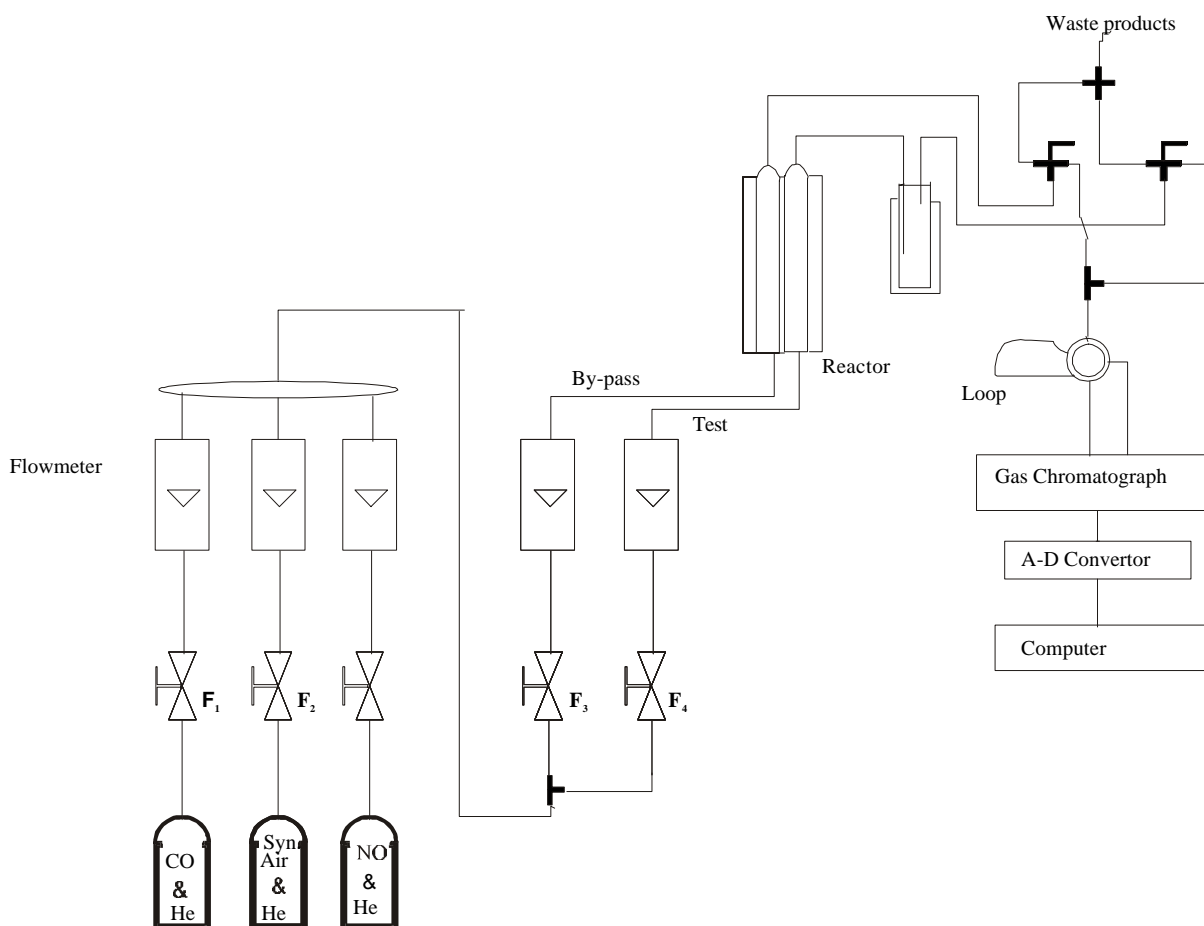


Fig. 3.10: Apparatus for the determination of catalytic activity

The oven with its contents, the reactor chambers, and the bottle, as well as the metal loop for storing the gas mixture prior to GC analysis are all housed in a stainless steel compartment with a transparent door made up of polycarbonate plastic material. A suction pump coupled to the compartment sucks the exhaust gas to the gas chimney.

The reactor chamber, the flow meter tubes and the thermostat devices were all made up of glass. The gas tubes and their joints, the valves and the loop for storing the gas mixture were all made up of stainless steel. Where necessary, especially where glass and metal joints are involved, Teflon was used for the fitting or as seal to ensure lack of leakage. The oven temperature, which is also the temperature of the reactor chambers, is controlled outside the steel vessel by a two-point switch (BITRIC). Iron - constantane thermo-element or filament was used in the determination of the oven temperature. The setup used in the CO oxidation was also used in the

CO/NO reduction-oxidation reaction. In place of the synthetic air NO in He was used. In the case of NO decomposition reaction the flow meters F_1 and F_2 and their corresponding valves were shut down completely and a direct connection of the reaction gas mixture, NO in He, to F_3 and F_4 via their corresponding valves as shown in the diagram was made.

Temperature of reactor and the catalyst substances

After inserting an empty reactor in the oven, the thermostat was set at the required temperature. The oven was heated up till an equilibrium temperature, which was measured by means of a thermoelement placed in the reactor, was reached. This was recorded after observing no further changes in the registered voltage after thirty minutes. The voltage, the correspondingly expected temperature, and the measured temperature were recorded. Plots of voltage against the fixed and measured temperatures are shown in Fig.3.11. The deviation of the expected temperature from the measured temperature can be inferred from the figure.

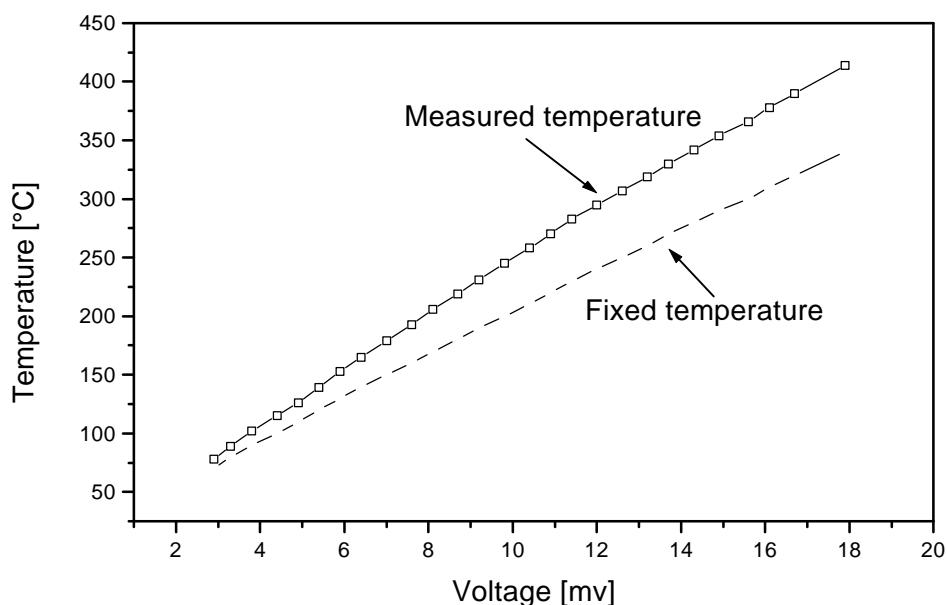


Fig.3.11 : Relation of fixed and measured temperatures with the recorded voltage.

Dead time

The dead time is the time that the reaction gas mixture takes from the storage tank to the switch at the entrance of the metal loop storing the reaction gas pending analysis with GC. Before beginning with every measurement, the dead time at the set flow rate and the corresponding reactant concentration(s) is measured. It is dependent mainly on the flow rate, the volume of the reactor as well as the length of the connecting tubes. No dependency of the dead time on the concentration of the reactants – within the measured range – is observed. The variation of the dead time with flow rate is measured by employing the By-pass lead, which is identically the same as the reactor lead, in consideration of its volume and the length of the connecting tubes. Keeping all other factors constant, the relation of dead time to flow rate found is as given in Fig.3.12.

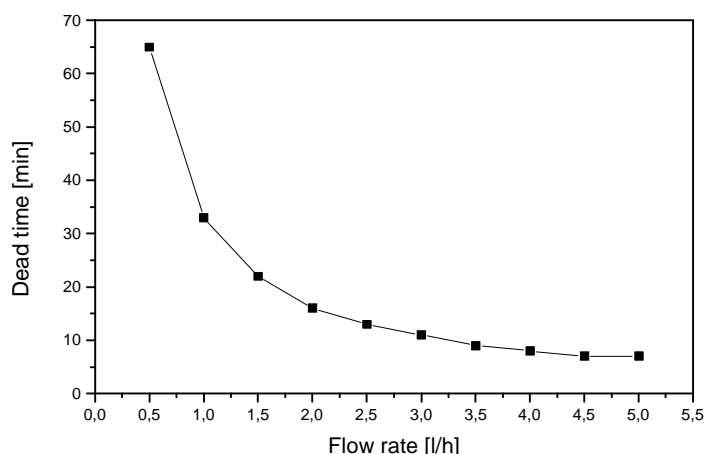


Fig.3.12 : Relation of dead time with flow rate

3.3.2 Measuring procedure

To assess the catalytic activities of the prepared samples it was necessary to find kinetic data such as reaction rate, rate constant, and activation energy under the measured reaction conditions. The extent of reaction reached in the CO Oxidation as well as in the in the CO/NO reduction-oxidation reaction was defined as the amount of CO consumed as compared to the initial concentration of the CO inserted in the reaction. The extent of reaction in the reduction-oxidation and in the NO decomposition could also be defined in terms of NO consumed in relation to the initial concentration of NO inserted in the reaction. As turned out in the investigation the total N_2

produced corresponded to NO consumed. The extent of reaction was therefore based on N₂ produced, N₂ being easier to trace and also to measure using the GC method of analysis. In all the reactions investigated the amount of relevant substances (CO, N₂) consumed or produced after reaction on the catalyst sample was separated and measured by means of gas chromatography.

The reaction test gas or gas mixture, after passing through the reactor chamber at the set temperature, was directed to a metal loop of known volume (0.5 and 10ml). The trapped gas mixture was then analysed by means of GC of the firm HEWLETT-PACKARD, identification number HP 5750. The separation of the gas mixture was made over CTR I column and the detection of the components with TCD of the GC. The results were recorded after a steady state had been achieved, that is after repeated measurement of a component at the investigated temperature was observed to be constant. To enable easy but accurate evaluation of the detected substances an Analogue-Digital (AD) converter of the firm ISSENDORF [P88] was used. The converter, connected to the GC outlet to printer and also to ATARI 1040 ST computer at its ROM-Port (with ROM-Port -Buffer, [Mey 87]), as its name implies, serves to convert the electric impulse, the analogue signal received at the printer out to a digital signal which is then passed on to the computer for ultimate evaluation. The AD converter, previously modified [E 93] to take readings only on the positive range, instead of the originally constructed measurement range of -5V to +5V and also to enable the amplification of the entering signal by factors of 1, 10, 100, 200 and 500, was used without further alteration.

A special GFA-Basic program, developed by H.P Eickhoff of our working group for the ATARI computer (Lit. 30) was used for the measurement, evaluation and storage of data values as well as for the presentation of the chromatographic diagrams. The GFA-Basic program, ADW-Version 2.36 enabled the registration of 12,000 pairs of data values per analysis. The capability of the program can well be appreciated by noting that a maximum of 10 data values per second is considered reasonable for the registration of a GC-Diagram. The evaluation of the data values, which is basically the evaluation of the areas under the chromatographic diagrams were performed with a program developed by T. Ressler [Re 95], also a former co-worker in our group. A table calculation program, Power Calc, was used to evaluate the measured areas under the curves or diagrams in terms of the number of moles of the measured reaction gases. To achieve that, a gas mixture comprising all the gases under consideration and with the

concentration of all individual gases known, was used as standard. It was supplied by the firm ALL TECH. This standard gas mixture was also run on the GC, evaluated with the ATARI computer with the aid of the AD-Converter.

Knowing the concentrations of the gases in the mixture, the volume of gas mixture inserted, the areas under the curves corresponding to the individual gases were evaluated. Taking these area values as our bases for the calculation of the mole values, we could evaluate the number of moles of the individual gases in the reaction mixture before and after passing through the reactor chambers. In all, 4 different measurements, and therefore 4 different chromatograms, were run for every reaction investigated at given experimental conditions. The 4 are the measurements of the standard gas mixture, the two reaction gas mixtures after leaving the reactor chambers containing the catalyst sample and blank, and the reaction gas mixture after passing through an empty reactor chamber at the given experimental conditions. For the analysis of a reaction mixture several GC-Diagrams-are registered and evaluated. The number of registrations depended on how long it took to achieve a steady state for the reaction. The steady state was achieved when a repeated constant value was measured for the reaction gas in question at the experimental conditions. After taking the dead time into consideration, 10 minutes' time intervals were given for every subsequent registration or measurement of GC data.

The course of CO oxidation could be followed by means of gas chromatographic measurements. The reactants and products, made up of CO, O₂ and CO₂, were separated as already mentioned, by employing CTR 1 column supplied by ALLTECH. NO decomposition could also be traced by analysing the N₂ formed in the course of the reaction. The CO – NO redox reaction was followed just as explained in the CO oxidation and NO decomposition reactions.

As already mentioned an ATARI-computer is used for the registration of the data, and it is therefore a necessity to know the basic operational functions of ATARI ST – series such as for example answering the dialogue box, which implies a knowledge of the special usage of the “mouse”.

After starting the program, the program logo appears, allowing an optional possibility of entering the date, which then appears on the analytic protocols. The offset time is then given, if found necessary. This time is very necessary, for example, in performing kinetic investigation. In an

analysis, where the registration of the first test is done, after allowing, for example, 5 minutes for chemical reaction to take place, this time is given as offset time. It is then considered in the registration time, the time set for analysis, in all the subsequent tests. This registration time is automatically taken as the time point of sample dispatch and of diagram registration start point.

The choice of **GC – AD** enables the registration of the GC diagram. A list of parameters appears, which can be called in by giving the corresponding number on the left edge of the diagram shown in the Fig.3.13.

1	Value is given (0 for –5V):	0 AD-Canal (0 – 3) : 0
2	Interval time in 1/10 sec:	2 ADW-Amplifier : 200
3	Offset time after injection in [s] given:	0
4	Running time in [min] given	10
5	Sample (max. 30 letters):	
6	Column (max. 30 letters):	
7	Detector (max. 5 letters): FID	
8	Working method Dual	
9	Scope (around 1 g):	2
10	Attenuation:	1
11	T (oven) [grd C]:	0
12	T (Det.) [grd C]:	0
13	T (Inj. Port) [grd C]:	0
14	Gas : Air [bar] :	0
	Hydrogen [bar]:	0
	Nitrogen [bar] / [Skt]:	0/0
	Helium [bar] / [Skt]:	0/25
15	Commentary (max. 30 letters): Test	

Shall parameter be changed (no change: 0)? ☐

Fig.3.13 : Parameter setting for the running of a GC - analysis

The parameters given under numbers 1, 2, 3, 4 9, and 10 were used in data evaluation whilst the rest were mainly of informative character covering the sample and the analytical conditions. The

parameters were stored in the parameter data (*.DA0). After taking the data, only the commentary (number 15) in the evaluation file can be changed.

After calling in number 1, three instructions are expected:

- A hexadecimal value is given to set an opposed voltage on the AD converter (0 for –5V, 800 for 0V and F00 for +5V). In order to make use of the whole measuring area of the 12-Bit AD converter, for the reasons already given in this section, an opposed voltage of –5V must be set.
- The data registration, as a rule, is performed over the AD-canal 0; this parameter therefore is kept unchanged.

The amplification setting of the AD-converter's amplifier should always be updated, to enable later comparisons of various diagrams registered with different amplification.

Number 3, the offset time, enables us to do away with data registration for this period, after starting the analysis. This helps us save information storage place and should not be taken as the offset time already discussed. The diagram registration therefore begins, after starting the analysis, with delay corresponding to the set offset time (in seconds).

The running time, number 4, gives the time from the start of the analysis to the end of data registration.

The other indicated numbers and their corresponding parameters are selfexplanatory. One quits the file after giving the number 0.

One is then called upon to inject the sample and at the same time with RETURN the data registration to begin. The current measuring points are then displayed in the diagram mask. At the same time, the current number of measuring points, the current run time and a value of the intensity of the measuring points are displayed.

The relevant information for the GC-analysis and the sample appear in the heading of the diagram. The data registration can be interrupted, by pressing a key on the keyboard. One has then the possibility of continuing with the data registration, the evaluation and saving of already gathered data, or directly a new analysis to begin.

Storage of data, diagrams and results

At the end of data registration, one has the possibility of saving the data by selecting EDIT, which delivers a dialogue box, as shown in Fig3.14, on the right side of the monitor. As a rule parameter data (*.DA0) and data file (*.DA1) are set up. The T is automatically replaced upon choosing number 1 and giving a name ending with DAT in the selection box. To be able to do the data evaluation using other evaluation programs, the data is split into 800 data points (*.DA1, *.DA2, etc.) and one chooses the number 2 in the data selection box and give a name with ending DAT.

After the data storage, a new run of the analysis can begin (number 0), or the data stored can be evaluated (number3). Number 4 and 5 can be called in after the evaluation of the diagram.

Number 4, the storage of results, offers the possibility of storing the date, description of the sample, the time of taking or injecting the sample, the peak number and the peak area (*.DAT).

After selecting number 5, the storage capability of the disk is checked. If enough storage place is available, the current diagram including the evaluated results are stored as 32kB-Picture (*.PIC).

With the zero and upon activation of the field DATA of the following dialogue box, one can begin a new data collection, else the program, can be closed with END.

Evaluation of a diagram

The current diagram appears on the right side of the monitor after the selection of the evaluation file (Fig.3.15). Number 5, corresponding to the evaluation, must be selected in this case. To reduce statistical raucousness, the data undergoes a5-point smoothing (number 3).

Quit, Data Registration
Give 0 !

Save Data

1 All

2 800 D.P./Dat.

3 Diagram
evaluation

Diagram / Results
Save

4 Save Results

5 32000 kB -
Picture

Which performance is
required?
■

Fig.3.14 : Dialogue box
“Save”

The choice of number 4, the base line, enables us, in case of high base line intensity, to reduce it to about 2% of its value. With the help of the mouse, 2 broad lines are chosen to give a sinful base line region. Here, only the x-position of the cursor is decisive. The left key of the mouse is pressed; by pressing the right mouse key, one gets back to the evaluation file.

The calling in of the spike elimination, number 6, leads to the sub file, which enables us to perform automatic as well as manual correction of “deviating values”. The automatic correction takes the average values of all 2 neighbouring data points over the whole measured region.

In cases where single values exceed the average value by a certain factor, the second value is equated to the first value. A corrected value is marked by a line parallel to the y – axis and cutting the x – axis. Maximum of 3 neighbouring values can be identified as spikes and corrected. The fourth value remains unchanged, while the following values are checked and if necessary corrected under the same condition. Finally, the number of corrected values, is indicated.

1	Standard evaluation
2	Original diagram
<hr/>	
3	Curve smoothing
4	Base line
5	Evaluation
6	Spike removal
7	Area y – axis
8	Hard copy
<hr/>	
9	Help
0	Data, Diagram save and quit

Which performance is required?
■

Quit, Data Registration
Give 0 !

Fig.3.15: Dialogue box
“Evaluation”

The selection of area y – axis, number 7, enables us to equate the highest peak to 100%. Where the base line correction has not been previously done, it is carried out automatically.

The selection of number 5 enables us to determine or calculate the retention time and the area under the peak. The calculation of the chromatogram (number 1 in this subfile) demands setting up boundaries for the peak to be analysed. This is done by using the left mouse key. The minimum values lying between the boarder lines and the peak are automatically sought out and the boarder lines are set at these positions. The average values of every five neighbouring points within the boarder lines are taken. They are added together and the background area (area under the line connecting the two boarder lines) is then subtracted. The result is then multiplied with the TCD units of the measuring region set at the GC and the attenuation factor. The outcome is then divided by the product of the amplification set at the AD converter and the number of

measurements made in seconds. Finally, the obtained value, is divided by 100, to account for easy handling or normalisation after setting the maximum peak to 100% as stated above. The evaluated peaks are then marked and indicated with numbers by means of the mouse. The left key of the mouse is held pressed down and the cursor brackets shifted. After all peaks, maximum of 30, have been evaluated, the right mouse key is operated. The cursor, in the form of a hand, appears. With the left mouse key pressed, a rectangle displaying the results, can be placed in the diagram.

Number 2, the analysis of a time dependent sample (its constituents' concentrations vary with time), permits the tracing of a reaction, for example by following the increase or decrease of a reaction partner in the course of time.

The evaluation of further diagrams in the course of the analysis, based on the same retention time, follows the choice of number 2 in the evaluation file automatically. The results are stored in the data file containing the results of the first analysis. All the results obtained in the course of the analysis can then be further treated using a table calculation program.

4 Results: Characterisation of Graphite Intercalation Compounds (GICs) and Exfoliated Products.

4.1 Characterisation of the $\text{AlCl}_3/\text{CuCl}_2$ – GICs and the Exfoliated Products.

X – ray diffraction, fluorescence, absorption spectroscopy and BET specific surface area determination methods of instrumental analyses were employed in the characterisation of the GICs and the exfoliated products. Density determination was also carried out on the exfoliated specimen. The results obtained in the ash analyses for the GICs were also used in ascertaining the chemical composition of the GICs. In such cases, total conversion of the intercalated compounds into metal oxides was undertaken.

X – ray diffraction analysis

In all cases of the intercalation compounds prepared in this work nearly pure stage compounds were obtained and typical examples of their X – ray diffraction diagrams as well as their d_{001} -values are given below. In Fig.4.1 and Tab.4.1 are the X – ray diffraction diagrams of investigated $\text{AlCl}_3/\text{CuCl}_2$ – GICs, and the d_{001} -values evaluated from the positions of the reflections respectively.

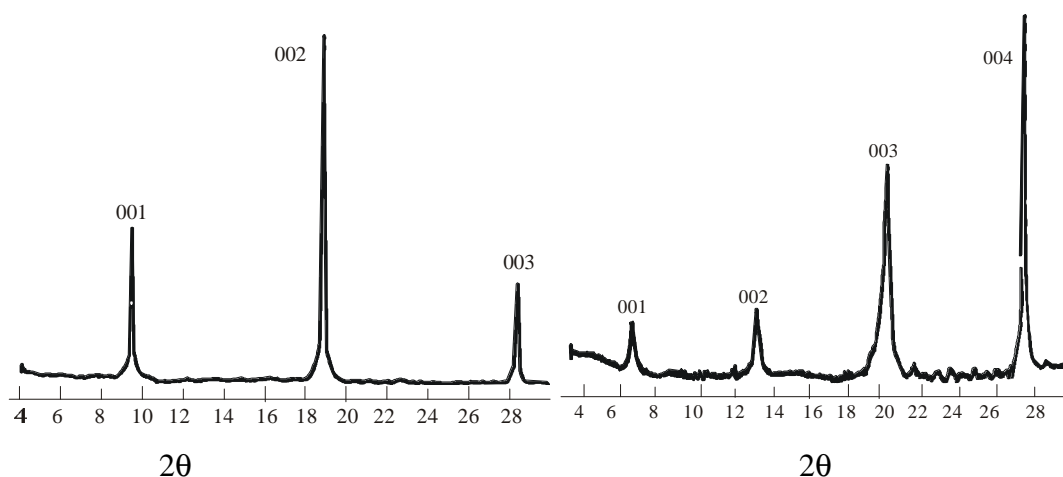


Fig.4.1: 1st and 2nd stage X-ray diffraction diagrams of $\text{AlCl}_3/\text{CuCl}_2$ GICs

Table 4.1: $d_{00\lambda}$ – values and the reflection peak positions (shown in brackets) for Cu-K α radiation ($\lambda = 154.2\text{pm}$) for the investigated $\text{AlCl}_3/\text{CuCl}_2$ GICs. The $d_{00\lambda}$ -values are given in pm and the angles (2θ) are measured in degrees.

$\text{AlCl}_3/\text{CuCl}_2$	001	002	003	004

1 st Stage	940 (9.41)	470 (18.88)	313 (28.49)	
2 nd Stage	1275 (6.93)	638 (13.89)	425 (20.90)	319 (27.79)

Gravimetric measurements (ash analyses)

To determine the intercalate content in a prepared GIC, the GIC was first dried in exsiccator over P_2O_5 . It was then weighed and the increase in weight of the inserted graphite determined. The oxides of the compounds intercalated are stable. For crude determination of the intercalate composition in the GIC, the GICs were burnt to ashes and the metal oxide residue measured. The results of the analyses are presented in Tab.4.2 and 4.3.

Table 4.2: Content of intercalate compound in the prepared GICs, expressed as % of the weight of GIC analysed.

GIC	Stage	Intercalate (weight %)

$\text{AlCl}_3/\text{CuCl}_2$	1	70.3
	2	53.5

Table 4.3: Results of total metal oxide composition in the GIC, expressed as % of the weight of GIC analysed.

GIC	Stage	Total oxides (weight %)

$\text{AlCl}_3/\text{CuCl}_2$	1	40.8
	2	31.2

X-ray fluorescence analysis

X – ray fluorescence measurements were carried on $\text{AlCl}_3/\text{CuCl}_2$ - GIC, to determine the Cu composition. Standard samples, composed of graphite, boric acid, ZnO and CuO, were prepared. Constant amounts of graphite (2mg) and boric acid (130mg) were put in each prepared sample. The mole proportions of the prepared standards are around 1:1, 1:2, 1:3, up to 1:10 (CuO : ZnO). Weighed amounts of the compounds in these proportions are ground in a mortar with a pestle for a period of about 10minutes, after which 4 to 6 X – ray fluorescence measurements are repeatedly made on each sample. A plot of the intensity relations, corresponding to the ratios of the radiation count rates ($\text{Cu-K}_\alpha / \text{Zn-K}_\alpha$), against the molar ratios ($n_{\text{CuO}} / n_{\text{ZnO}}$) was made. Fig. 4.2 shows the standard curve and the results obtained are provided in Tab. 4.4.

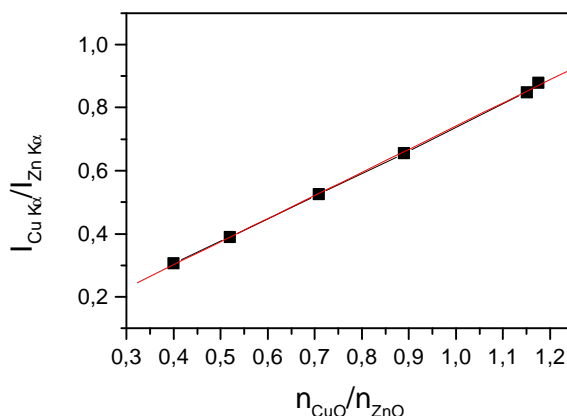


Fig.4.2: Cu and Zn intensity ratio (K_α radiation)
as a function of their mole ratio

Table 4.4: Cu content in $\text{AlCl}_3/\text{CuCl}_2$ GICs obtained from X-ray fluorescence analysis.

GICs	Stage	Cu Content (%)
<hr/>		
$\text{AlCl}_3/\text{CuCl}_2$	1	32,1
	2	24,3

X - ray absorption measurements

The absorption spectra of a mixture of pristine CuCl_2 and graphite, and of the $\text{AlCl}_3 / \text{CuCl}_2$ GIC, after being heated in air for 20 minutes at 700° , are given in Fig.4.3.

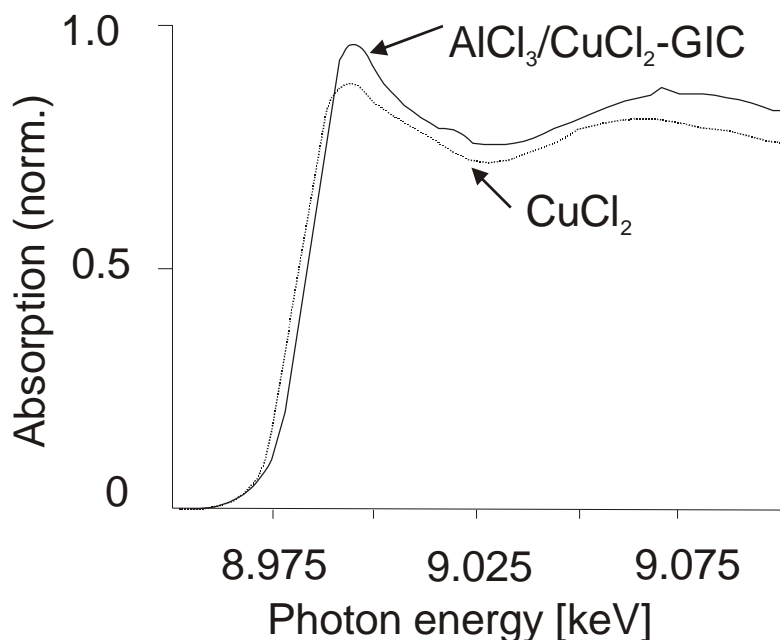


Fig. 4.3: X-ray absorption spectra (CuK edge) of exfoliated $\text{AlCl}_3 / \text{CuCl}_2$ GIC and of a correspondingly treated mixture of pristine CuCl_2 and graphite.

The position of the Cu-K absorption edge in exfoliated $\text{AlCl}_3 / \text{CuCl}_2$ GIC is shifted towards higher energy in comparison to pristine CuCl_2 (or the product CuO , respectively). This effect can be interpreted as consequence of the charge transfer to graphite, which must be expected in the formation of acceptor type GICs.

The EXAFS function $\chi(k)$ with k ranging from $k = 0.019$ to 0.095 pm^{-1} was weighted with k^2 and multiplied by a Bessel window function and Fourier-transformed into R space to obtain the radial distribution function. The main coordination shell in the FT was back transformed. The Fourier transform of the exfoliated product and the standard are shown in Fig.4.4. The back transform and the EXAFS fit are shown in Fig 4.5.

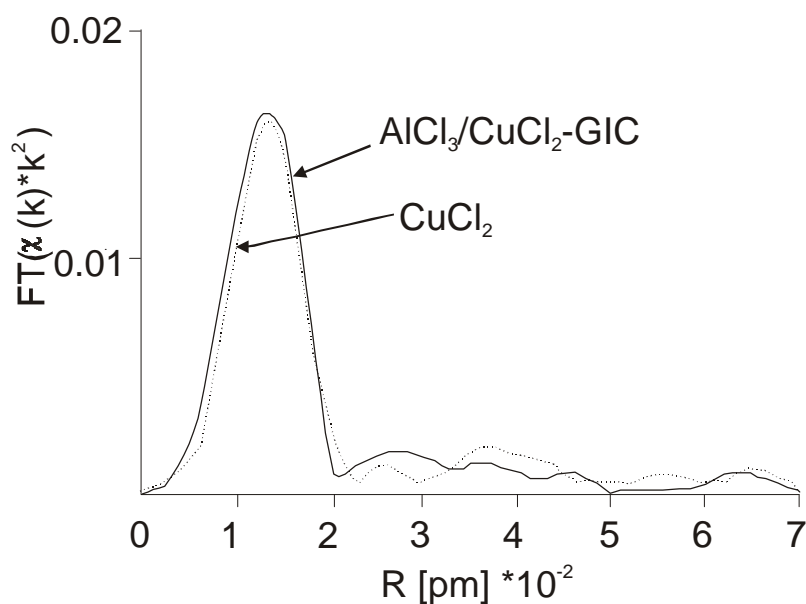


Fig. 4.4: The Fourier transformed $\chi(k)$ of exfoliated $\text{AlCl}_3 / \text{CuCl}_2$ GIC and of a correspondingly treated mixture of CuCl_2 and graphite. ($k = 0.019$ to 0.095 pm^{-1})

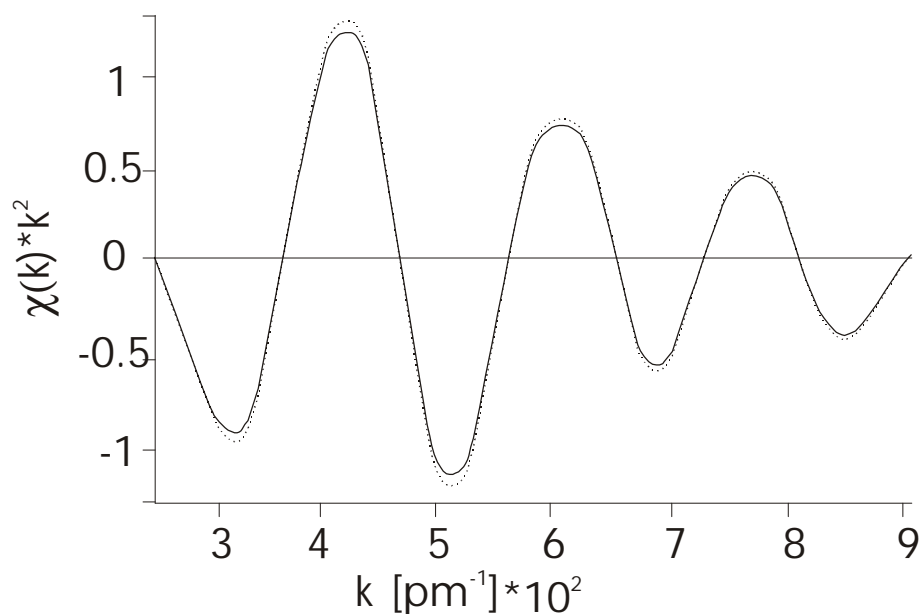


Fig. 4.5: Back transform of exfoliated $\text{AlCl}_3 / \text{CuCl}_2$ GIC (.....) and EXAFS Fit (____) derived from phase and amplitude functions obtained by measurement of a standard Cu – O coordinated compound. $\text{FT}(1.9 - 9.5) * 10^{-2} \text{ pm}^{-1}$ Back transform 70 – 245 pm

The exfoliated $\text{AlCl}_3 / \text{CuCl}_2$ GIC resembles the oxygen treated product obtained from CuCl_2 . In both cases CuO is obtained and no appreciable Cu(I) and Cu(0) products are obtained

The parameters of the fit – the coordination number of the ensuing copper oxide after the exfoliation and the Cu- O distance of the first coordination shell – are presented in Tab. 4.11 together with the results obtained for the exfoliated product of $\text{FeCl}_3 / \text{CuCl}_2$ – GIC. For comparison purposes, the results obtained for measurements made on Cu_2O and CuO are also presented.

A further discussion of the results is given in section 4.2 in order to compare them with the corresponding results obtained from $\text{FeCl}_3/\text{CuCl}_2$ GIC

Changes in mass, density, and specific surface area

In this work the exfoliation is done at high temperature and geared to correspond to the end of region 4 and the beginning of region 5 of Eickhoff's exfoliation diagram as shown in Fig.2.4. In all cases the exfoliation temperatures are above the decomposition or the vaporisation temperature of the intercalated substances. The exfoliation temperature is also the oven temperature, making it possible to follow the exfoliation process at a constant temperature. As can be inferred from the exfoliation procedure described in section 3.2.2, the temperature at which the exfoliation is performed is equal to the measured equilibrium temperature of the oven and its contents, i.e. the quartz glass tube and the porcelain bowl. Prior to inserting the sample in the porcelain bowl, the 'oven-quartz glass-porcelain system' is heated to the so-called exfoliation temperature. It is to be noted here that the mass of the sample exfoliated at a time is negligibly small in comparison to that of the system, and the change in temperature occurring after inserting the sample is consequently negligible as confirmed by temperature measurements after sample insertion. Time dependency of the exfoliation process, in which loss of mass, density changes and specific surface area variations take place at a constant temperature, is carried out in this work. The results of the experiment for the various series of measurement on the exfoliated products are presented taking the temperature as a constant and time as variable.

Table 4.5 and Fig.4.6 and 7 provide a summary of the results of the exfoliation experiment for the prepared GICs. The exfoliation temperature $T_{\text{exf.}}$, exfoliation time $t_{\text{exf.}}$, the stage number of GIC prior to exfoliation, the loss in mass of GIC Δm , the density ρ , and the specific surface area S of the exfoliated products are presented.

Table 4.5: Results of the exfoliation experiment with $\text{AlCl}_3/\text{CuCl}_2$ -graphite

Stage number	$T_{\text{exf.}}(^{\circ}\text{C})$	t (min)	Δm (%)	ρ	S
1	700	1	10	1.2	28
1	700	2	12	1.63	30
1	700	3	15	1.93	40
1	700	4	20	2.08	58
1	700	5	25	2.2	66
1	700	6	29	2.29	69
1	700	7	29	2.3	69

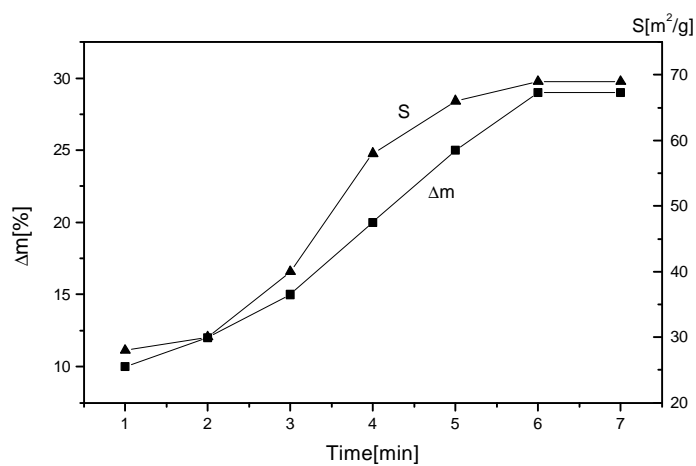


Fig.4.6: Change of mass and specific surface area of $\text{AlCl}_3/\text{CuCl}_2$ GIC as a function of exfoliation time at 700°C

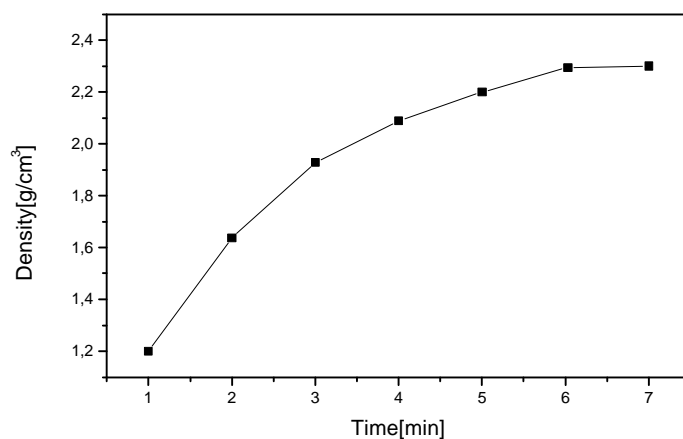


Fig.4.7: Variation of $\text{AlCl}_3 / \text{CuCl}_2$ GIC's density as a function of exfoliation time at 700°C

Deductions made from the analyses of $\text{AlCl}_3 / \text{CuCl}_2$ – GICs and of the exfoliated products

Almost pure stage first and second stage products were obtained under the reaction conditions investigated as shown by X-ray diffraction Fig.4.1. Under the same experimental conditions, a trial to intercalate AlCl_3 and CuCl_2 independent of each other was not successful. It is an already known fact that AlCl_3 acts as a carrier in fixing metal chlorides in graphite layers. Here, the question that arises is, whether it acts only as a transporting means or after the complex formation with the CuCl_2 , the Al_2CuCl_6 complex formed is intercalated, implying the co-intercalation of AlCl_3 . Or, does the complex decompose, setting the AlCl_3 free, which then leaves the graphite interlayer? . For the clarification of possible co-intercalation see Ref. [Stu92].

The gravimetric measurements of the products delivered 70 and 54 weight percent composition for the first and second stage GIC respectively. Ash analysis gave 41 and 31 weight percent metal oxides for the first and second stage products respectively. Theoretically, 37 or 41 percent is expected for the first stage for total conversion to Cu_2O or CuO , and 28 or 31 percent for the second stage conversion to Cu_2O or CuO . The results of the ash analyses conform to good extent the theoretical results. The deviations can be solely attributed to partial reduction of CuO to Cu_2O and possibly to elemental Cu , all leading to small weight percent of CuO as observed in the ash analyses. The results obtained can be taken as supporting the sole intercalation of CuCl_2 . This is also confirmed by the results obtained in the exfoliation investigation. The maximum loss in mass was found to be 29 percent for the first stage and 20 for the second. Theoretically, neglecting graphite burnt out, complete conversion of the GIC in its chloride form to its oxide, results with 28 and 22 percent loss in mass for the first stage and the second stage – assuming that the GIC contains only CuCl_2 as intercalate and that no de-intercalation took place during the exfoliation process. Quantitative X – ray fluorescence measurement (intensity measurement of the $\text{Cu-K}\alpha$ radiation as a function of mole ratio), carried out on the exfoliated $\text{AlCl}_3/\text{CuCl}_2$ -GIC products also confirmed the amount of Cu in the products. The ratio of Cu in the first stage to that in the second is roughly 1.3 and is in conformity with that obtained from gravimetric measurements (32: 41). The results obtained from X –ray absorption spectroscopy of the exfoliated products showed overwhelming Cu(II) – implying, if any at all, a negligible amount of Cu(I) and Cu(0) .

Table 4.6: Weight % Cu in the prepared $\text{AlCl}_3/\text{CuCl}_2$ GICs obtained from X-ray fluorescence analysis.

GIC	Stage number	Weight % of Cu in GIC
$\text{AlCl}_3/\text{CuCl}_2$	2	33
$\text{CuCl}_3/\text{CuCl}_2$	1	25

4.2 Characterisation of the $\text{FeCl}_3/\text{CuCl}_2$ GICs and the Exfoliated Products

X – ray diffraction analysis

Just as in the case of $\text{AlCl}_3/\text{CuCl}_2$ -GIC nearly pure stage compounds were obtained in the preparation of $\text{FeCl}_3/\text{CuCl}_2$ – GICs and typical examples of their X – ray diffraction diagrams as well as their d_{001} -values are given below. X – ray diffraction diagrams of investigated graphite intercalation compounds, and the d_{001} -values evaluated from the positions of the reflections are respectively shown in Fig.4.8 and Tab.4.7.

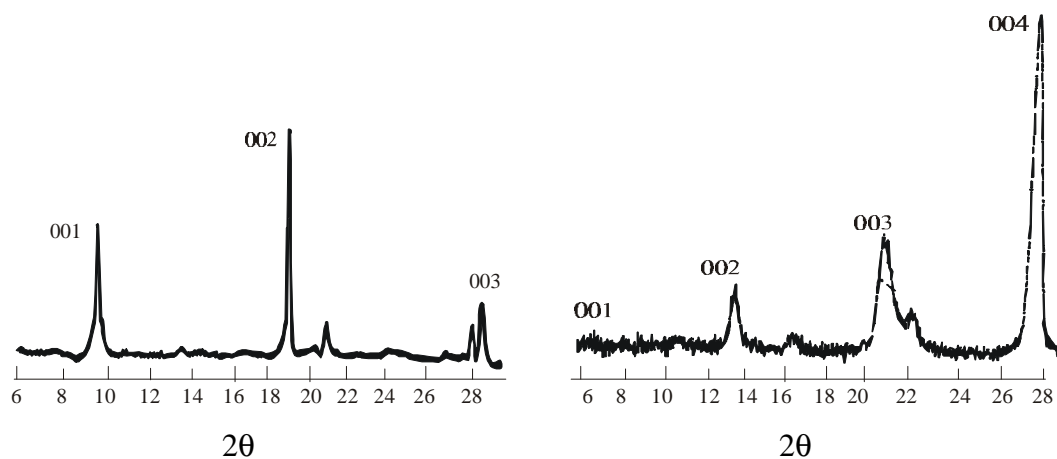


Fig.4.8: 1st and 2nd stage X-ray diffraction diagrams of $\text{FeCl}_3/\text{CuCl}_2$ GICs

Table 4.7 : $d_{00\lambda}$ values and the reflection peak positions (shown in brackets) for Cu-K α radiation ($\lambda = 154.2\text{pm}$) for $\text{FeCl}_3/\text{CuCl}_2$ – GICs. The $d_{00\lambda}$ values are given in pm and the angles (2θ) are measured in degrees.

$\text{FeCl}_3/\text{CuCl}_2$	001	002	003	004
1 st Stage	941 (9.40)	470.1 (18.88)	313.2 (28.50)	
2 nd Stage	1272.3 (6.95)	626 (13.90)	424.8 (20.92)	318.9 (27.98)

Gravimetric measurements (ash analyses)

The results of the analyses are presented in Tab. 4.8 and 9.

Table 4.8: Content of intercalate compound in the prepared GICs, expressed as weight % of the of GIC analysed.

GIC	Stage	Intercalate (weight %)
$\text{FeCl}_3/\text{CuCl}_2$	1	74.1
	2	58.9

Table 4.9 Results of total metal oxide composition in the GIC, expressed as weight % of GIC analysed.

GIC	Stage	Total oxides (weight %)
$\text{FeCl}_3/\text{CuCl}_2$	1	43.1
	2	32.6

X-ray fluorescence analysis

By employing this method one is in a position to find the mole relation of Cu and Fe in the $\text{FeCl}_3 / \text{CuCl}_2$ GIC. Standard samples containing defined or specified mole proportions of Fe and Cu were prepared from $\text{CuCl}_2 \cdot 2\text{H}_2\text{O}$ and $(\text{NH}_4)_2\text{SO}_4\text{FeSO}_4 \cdot 6\text{H}_2\text{O}$ (Mohr's salt).

Compounds of Fe(III) such as $\text{FeCl}_3 \cdot 6\text{H}_2\text{O}$ could not be used because they are hygroscopic and do not ensure the maintenance of stoichiometric relations in the course of weighing the substances. Contrary to other Fe(II) compounds, the Mohr's salt does not have the disadvantage of easily changing into the oxidation state (III). An adulteration of the results by employing a compound containing sulphate instead of chloride can be considered negligible, in view of the fact that sulphur and chlorine are neighbouring elements in the periodic table and therefore possess similar X-ray absorption coefficient. The elements hydrogen, nitrogen and oxygen, which are in the standard samples but not in the graphite intercalation compounds can be neglected in their effect upon the intensity relations of Cu-K_α and Fe-K_α , because of their very small mole masses and consequently of their very small X - ray absorption coefficient.

The mole proportions of the prepared standards are around 0.1:1, 1:1, 10:1, and 100:1 (Cu: Fe). Weighed amounts of the compounds in these proportions are ground in a mortar with a pestle for a period of about 10 minutes, after which 4 to 6 X – ray fluorescence measurements are repeatedly made on each sample. The count rates corresponding to the background radiation are deducted from that of Cu-K_α / Fe-K_α radiation, after which the intensity relation are formed. Fig. 4.9 shows the standard curve in logarithmic scale (both axis).

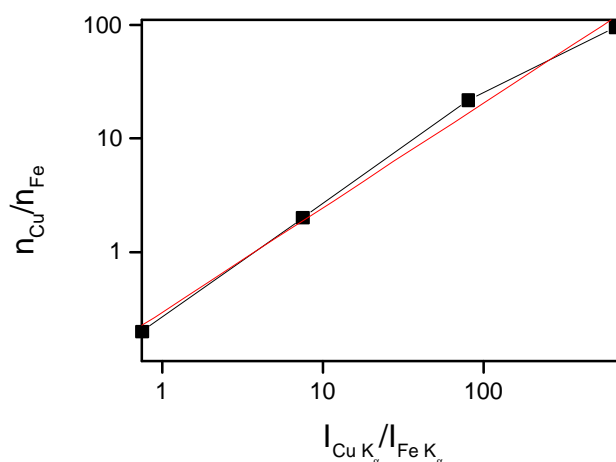


Fig. 4.9: Mole proportions (Cu : Fe) as a function of their K_α radiation intensity relations.

The results of the X-ray fluorescence measurements, illustrating the mole proportions of Cu to Fe in the GICs are presented in Tab. 4.10.

Table 4.10: Reaction products (GICs), their stage numbers and mole proportions of Cu to Fe obtained from X-ray fluorescence analysis.

GIC	Stage number	Mole proportions of Cu to Fe
$\text{FeCl}_3/\text{CuCl}_2$	2	4:1
$\text{FeCl}_3/\text{CuCl}_2$	1	3.9:1

X - ray absorption measurements

X – ray absorption measurements were also carried out on the exfoliated products of FeCl_3 / CuCl_2 GIC. The measurements were performed as already stated above at the Cu and Fe K-edges ($E = 8.979$ and 7.112 keV. respectively).

Results of absorption measurements

The absorption spectrum of FeCl_3 / CuCl_2 GIC , after being heated in air for 20 minutes at 700° , is combined with the spectra of AlCl_3 / CuCl_2 and pristine CuCl_2 , and given in Fig.4.10.

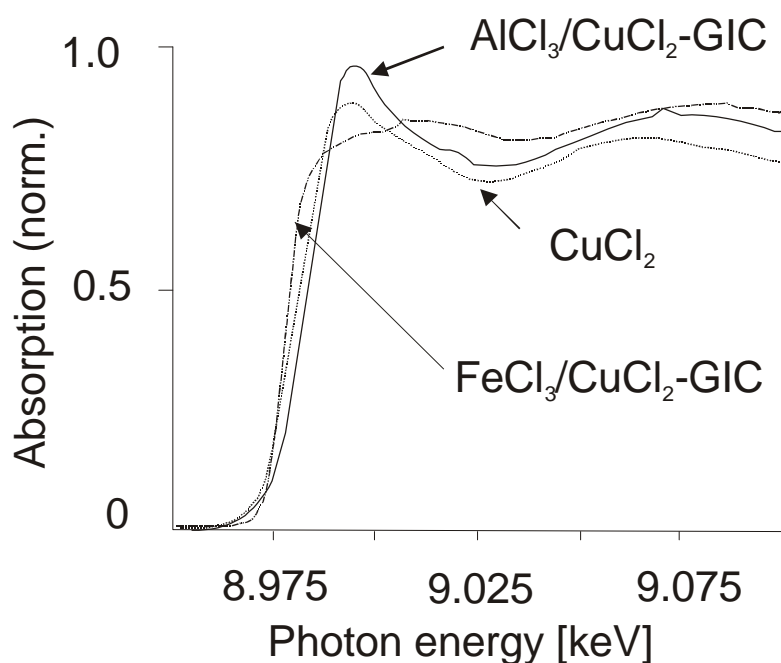


Fig. 4.10: X-ray absorption spectra (CuK edge) of exfoliated AlCl_3 / CuCl_2 GIC, FeCl_3 / CuCl_2 GIC, and of a correspondingly treated mixture of CuCl_2 and graphite.

The position of the Cu-K absorption edge in the exfoliated $\text{FeCl}_3 / \text{CuCl}_2(\text{CuO})$, just as that in the case of the exfoliated $\text{AlCl}_3 / \text{CuCl}_2$ and $\text{CuCl}_2 (\text{CuO})$, lies within the expected range required for Cu(II) compounds.

After transforming the EXAFS function $\chi(k)$, the FT with k ranging from $k = 0.019$ to 0.095 pm^{-1} was back transformed. In order to obtain the Fourier transform, the radial distribution function FT, the experimental $\chi(k)$ was weighted with k^2 and multiplied with a Bessel window and transformed into R space. The Fourier transform for the exfoliated products and the oxygen treated pristine CuCl_2 is presented in Fig 4.11 and back transform for oxygen treated pristine $\text{CuCl}_2(\text{CuO})$ and CuCl_2 standard are shown in Fig. 4.12 and Fig. 4.13 respectively.

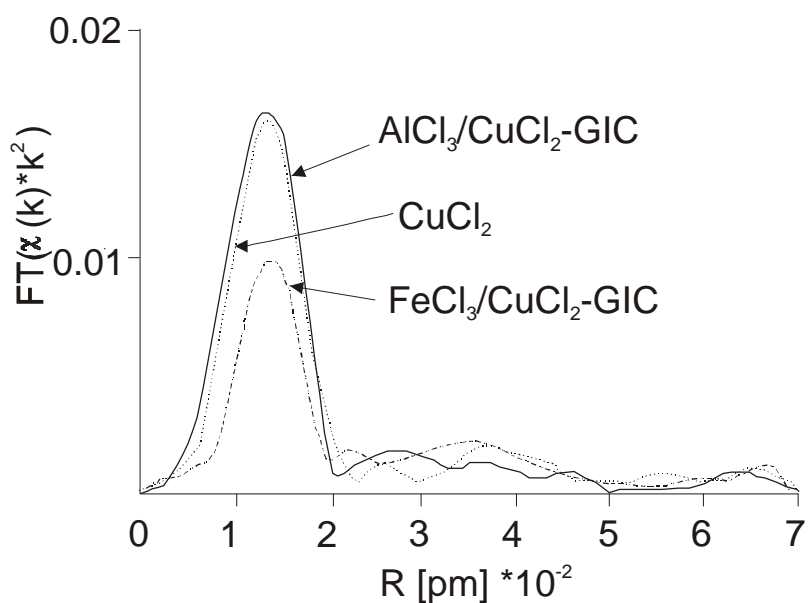


Fig. 4.11: The Fourier transformed $\chi(k)$ of exfoliated $\text{FeCl}_3 / \text{CuCl}_2$ GIC and of a correspondingly treated mixture of CuCl_2 and graphite, in comparison with $\text{AlCl}_3 / \text{CuCl}_2$ GIC ($k = 0.019$ to 0.095 pm^{-1}).

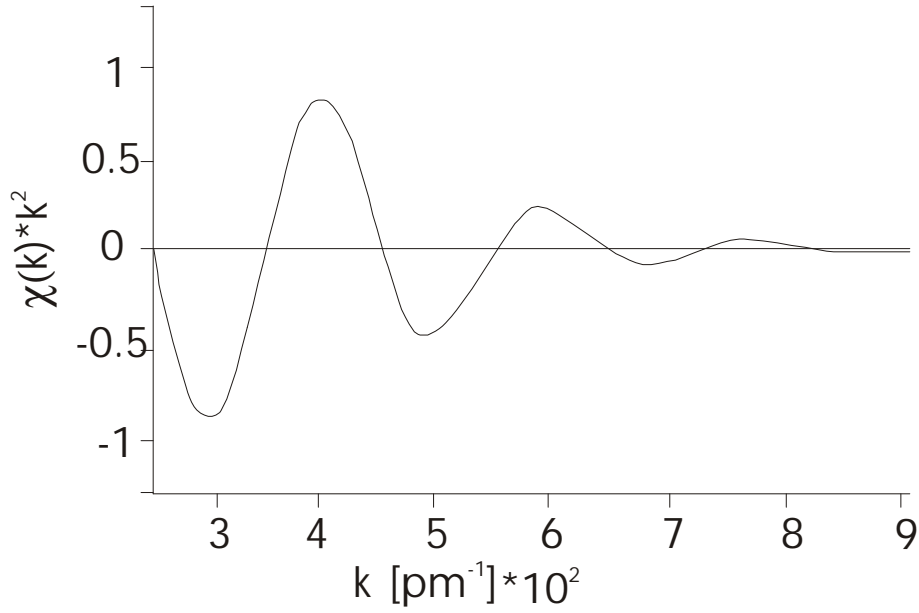


Fig. : 4.12: Back transform of exfoliated $\text{FeCl}_3 / \text{CuCl}_2$ GIC . $\text{FT}(1.9 - 9.5) \cdot 10^{-2} \text{ pm}^{-1}$, back transform 70 – 245 pm .

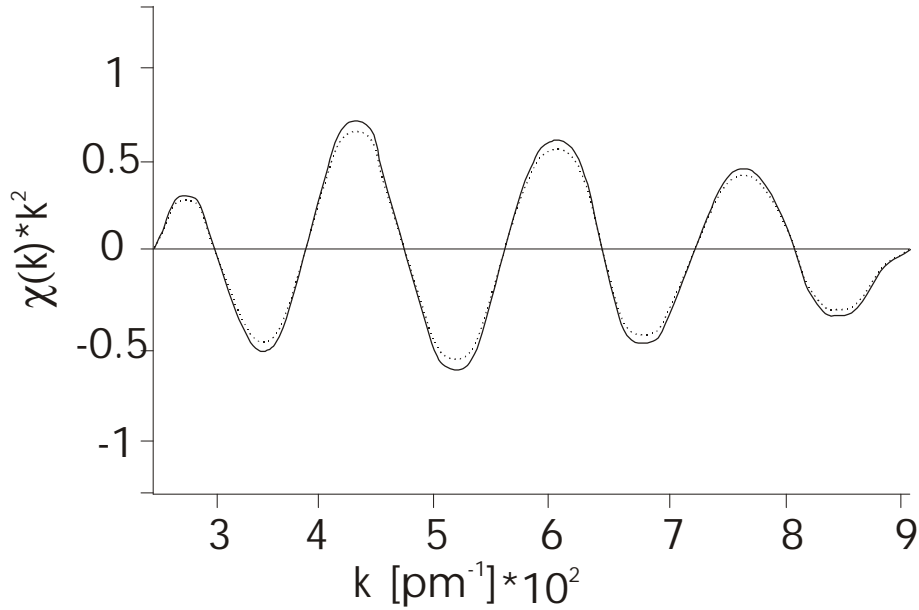


Fig. : 4.13: Back transform for pristine CuCl_2 . $\text{FT}(1.9 - 9.5) \cdot 10^{-2} \text{ pm}^{-1}$, back transform 70 – 245 pm.

A comparison of the inverse transform for pristine CuCl_2 (Fig.4.13) and that for the exfoliated $\text{AlCl}_3 / \text{CuCl}_2$ GIC shown in Fig. 4.5 indicates qualitatively the conversion of copper chloride in the GIC to copper oxide. The EXFAS fit for the exfoliated $\text{AlCl}_3 / \text{CuCl}_2$ GIC shown in Fig. 4.5 can reasonably be taken as representative of that for the oxygen treated mixture of pristine CuCl_2 and graphite. From Fig.4.11 we observe that the position and amplitude of the FT curves for both products conform perfectly to one another. The difference

in the EXAFS fit for the exfoliated $\text{AlCl}_3 / \text{CuCl}_2$ GIC from that of the pristine can also be justifiably assumed for the oxygen treated mixture of pristine CuCl_2 and graphite. This change can only be attributed to the conversion of the oxygen treated pristine copper chloride into oxide. Similarly, the difference in Fig. 4.2.6 and Fig. 4.2.5K – the inverse transform for exfoliated $\text{FeCl}_3 / \text{CuCl}_2$ GIC – shows clearly the conversion of copper chloride.

A clear difference in the exfoliation products of $\text{FeCl}_3 / \text{CuCl}_2$ and $\text{AlCl}_3 / \text{CuCl}_2$ GICs is evident from the near edge region of the measured Cu K edge spectra (see Fig. 4.10). A remarkable edge shift towards lower photon energies is observed for $\text{FeCl}_3 / \text{CuCl}_2$ indicating a reduction of the copper species. A remarkable reduction observed in the ‘white line’ is a clear indication of structural change in the copper coordination geometry. The oxygen peak height (see Fig. 4.11) of the resulting copper oxide species is smaller compared to the oxides obtained from $\text{AlCl}_3 / \text{CuCl}_2$ or CuCl_2 . This indicates the formation of both Cu(II) and Cu(I) oxides in the course of the exfoliation process. In order to justify these conclusions, comparative measurements and evaluations were carried out on CuO , CuCl_2 and Cu_2O , see Fig. 4.14. The occurrence of these two products side by side in the exfoliated products is explained later in this section. This phenomenon observed in the course of the exfoliation process of $\text{FeCl}_3 / \text{CuCl}_2$ GIC is in sharp contrast to that observed in $\text{AlCl}_3 / \text{CuCl}_2$ GIC exfoliated product and in the product obtained after treating a mixture of pristine CuCl_2 and graphite in oxygen. In the last two cases almost only Cu(II) oxides are obtained.

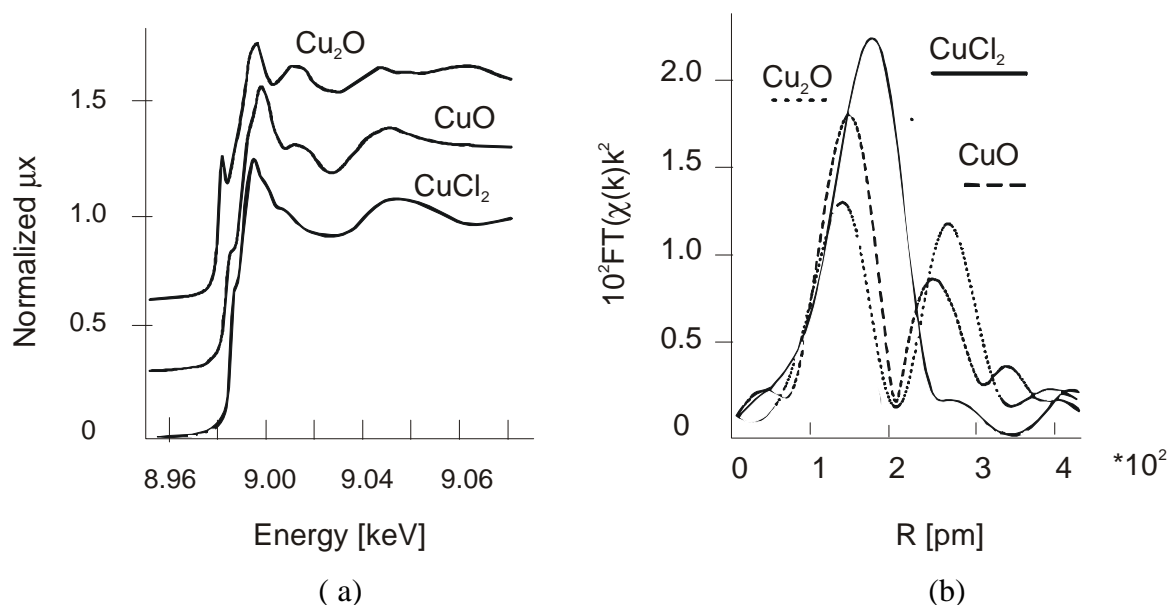


Fig.4.14: X – ray absorption spectra of CuCl_2 , CuO and Cu_2O showing the Cu K edges (a) and the corresponding Fourier transform (b)

Tab. 4.11 :

The Cu coordination numbers N (for the first oxygen shell) and the Cu – O inter atomic distances R obtained from X – ray absorption measurements for the exfoliated FeCl₃ / CuCl₂ and AlCl₃ / CuCl₂ GICs as well as the correspondingly treated pristine CuCl₂ / graphite and other comparable copper oxides. Experimental phases and amplitudes for oxygen shell in Cu₂O were used. Fourier transform FT(0.019 – 0.095pm⁻¹) and back transform (60 – 230pm)

Exfoliated GICs			Comparable copper oxides		
	N	R (pm)		N	R (pm)
CuCl ₂ / graphite	3.6(0)	196(2)	Cu ₂ O	1.9 (1)	201
AlCl ₃ / CuCl ₂	3.6(3)	202(1)	CuO	3.9(1)	199
FeCl ₃ / CuCl ₂	2.0(0)	198(2)			

X-ray absorption measurements made at the Fe K edge give the following results: Fig.4.15 indicates the Fe K edge of the exfoliated product of FeCl₃ / CuCl₂ GIC and the Fourier transform, the radial distribution function FT. Fig.4.16 illustrates the absorption spectra of FeCl₃ and FeCl₂ as basis for the absorption analysis.

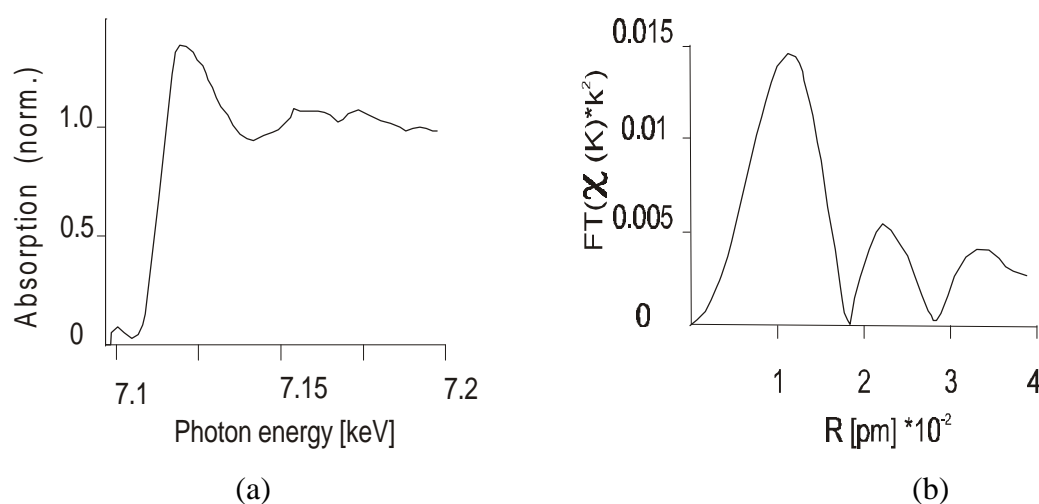


Fig.4.15: (a) X – ray absorption spectrum indicating the Fe K edge of the exfoliated product of FeCl₃ / CuCl₂ GIC and (b) the Fourier transform, k ranging from 1.9 to 7.6 *10⁻² pm⁻¹.

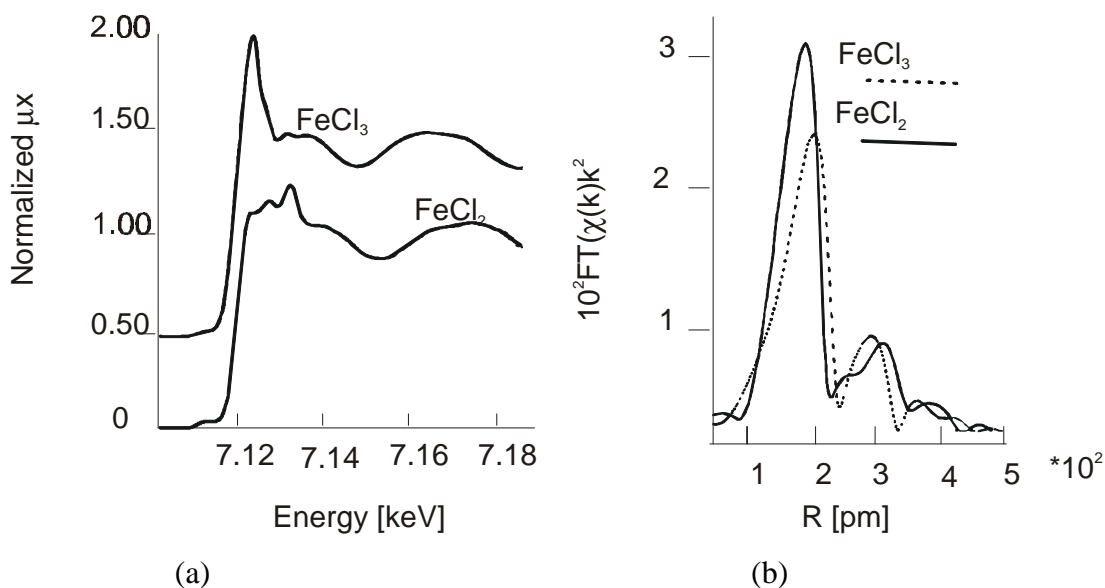


Fig.4.16: X – ray absorption spectra of FeCl₂ and FeCl₃ showing the Fe K edges (a) and the corresponding Fourier transform (b)

Pre-edge peak of FeCl₂ is also found in the absorption spectrum of FeCl₃ / CuCl₂ prior to exfoliation and indicates the co-existence of FeCl₃ and FeCl₂ in this graphite interaction compound.

At the exfoliation temperature the Fe(II) seems to be oxidised. This conforms with the reduction of Cu(II) to Cu(I) as already indicated. The oxidation of Fe(II) as a result of disproportionation ($2\text{FeCl}_2 \rightarrow \text{FeCl}_3 + \text{Fe}$) cannot be ruled out completely.

For more detailed information, especially concerning the time dependence of the exfoliation process, see [Re95]

Changes in mass, density and specific surface area

Table 4.12 and Fig.4.17 and 4.18 provide a summary of the results of the exfoliation experiment for the prepared FeCl₃ / CuCl₂ -GICs. The exfoliation temperature $T_{\text{exf.}}$, exfoliation time $t_{\text{exf.}}$, the stage number of GIC prior to exfoliation, the loss in mass of GIC Δm , the density ρ , and the specific surface area S of the exfoliated products are presented.

Table 4.12 Results of the exfoliation experiment with $\text{FeCl}_3/\text{CuCl}_2$ -graphite

Stage number	$T_{\text{exf.}}(^{\circ}\text{C})$	$t \text{ (min)}$	$\Delta m \text{ (\%)}$	ρ	S
1	700	1	8	1.74	5
1	700	2	11	1.75	9
1	700	3	18	1.91	15
1	700	4	22	2.03	20
1	700	5	26	2.2	32
1	700	6	29	2.32	37
1	700	7	32	2.41	48
1	700	8	35	2.46	59
1	700	9	35	2.47	59

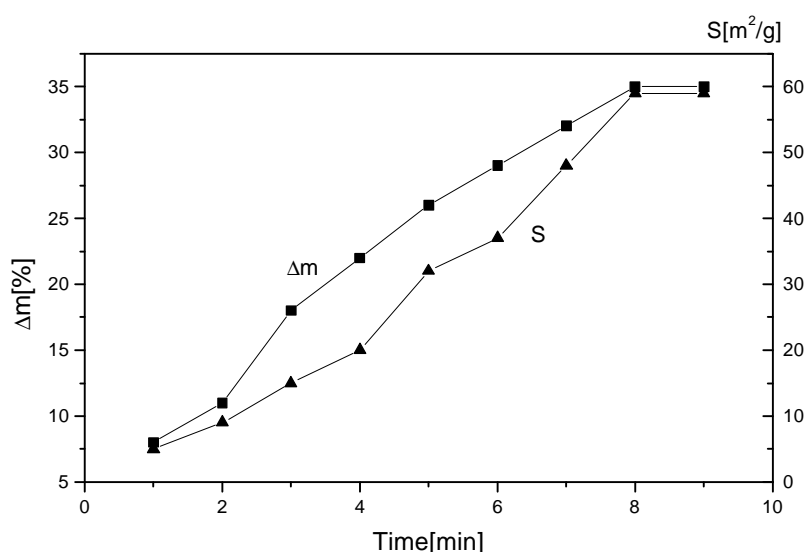


Fig. 4.17: Change of mass and specific surface area of $\text{FeCl}_3/\text{CuCl}_2$ GIC as a function of exfoliation time at 700°C

Deductions made from the analyses of $\text{FeCl}_3 / \text{CuCl}_2 - \text{GICs}$ and of the exfoliated products

Just as obtained for $\text{AlCl}_3/\text{CuCl}_2$ -GIC, nearly first stage and second stage products were obtained under the reaction conditions investigated as shown by X-ray diffraction Fig.4.8. The d_{00l} -values of the reflections are presented in Tab.4.8. Under the same experimental conditions, a trial to intercalate AlCl_3 and CuCl_2 independently of each other was not successful. As already known FeCl_3 forms a complex just as AlCl_3 does with CuCl_2 before

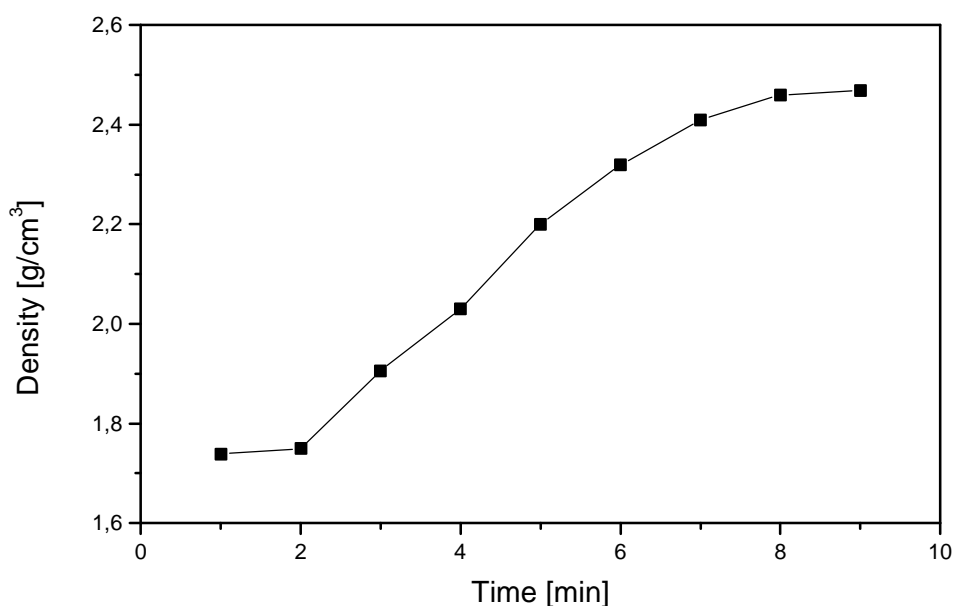


Fig.4.18: Variation of density as a function of exfoliation time at 700°C

intercalation takes place. From the reflection peaks in both the first and second stage GICs, an assumption of co-intercalation in which a complex or an adduct of both metal chlorides or the intercalation of only one of them can be made. The intercalation of only FeCl_3 can also be ruled out, while no prominent peaks corresponding to FeCl_3 -GIC reflections were observed. Roughly 74 and 59 percent by weight of metal chlorides were obtained from the gravimetric measurements of the first and second stage GICs respectively. X – ray fluorescence analyses (Tab.4.10) showed a Cu to Fe mole relations of 4:1 for both the first and second stage GICs. These results were also confirmed by the ash analyses, which delivered roughly 43 and 33 percent by weight of metal oxides in the first and second stage GICs, after being converted from their chloride form to their oxides. From the metal chloride compositions of the GICs and the results obtained from the X – ray fluorescence analyses, the empirical formulae $\text{C}_{4.9}\text{CuCl}_2(\text{FeCl}_3)_{0.25}$ and $\text{C}_{9.8}\text{CuCl}_2(\text{FeCl}_3)_{0.25}$ could be postulated for the first and second stage GICs respectively. Theoretically, conversion of the metal chlorides into their oxides (CuO and Fe_2O_3) should deliver 43 and 34 percent by weight of total metal oxides for the first and second stage GICs respectively. X – ray absorption measurements also confirmed the presence of FeCl_2 in the prepared GICs. Replacing all FeCl_3 in the GICs by FeCl_2 , we expect total metal oxides composition in the GICs after conversion from their metal chlorides to be 35 percent for the second stage and 44 for the first stage. A consideration of the metal oxide residue obtained in the ash analyses as consisting of Cu(II) and Fe(III) , and other low

oxidation states of the two, cannot be ruled out here. The results obtained from the ash analyses and the X – ray fluorescence measurements can be taken as fairly supporting the empirical formulae and therefore the composition of the GICs.

4.3 Characterisation of the $\text{AlCl}_3 / \text{MoOCl}_3 / \text{CuCl}_2$ – GICs and the Exfoliated Products.

X – ray diffraction analysis

Fig.4.19 and Tab.4.13 show the X – ray diffraction diagrams of investigated $\text{AlCl}_3 / \text{MoOCl}_3 / \text{CuCl}_2$ – GICs and the $d_{00\lambda}$ -values evaluated from the positions of the reflections respectively. Fig.4.20 and 4.21 show the 1st and 2nd stage MoOCl_3 GIC diffraction diagrams.

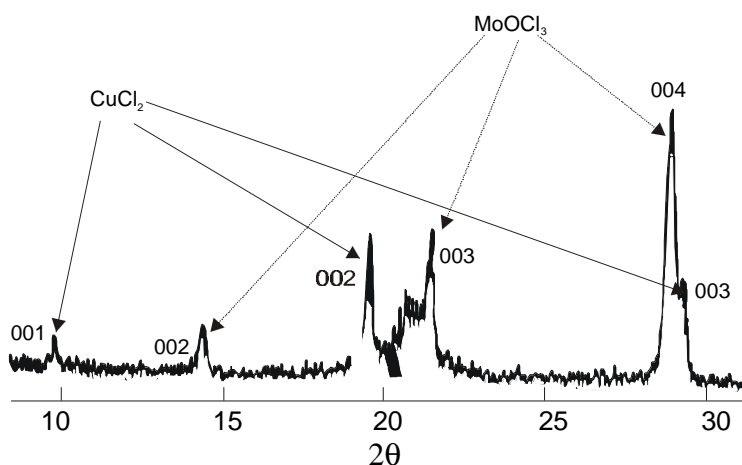


Fig.4.19: X-ray diffraction diagram of $\text{AlCl}_3/\text{MoOCl}_3/\text{CuCl}_2$

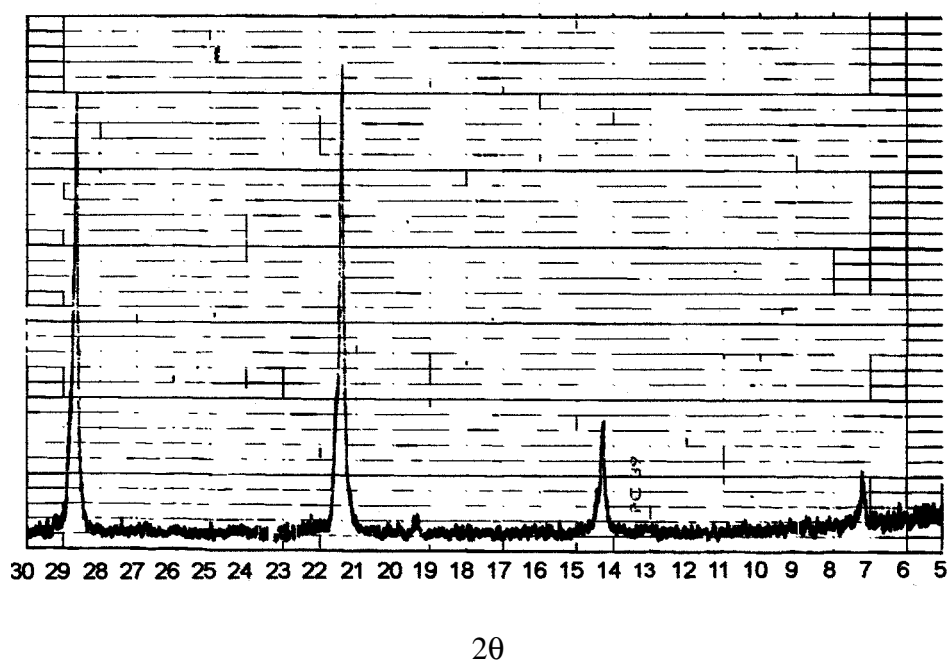


Fig.4.20: 2.stage X-ray diffraction diagram of MoOCl_3 GIC

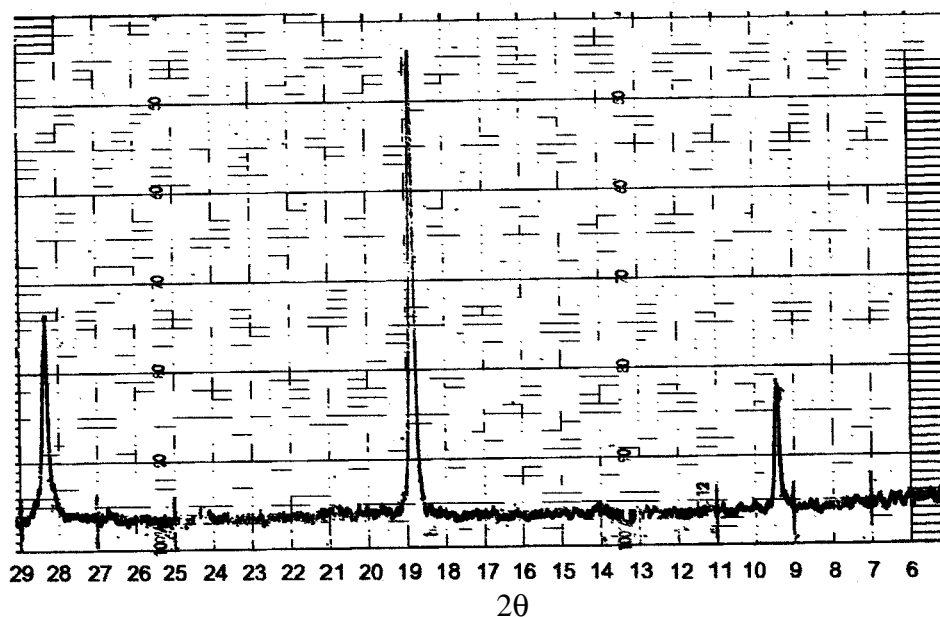


Fig. 4.21: 1.stage X-ray diffraction diagram of MoOCl₃ GIC

Table 4.13 : d_{001} – values and the reflection peak positions (shown in brackets) for Cu-K α radiation ($\lambda = 154.2\text{pm}$) for AlCl₃/MoOCl₃/CuCl₂ GICs.

The - d_{001} values are given in pm and the angles (2θ) are measured in degrees.

	001	002	003	004
1st. Stage	940.1 (9.40)	470 (18.85)	303 (29.40)	
2nd. Stage	12.75 (7.00)	6.38 (14.15)	4.25 (21.25)	3.19 (28.40)

Gravimetric measurements (ash analyses)

Composition of intercalated compounds in the AlCl₃ / MoOCl₃ / CuCl₂ GIC was found to be 71.4 weight percent and total metal oxides obtained was 41 weight percent .

Changes in mass, density and specific surface area

A summary of the results of the exfoliation experiments obtained for AlCl₃ / MoOCl₃ / CuCl₂ - GIC is presented in Table 4.14 and Fig.4.22 and 4.23. The exfoliation temperature $T_{\text{exf.}}$,

exfoliation time $t_{\text{exf.}}$, the stage number of GIC prior to exfoliation, the loss in mass of GIC Δm , the density ρ , and the specific surface area S of the exfoliated products are presented.

Table 4.14

Results of the exfoliation experiment with $\text{AlCl}_3/\text{MoOCl}_3/\text{CuCl}_2$ -graphite

Stage number	$T_{\text{exf.}}(^{\circ}\text{C})$	t (min)	Δm (%)	ρ	S
1	700	1	14	1.32	25
1	700	2	16	1.41	31
1	700	3	17	1.56	43
1	700	4	19	1.8	52
1	700	5	23	2.1	65
1	700	6	27	2.3	65
1	700	7	27	2.3	65

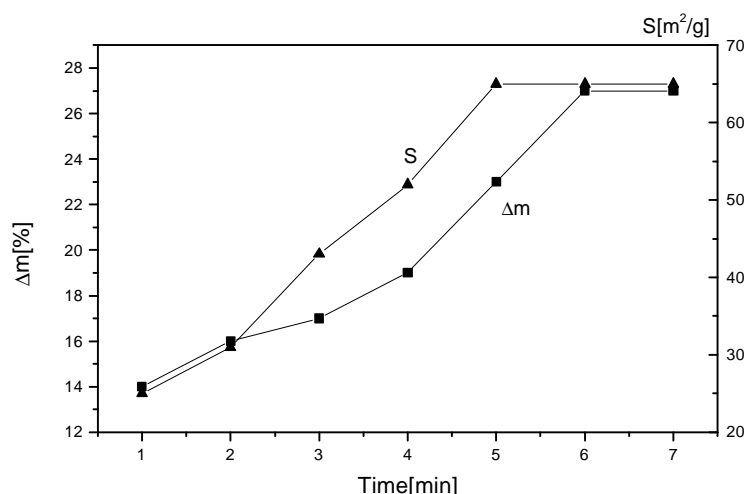


Fig.4.22: Change of mass and specific surface area of $\text{AlCl}_3 / \text{MoOCl}_3 / \text{CuCl}_2$ as a function of exfoliation time at 700°C

Deductions made from the analyses of $\text{AlCl}_3 / \text{MoOCl}_3 / \text{CuCl}_2$ – GICs and of the exfoliated products

A mixture of nearly pure stages intercalation product was obtained as indicated by the X – ray diffraction diagram in Fig.4.19. First stage intercalation attributed to CuCl_2 and second stage to MoOCl_3 are shown in the diagram. The preparation of MoOCl_3 -GICs (as control) was also undertaken. X-ray diffraction diagrams of the first and second stage products obtained are shown in Fig.4.20 and 4.21. The first and second stage MoOCl_3 -GICs could also be

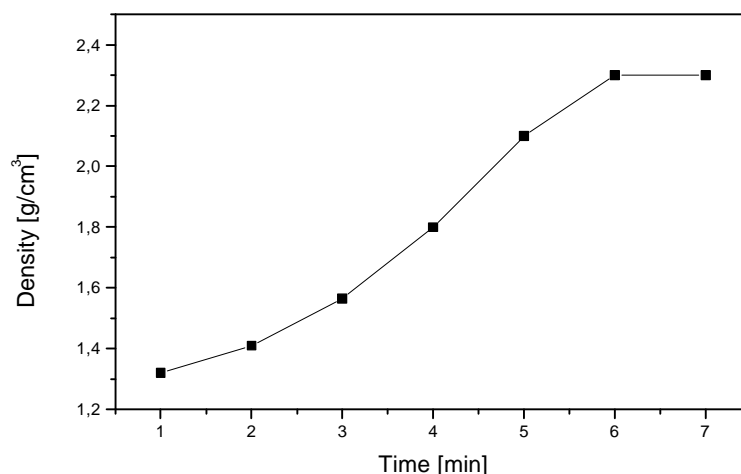


Fig.4.23: Variation of AlCl_3 / MoOCl_3 / CuCl_2 – GIC density as a function of exfoliation time at 700°C

prepared without the addition of chlorine or AlCl_3 . The d_{001} -values calculated from reflections pertaining to the first and second stage MoOCl_3 -GICs are presented in Tab. 4.13. The d_{001} - values of the first stage MoOCl_3 -GIC tally well with the values obtained from the reflections corresponding to those of MoOCl_3 -GIC in the first stage bi-intercalation compound $\text{AlCl}_3/\text{MoOCl}_3/\text{CuCl}_2$. The $d_{00\lambda}$ -values calculated from the reflections attributed to the CuCl_2 in the bi-intercalation compound agree well with those calculated from the first stage reflections of $\text{AlCl}_3/\text{CuCl}_2$ -GIC. 71 weight percent of the intercalated metal chlorides was measured for the first stage $\text{AlCl}_3/\text{MoOCl}_3/\text{CuCl}_2$ -GIC. Taking the CuCl_2 -GIC in the bi-intercalation to be the same in structure as that in the $\text{AlCl}_3/\text{CuCl}_2$ -GIC, a reasonable assumption based on the CuCl_2 reflection positions in the two products, roughly 25 weight percent was calculated for CuCl_2 and 47 percent for MoOCl_3 . The weight of the metal oxide left after burning out graphite in the presence of oxygen was 41 percent of the $\text{AlCl}_3/\text{MoOCl}_3/\text{CuCl}_2$ -GIC. The CuO in the metal oxide mixture was found from X-ray fluorescence measurement to be 35 percent. This indicates that the composition of CuO and MoO_3 in the metal oxide mixture is roughly 1:1.

4.4 Characterisation of the Ce(IV)nitrate - GICs and the Exfoliated Products

X – ray diffraction analysis Fig. 4.24 and 4.25 and Tab.4.15 show the X –ray diffraction diagrams of the 2nd and 3rd stage Ce(IV)nitrate - GICs investigated and the d_{001} -values evaluated from the positions of the reflections respectively.

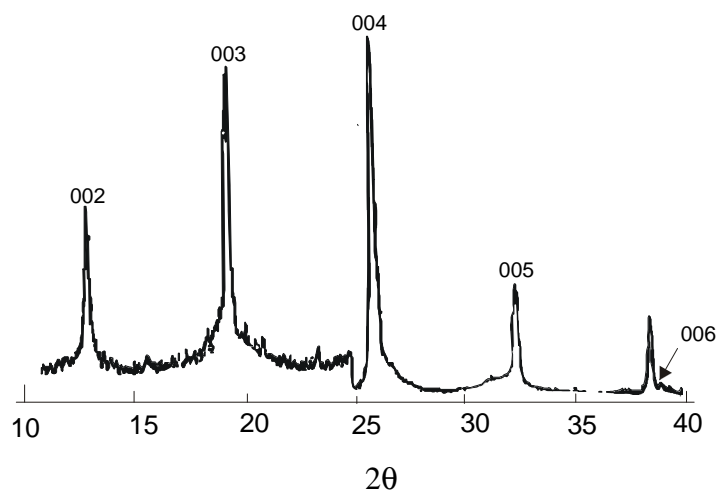


Fig. 4.24: 3.stage X-ray diffraction diagram of Ce(IV)nitrate GIC

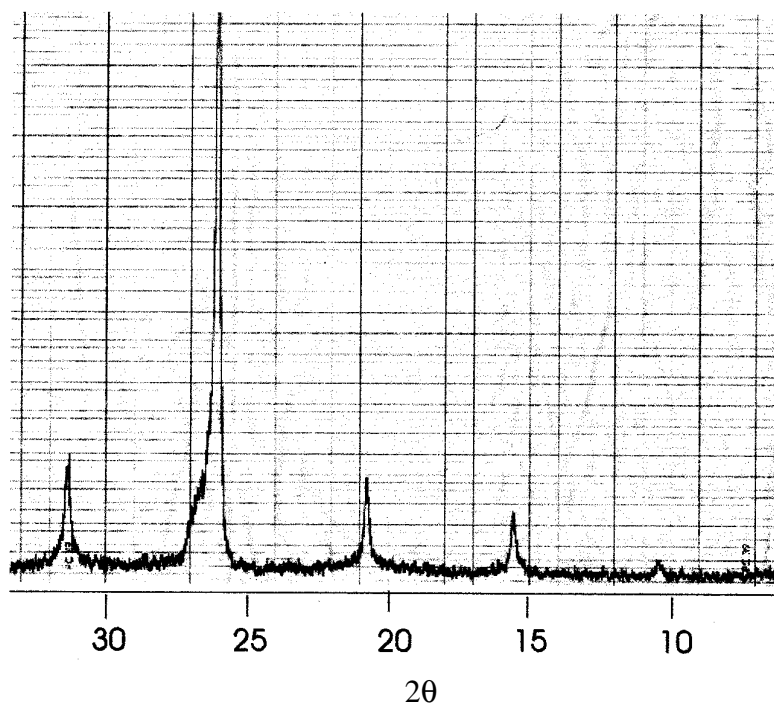


Fig. 4.25: 2.stage X-ray diffraction diagram of Ce(IV)nitrate GIC

Table 4.15 : d_{001} – values and the reflection peak positions (shown in brackets) for Cu- K_{α} radiation ($\lambda = 154.2\text{pm}$) of the investigated Ce(IV)nitrate - GICs. The d_{001} -values are given in pm and the angles (2θ) are measured in degrees.

Ce(IV)nitrate	001	002	003	004	005
----	--	---	---	---	--
3rd. Stage		689.5(12.84)	461.1(19.25)	346.4(25.72)	277.9(32.22)
2nd. Stage	850.7(10.4)	568.1(15.6)	427.1(20.8)	342.7(26.0)	

Gravimetric measurements (ash analyses)

The results delivered from the ash analyses are shown in Tab. 4.16 and 4.17.

Table 4.16: Content of intercalate compound in the prepared GICs, expressed as weight % of the of GIC.

Ce(IV)nitrate GIC	Stage	Intercalate (weight %)
	2	65.2
	3	48.7

Table 4.17: Results of total metal oxide composition in the GIC, expressed as weight % of the of GIC .

Ce(IV)nitrate GIC	Stage	Total oxides (weight %)
	2	19.1
	3	13.9

Changes in mass, density and specific surface area

Table 4.18 and Fig.4.26 and 4.27 provide a summary of the results of the exfoliation experiments for the prepared Ce(IV)nitrate - GICs. The exfoliation temperature $T_{\text{exf.}}$, exfoliation time $t_{\text{exf.}}$, the stage number of GIC prior to exfoliation, the loss in mass of GIC Δm , the density ρ , and the specific surface area S of the exfoliated products are presented.

Table 4.18: Results of the exfoliation experiments with Ce(IV)nitrate-graphite

Stage number	$T_{\text{exf.}}(\text{K})$	$t \text{ (min)}$	$\Delta m \text{ (\%)}$	ρ	S
2	700	1	32	1.9	43
2	700	2	35	2.03	51
2	700	3	38	2.15	70
2	700	4	41	2.23	78
2	700	5	44	2.27	83
2	700	6	44	2.27	83

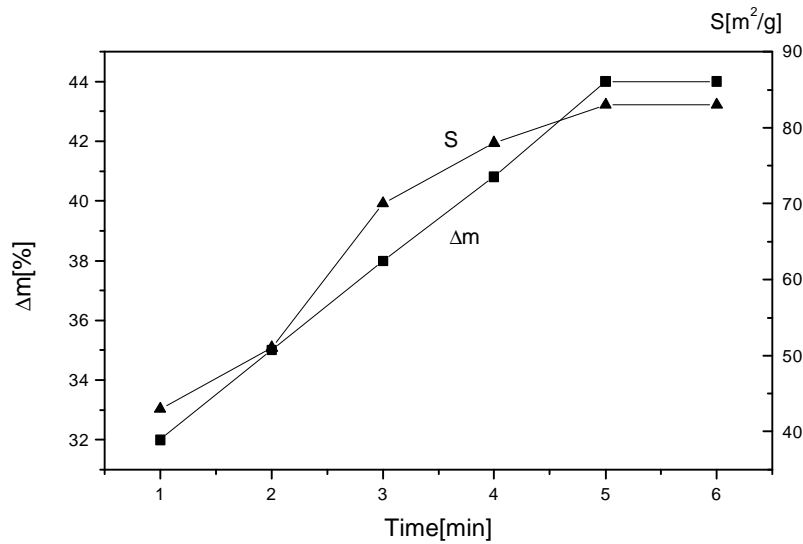


Fig.4.26: Change of mass and specific surface area of Ce(IV)nitrate as a function of exfoliation time at 700°C

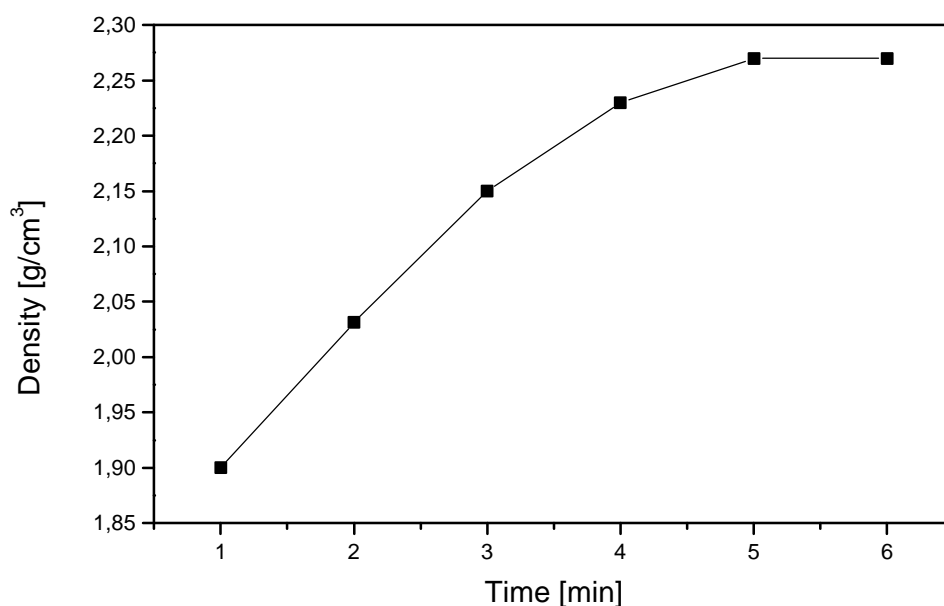


Fig.4.27: Variation of Ce(IV)nitrate density as a function of exfoliation time at 700°C

Deductions made from the analyses of Ce(IV)nitrate GICs and of the exfoliated products

The X – ray diffraction diagrams of the products obtained in the preparation of the Ce(IV)nitrate – GIC revealed that almost pure stage third and second stage products were obtained under the operated experimental reaction conditions. The d_{001} -values of the reflections are presented in Tab. 4.15. The results obtained from gravimetric measurements depicting the weight percent intercalate are shown in Tab.4.16 and 4.17. 65.2 and 48.7 weight percent composition were obtained for the second and third stage GIC respectively. Ash analyses of the exfoliated products delivered 19.1 and 13.9 weight percent metal oxides for the second and third stage products respectively. These results also lead to composition formulae of $C_{52.4}CeO_2$ and $C_{26.2}CeO_2$ for the second and third stage exfoliated products, assuming no carbon oxidation and subsequent loss of carbon in the course of the exfoliation process. Taking these formulae and the weight percent of the intercalate into consideration, the empirical formulae of the second and third stage Ce(IV)nitrate – GIC were evaluated to be $C_{52.4}Ce(NO_3)_4(HNO_3)_{4.3}$ and $C_{26.2}Ce(NO_3)_4(HNO_3)_{4.3}$ respectively. The maximum loss in weight of the second stage GIC in the exfoliation process, which also corresponds to complete conversion of the intercalated compound into its metallic oxide, was found to be 44%

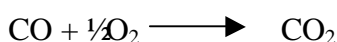
(s. Fig.4.26 and Tab.4.18). Theoretically, the expected percentage loss in mass of the second stage GIC as given by the formula above, in its total conversion to CeO_2 – GIC without loss of graphite is 45.3. The deviation of the practical result from the theoretically determined result can be attributed to the possibility of partial de-intercalation and the loss of graphite as a result of its conversion into carbon monoxide and dioxide during the exfoliation process.

5 Results: Catalytic Activities

5.1 CO Oxidation

The variations of CO turnover with the investigated operational temperatures are measured for all the prepared catalysts and the CuO / graphite – mixture of graphite and CuO with mole proportions corresponding to that of the prepared catalyst samples.

For the CO oxidation reaction tests 0.1% Volume of CO in He and 0.1% Volume of synthetic air (O₂/N₂ ratio 1:4) in He are employed. A reaction mixture of CO and O₂ – with overwhelming proportion of O₂ – was tested. The ratio of the initial CO concentration to that of O₂ in the reaction mixture was always held constant at a particular reaction temperature. The CO oxidation reaction is represented as:



The results of the tests for the various catalysts are presented diagrammatically below. In the figures shown below the conversion, x_{CO} , of CO to CO₂ at the tested reaction temperatures and the corresponding flow rates as a function of contact time, CT are presented. The expressions are defined in section 3.1.8. The relations of CO conversions to CO concentrations at a particular reaction temperature are used to determine the reaction rate for the various samples. Reaction rate constants and activation energies of CO oxidation reaction, using the prepared samples as catalysts, are consequently determined.

Sample AlMo-Graphite exhibited no catalytic activity in the temperature range and the flow rate range investigated and is therefore not further discussed. The results obtained for all the other samples are presented.

First order CO oxidation reaction kinetics (see Section 3.1.7) is tested for all the measured values in the GC analysis. Plots of x_{CO} against CO concentration and of $\ln(1/(1-x_{\text{CO}}))$ against S/v_o - where x_{CO} , S and v_o are CO converted in the oxidation reaction, surface area of the amount of catalyst sample inserted in the reaction, and the flow rate of the reaction mixture respectively - are made at every measured temperature for all the tested samples. This evaluation is based on the formula given in 3.1.8, $k \int dV / v_o = \ln 1/(1 - x_A)$, which is integrated over the reactor volume V . In order to refer to the surface area S , the volume is replaced by S . In consequence of this, the rate constant k changes its dimension and the plots given in this chapter are executed according to the equation

$$\ln (1/(1-x_{\text{CO}})) = k S/v_o .$$

Plots of $\ln(1/(1-x_{\text{CO}}))$ versus S/v_0 at the investigated temperatures are presented for all the prepared samples and give a measure of the reaction rate constants at all the investigated reaction temperatures.

The activation energies for the prepared catalysts are determined by employing the Arrhenius' equation.

5.1.1 CO oxidation – using CuO / graphite mixture as catalyst

The mixture of CuO and graphite was used as basis for comparing the catalytic activities of the different exfoliated graphite compounds. The results from the CO oxidation at the various flow rates and reaction temperatures investigated are shown in Fig. 5.1. The figure indicates the CO conversion as a function of contact time at the operating reactor temperature, which is shown in the diagram and reasonably equated to reaction temperature.

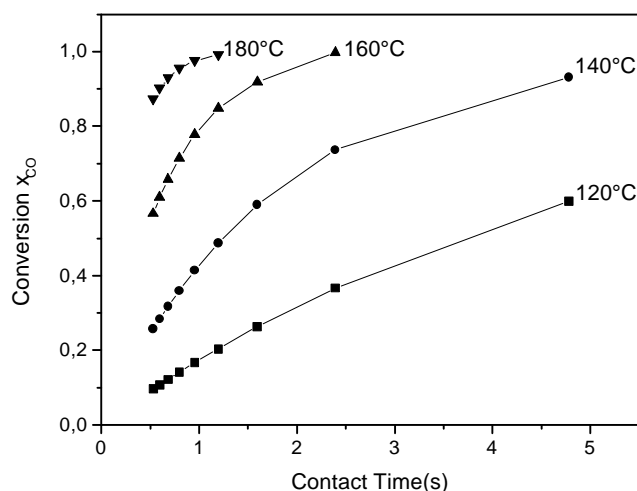
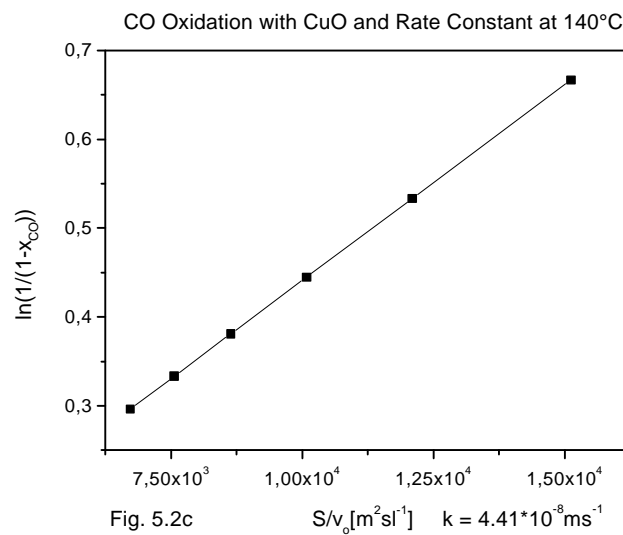
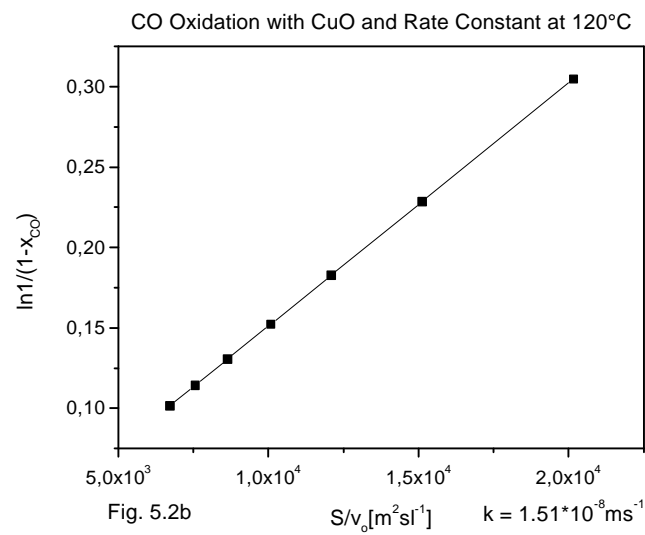
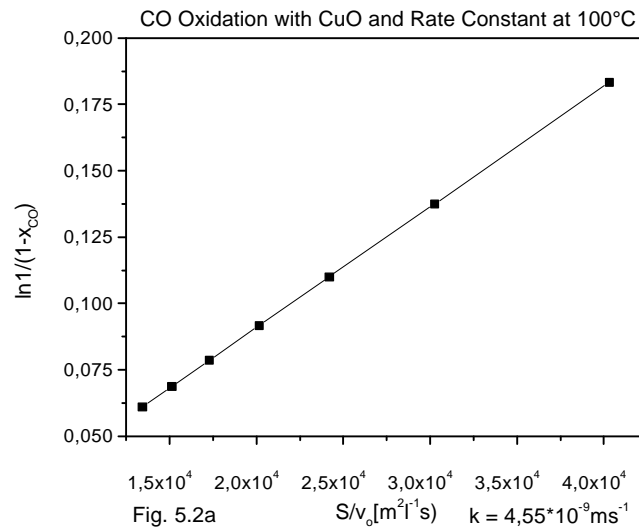
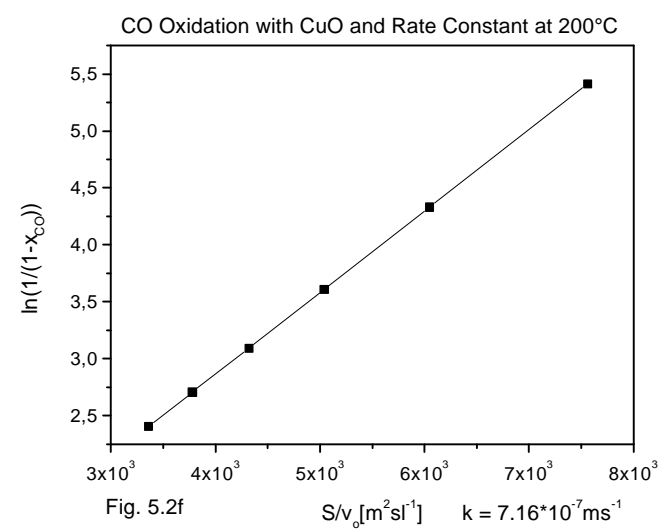
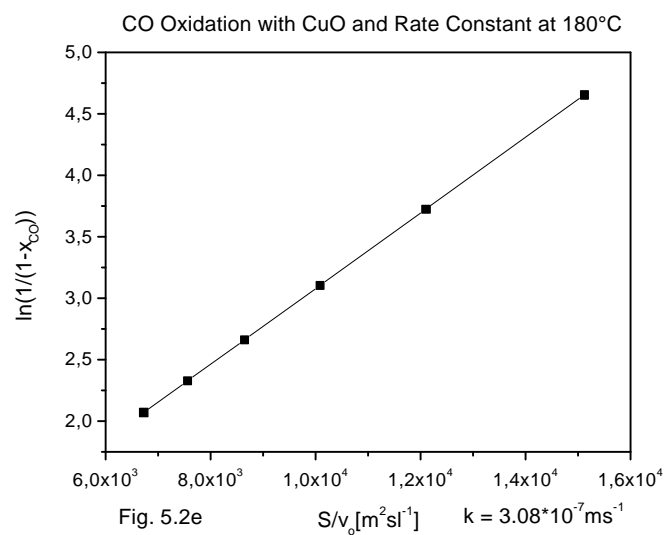
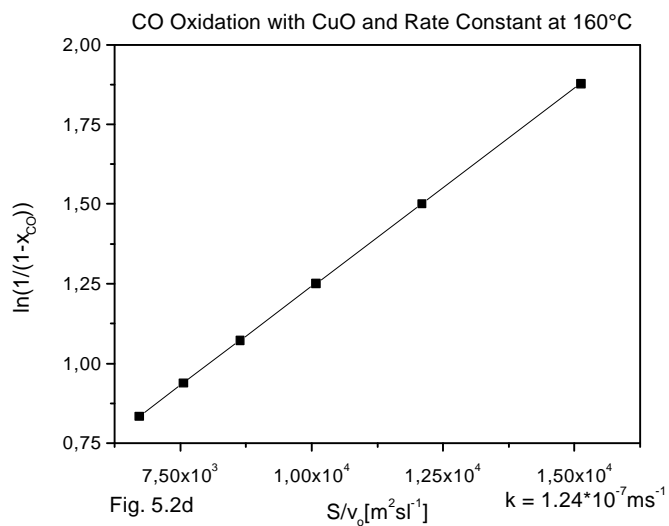


Fig. 5.1 : CO conversion as a function of contact time.
Mixture of CuO and graphite.

Reaction rate constants – using CuO / graphite mixture as catalyst

Plots of $\ln(1/(1-x_{\text{CO}}))$ versus S/v_0 at the investigated temperatures are presented for CuO / graphite in Fig. 5.2a to 5.2f. The gradients of the graphs are measures of the rate constants at the investigated reaction temperatures.





Activation energy – using CuO / graphite mixture as catalyst

A plot of the Arrhenius function using the rate constants and the corresponding reaction temperatures is shown in Fig. 5.3. The apparent activation energy determined is also indicated in the figure.

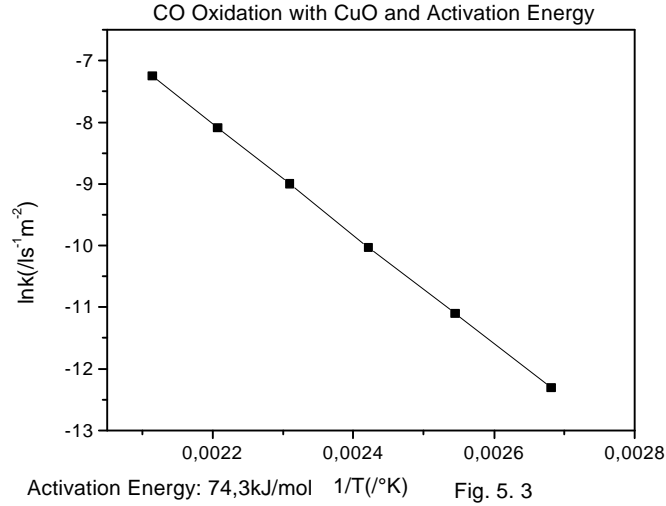


Fig. 5.3: Arrhenius plot for the CuO / graphite mixture. An apparent activation energy of 74.3 kJ/mol is determined.

5.1.2 CO oxidation – using AlCu graphite as catalyst

The results from the CO oxidation at the various flow rates and reaction temperatures investigated are shown in Fig. 5.4. The figure shows the CO conversion as a function of contact time at the operating reactor temperature, which is shown in the diagram.

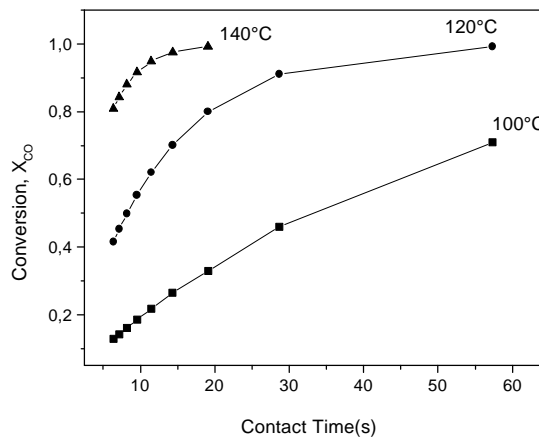
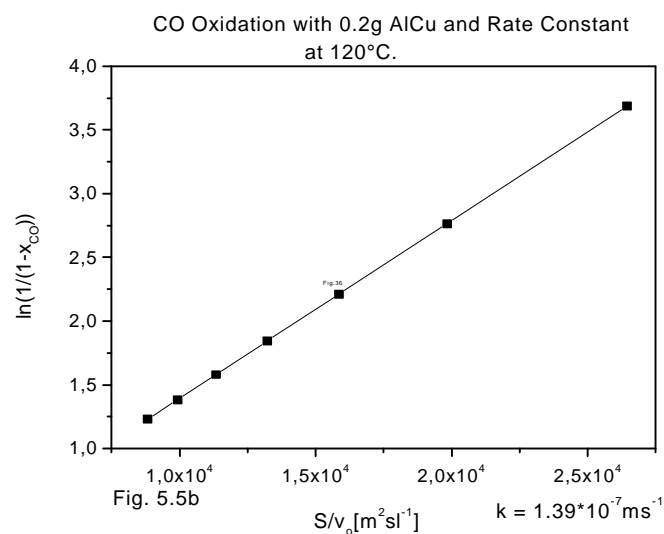
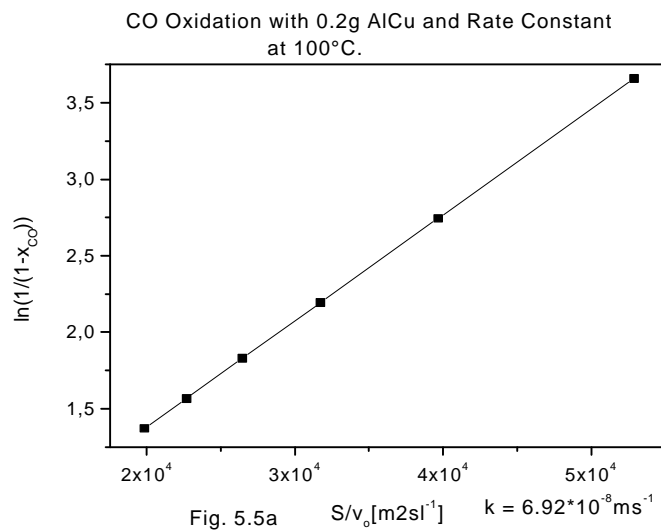


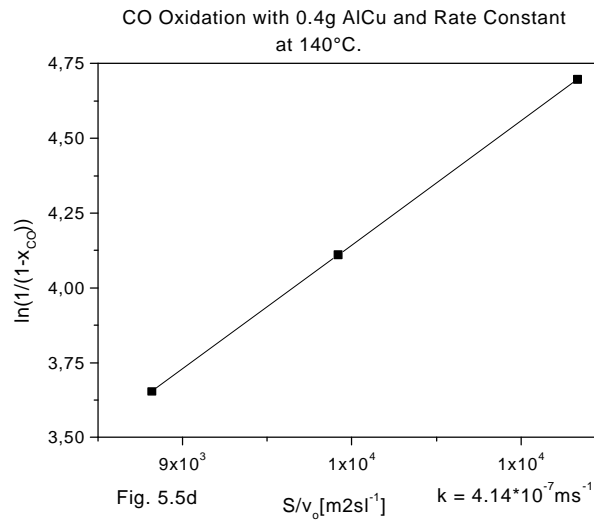
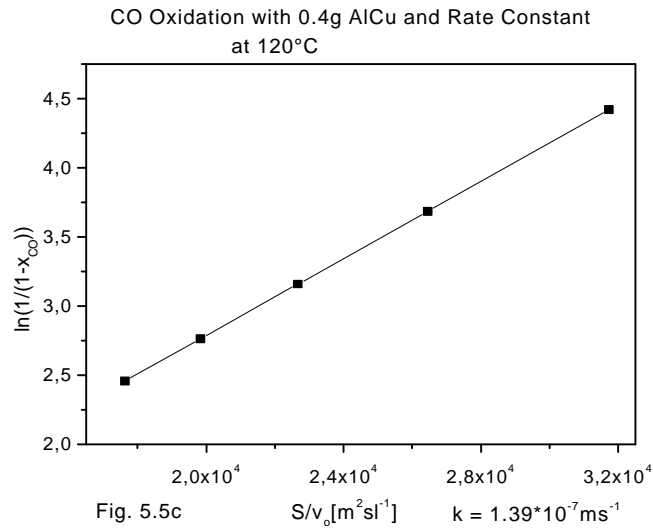
Fig. 5.4 : CO conversion as a function of contact time.
AlCu graphite.

The conversions at the various contact times and investigated temperatures 140°C and above are not indicated on the graph. For these temperatures very high conversions were obtained.

Reaction rate constants – using AlCu graphite as catalyst

Plots of $\ln(1/(1-x_{CO}))$ versus S/v_o at the investigated temperatures are presented for AlCu graphite in Fig. 5.5a to 5.5d. The gradients of the graphs are measures of the rate constants at the investigated reaction temperatures.





Activation energy – using AlCu graphite as Catalyst

A plot of the Arrhenius function using the rate constants and the corresponding reaction temperatures is shown in Fig. 5.6. The apparent activation energy determined is also indicated in the figure.

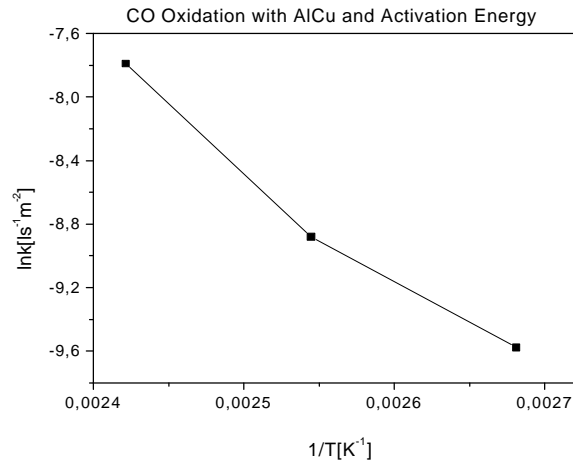


Fig. 5.6: Arrhenius plot for the AlCu graphite. An apparent activation energy of 59.1 kJ/mol is determined.

5.1.3 CO oxidation – using MoCu graphite as catalyst

The results from the CO oxidation at the various flow rates and reaction temperatures investigated are shown in Fig. 5.7. The figure shows the CO conversion as a function of contact time at the operating reactor temperature, which is shown in the diagram.

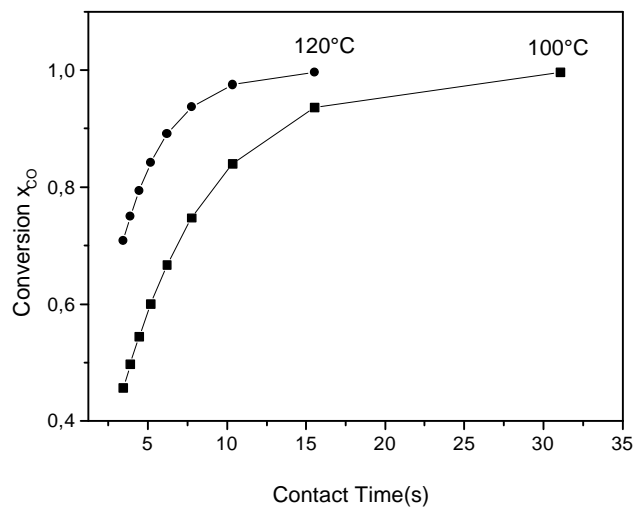
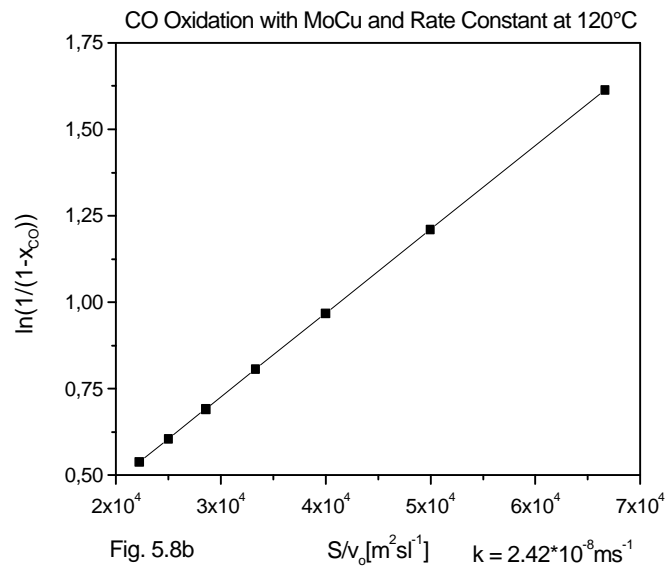
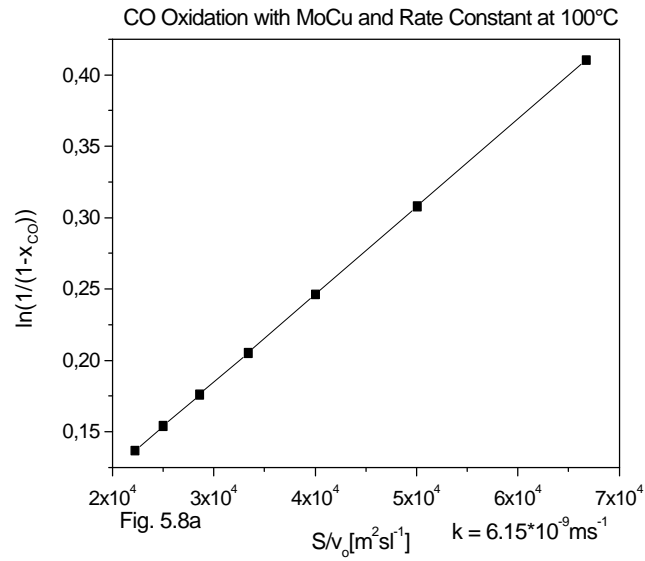
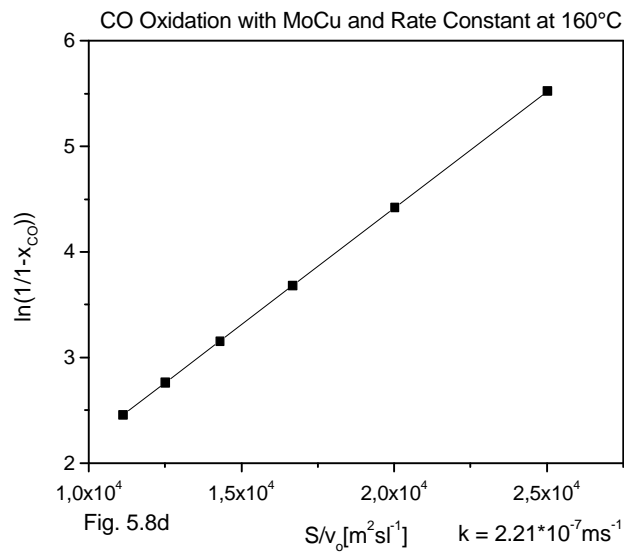
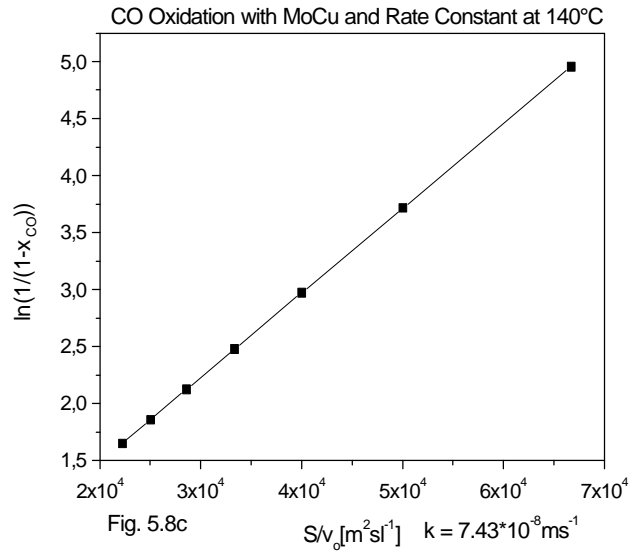


Fig. 5.7 : CO conversion as a function of contact time.
MoCu graphite.

Reaction rate constants – using MoCu graphite as catalyst

Plots of $\ln(1/(1-x_{CO}))$ versus S/v_o at the investigated temperatures are presented for MoCu graphite in Fig. 5.8a to 5.8f. The gradients of the graphs give indication of the rate constants at the investigated reaction temperatures.





Activation energy – using MoCu graphite as Catalyst

A plot of the Arrhenius function using the rate constants and the corresponding reaction temperatures is shown in Fig. 5.9. The apparent activation energy determined is also indicated in the figure.

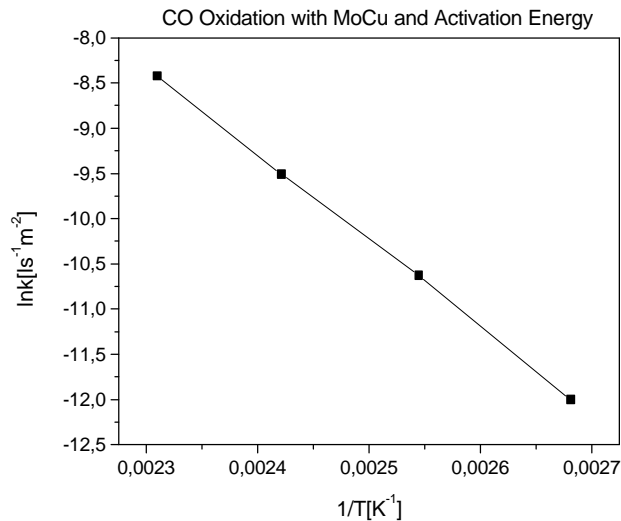


Fig. 5.9: Arrhenius plot for the MoCu graphite. An apparent activation energy of 79.7 kJ/mol is determined.

5.1.4 CO oxidation – using AlMoCu graphite as catalyst

The results from the CO oxidation at the various flow rates and reaction temperatures investigated are shown in Fig. 5.10. The figure shows the CO conversion as a function of contact time at the operating reactor temperature, which is shown in the diagram.

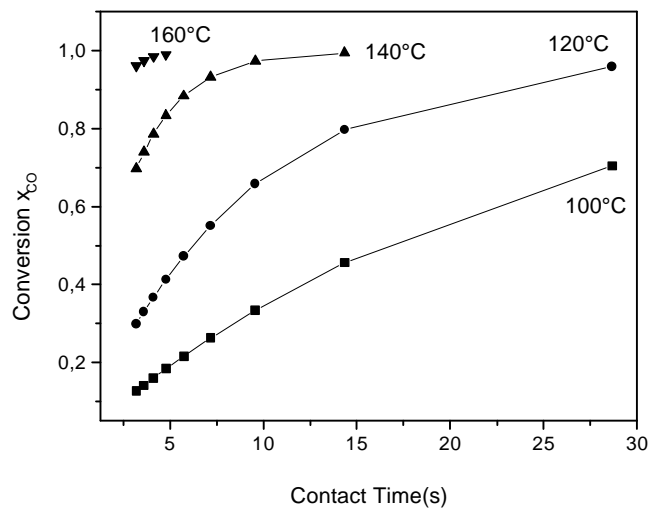
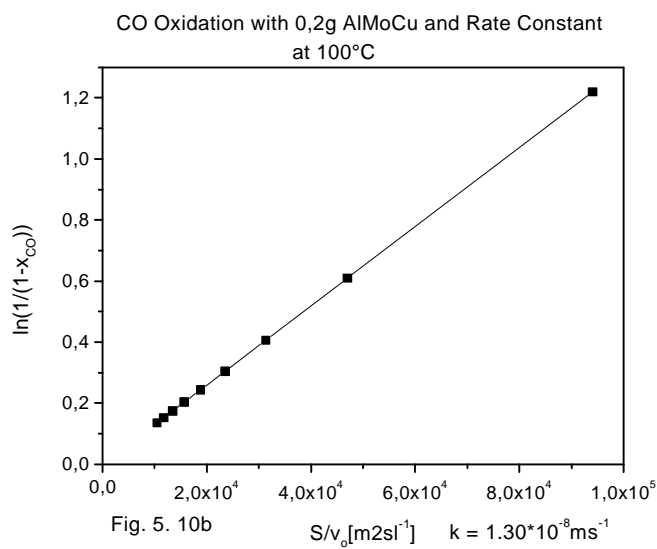
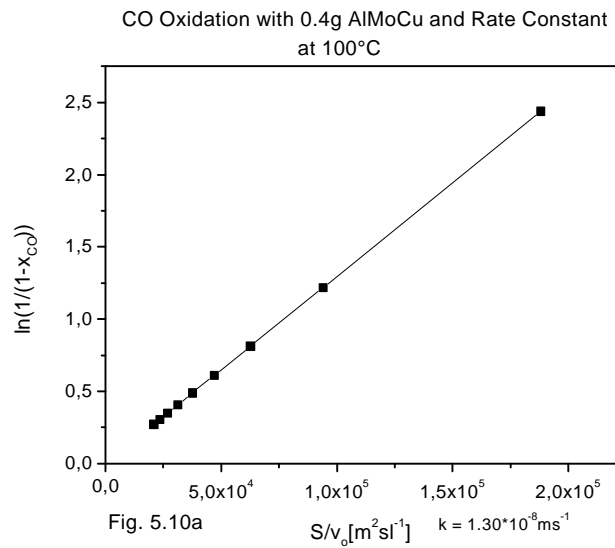
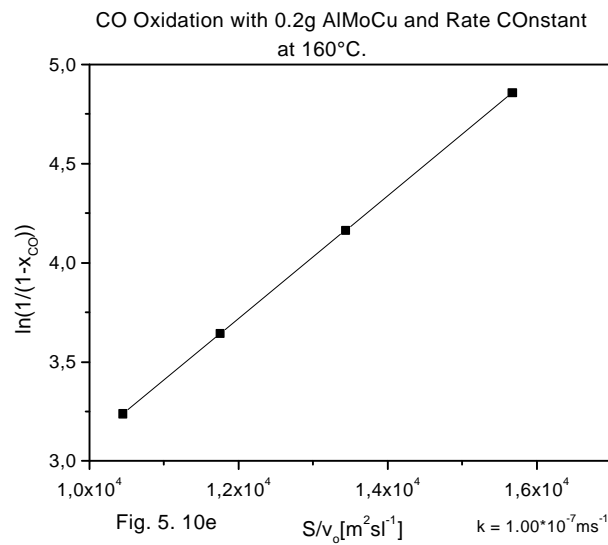
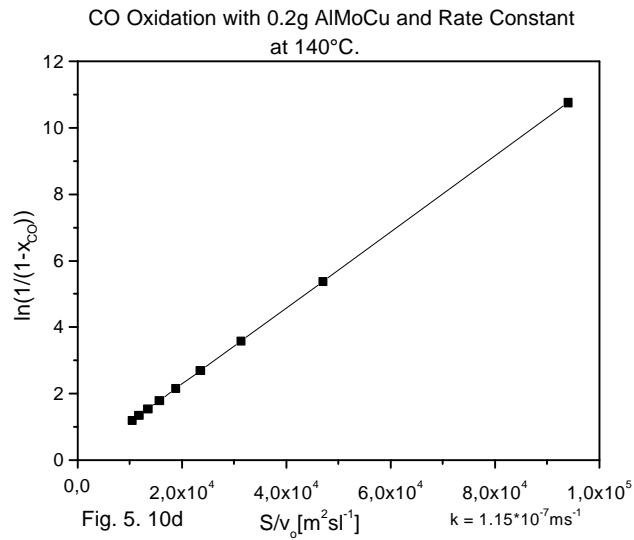
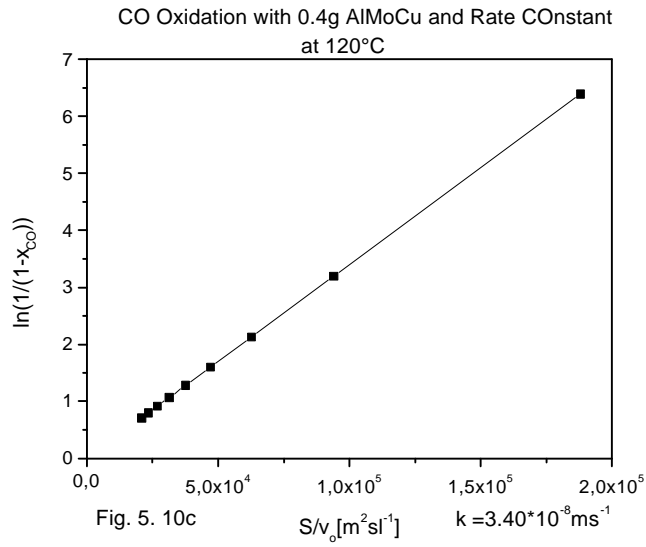


Fig. 5.10 : CO conversion as a function of contact time.
AlMoCu graphite.

Reaction rate constants – using AlMoCu graphite as catalyst

Plots of $\ln(1/(1-x_{\text{CO}}))$ versus S/v_0 at the investigated temperatures are presented for AlMoCu graphite in Fig. 5.10a to 5.10f. The gradients of the graphs give indication of the rate constants at the investigated reaction temperatures.





Activation energy – using AlMoCu graphite as Catalyst

A plot of the Arrhenius function using the rate constants and the corresponding reaction temperatures is shown in Fig. 5.11. The apparent activation energy determined is also indicated in the figure.

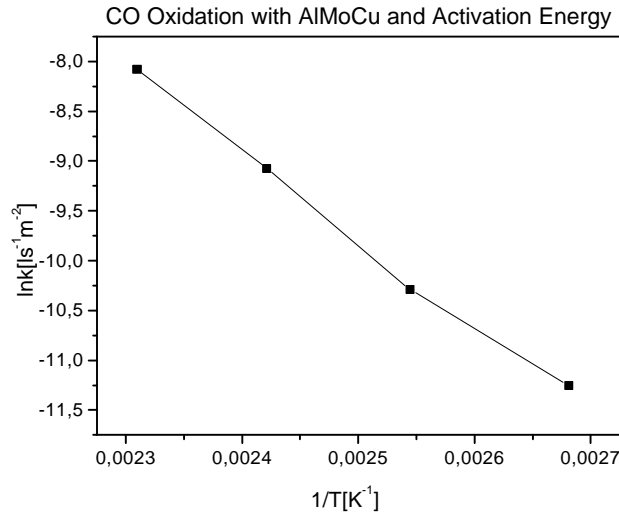


Fig. 5.11: Arrhenius plot for the AlMoCu graphite. An apparent activation energy of 71.9kJ/mol is determined.

5.1.5 CO oxidation – using FeCu graphite as catalyst

The results from the CO oxidation at the various flow rates and reaction temperatures investigated are shown in Fig. 5.12. The figure shows the CO conversion as a function of contact time at the operating reactor temperature, which is shown in the diagram.

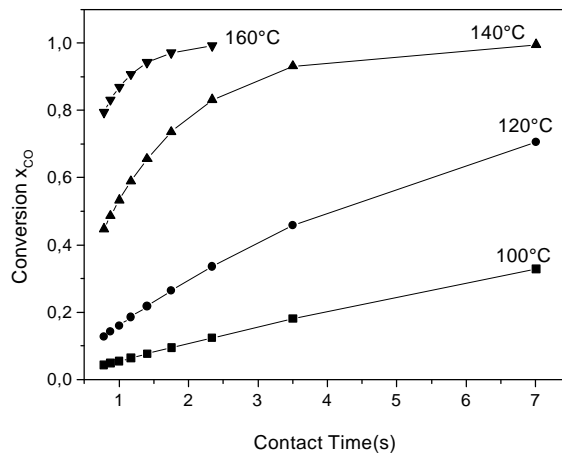
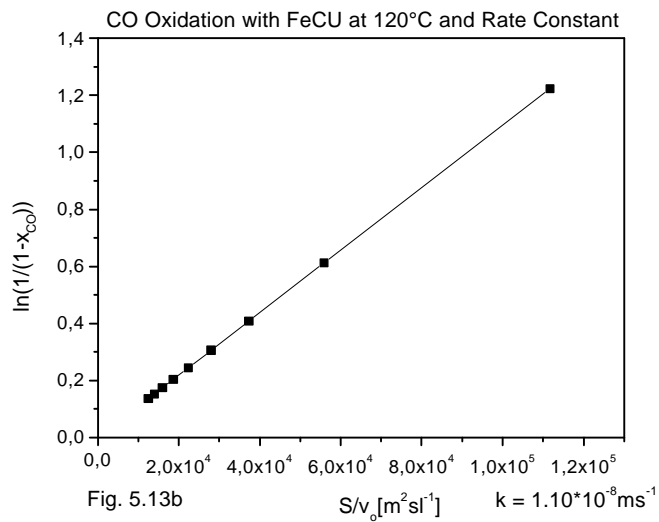
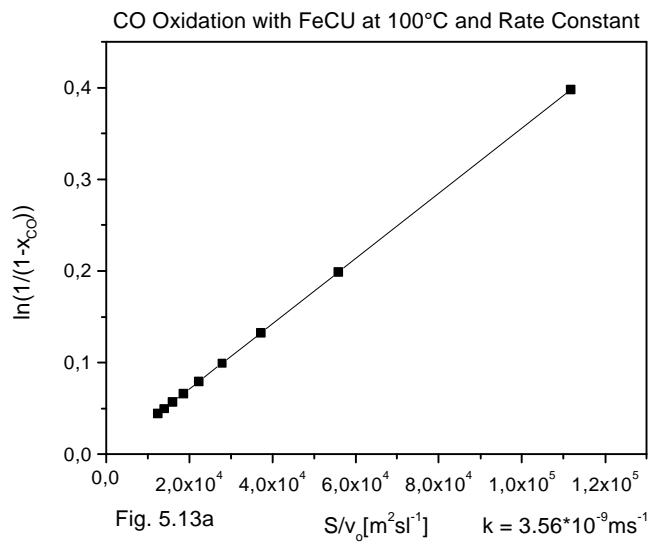
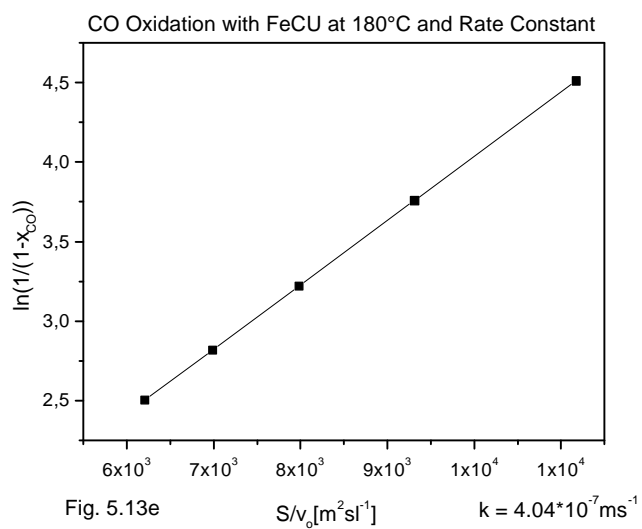
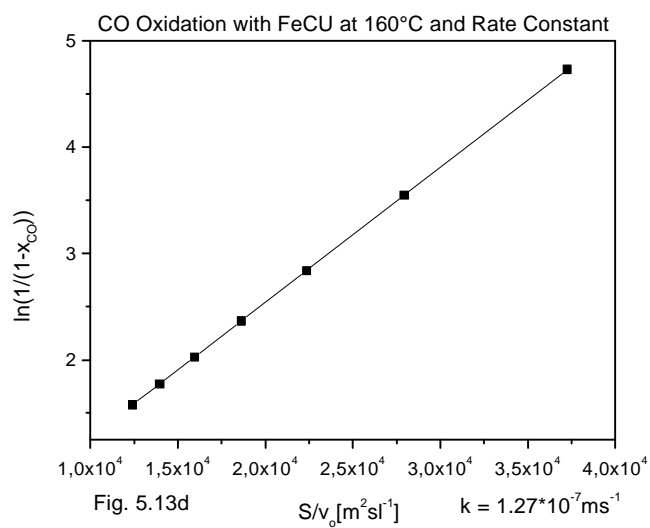
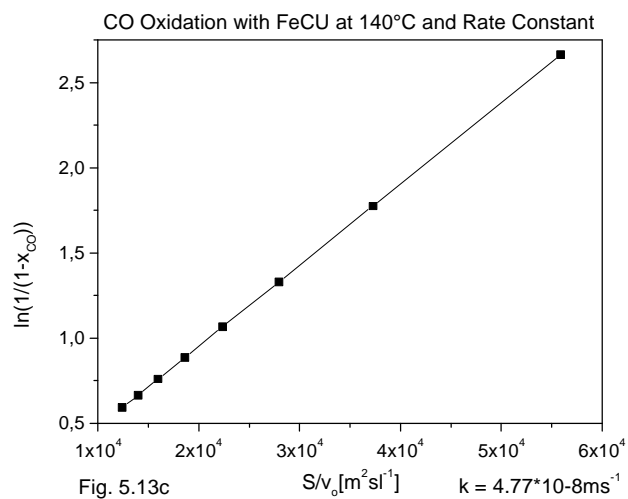


Fig. 5.12 : CO conversion as a function of contact time. FeCu graphite.

Reaction rate constants – using FeCu graphite as catalyst

Plots of $\ln(1/(1-x_{\text{CO}}))$ versus S/v_o at the investigated temperatures are presented for FeCu graphite in Fig. 5.13a to 5.13f. The gradients of the graphs give indication of the rate constants at the investigated reaction temperatures.





Activation energy – using FeCu graphite as Catalyst

A plot of the Arrhenius function using the rate constants and the corresponding reaction temperatures is shown in Fig. 5.14. The apparent activation energy determined is also indicated in the figure.

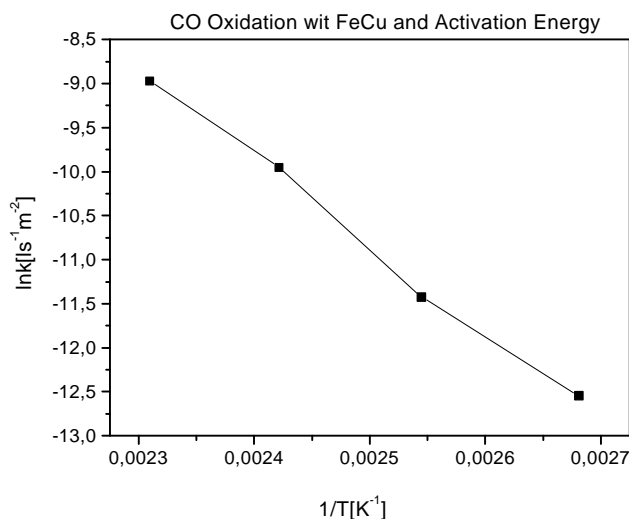


Fig. 5.14: Arrhenius plot for the FeCu graphite. An apparent activation energy of 81.8 kJ/mol is determined.

5.2 NO Decomposition

The decomposition of NO was done in the absence of O_2 . Reaction gas mixtures made up of various NO concentrations in He were used. Test gas was prepared by diluting the 1 volume percent NO in helium by increasing the helium component. Results for the catalytic NO decomposition reaction for the various catalytic substances prepared are presented. The reaction gas flow rate ranged from 0.5 l/hr to 4.5 l/hr. Different quantities (0.2 g to 0.8 g) of each catalyst were also tested. Similar to the presentation of the results in the CO oxidation reaction, the conversion of NO, based on N_2 turnover in the decomposition reaction, are plotted against contact time for all the catalysts tested. The NO turnover as a function of its concentration was found to follow first order reaction mechanism. Consequently, the rate constants at the various investigated reaction temperatures were determined. The apparent activation energies for the catalysts were also determined and are presented.

The NO decomposition reaction is represented as:



A plot of NO conversion into N_2 at the measured reaction gas flow rates and the corresponding temperatures is indicated in Fig. 5.15. In the figure S represents the surface area of the catalyst used. ω_{NO_0} (see section 3.1.8) represents the initial nitric oxide molar flow rate. In each trial 0.4g of catalyst material is used. The initial NO concentrations in He were roughly 500ppm in all the trials.

Further evaluation is based on the formula given in 3.1.8, $r = (x_A - x_{A0})/(V_a/\omega_{A0})$, where the volume of the reactor is replaced by S , the surface area of the catalyst, as explained in 3.1.8. In consequence of this, the reaction rate k and all dependent parameters changes their dimension.

Plots of reaction rates versus concentration at the investigated temperatures are presented for all the prepared samples and give the reaction rate constants. These values are used in the Arrhenius equation to determine the activation energies of NO decomposition reaction for all prepared catalysts.

5.2.1 NO decomposition – using CuO / graphite mixture as catalyst

In each trial 0.4 g of catalyst material is used. The initial NO concentrations in He were roughly 500 ppm in the following trials.

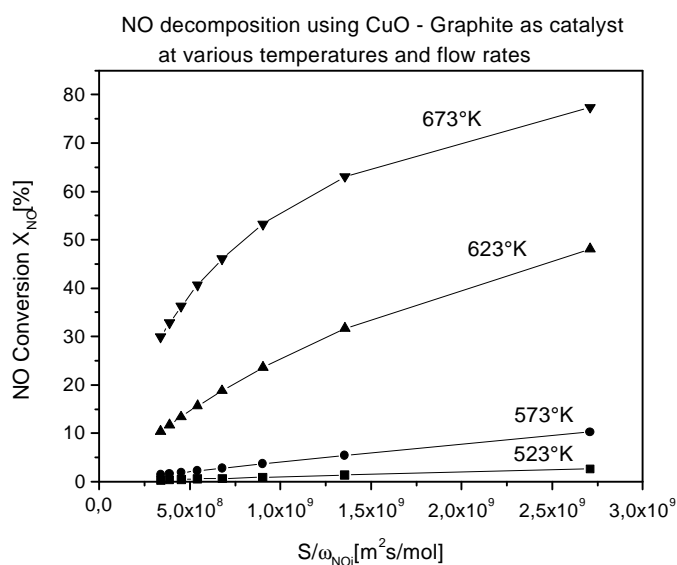
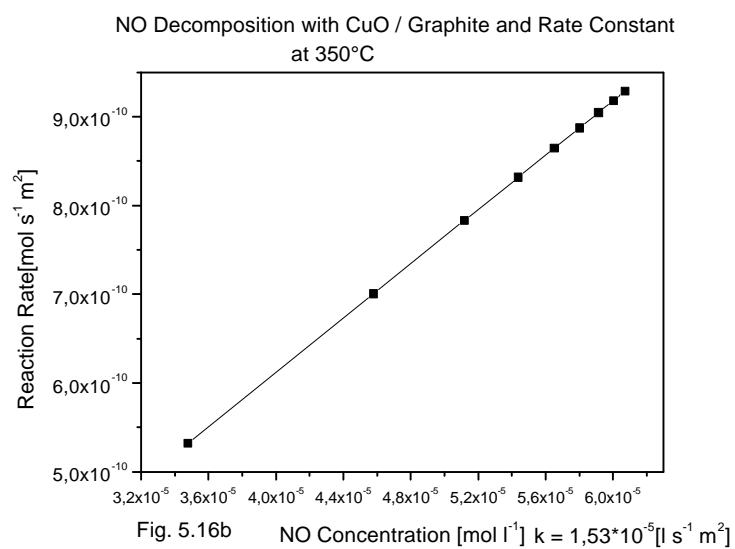
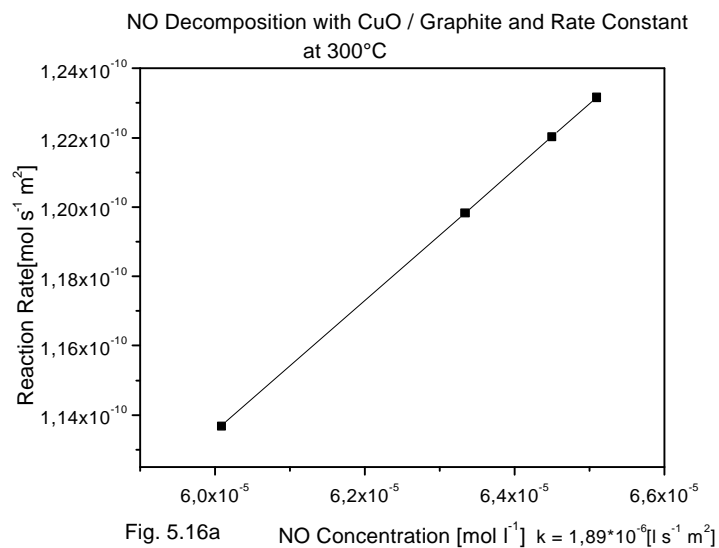
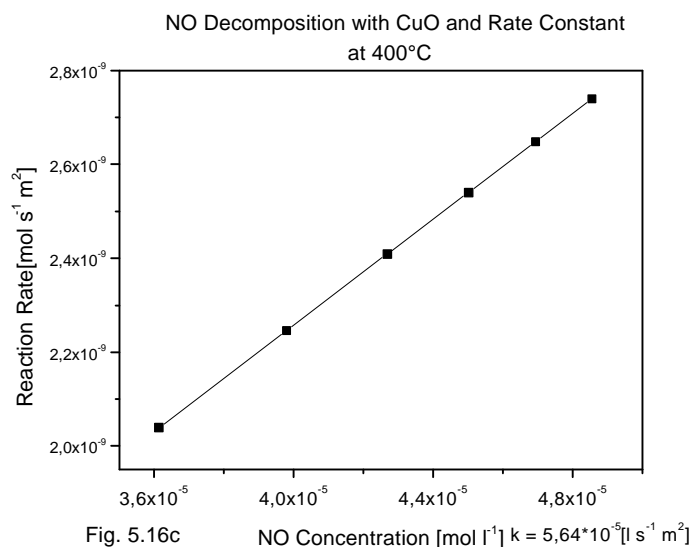


Fig. 5.15 : NO conversion as a function of molar feed rate.
Mixture of CuO and graphite.

Reaction rate constants – using CuO / graphite mixture as catalyst

Plots of reaction rate versus concentrations at the investigated temperatures are presented for CuO/ graphite mixture in Fig. 5.16a to 5.16c. The initial concentrations of NO were 1500 ppm in He.





Activation energy – using CuO / graphite mixture as catalyst

A plot of the Arrhenius function using the rate constants and the corresponding reaction temperatures is shown in Fig. 5.17. The apparent activation energy determined is also indicated in the figure.

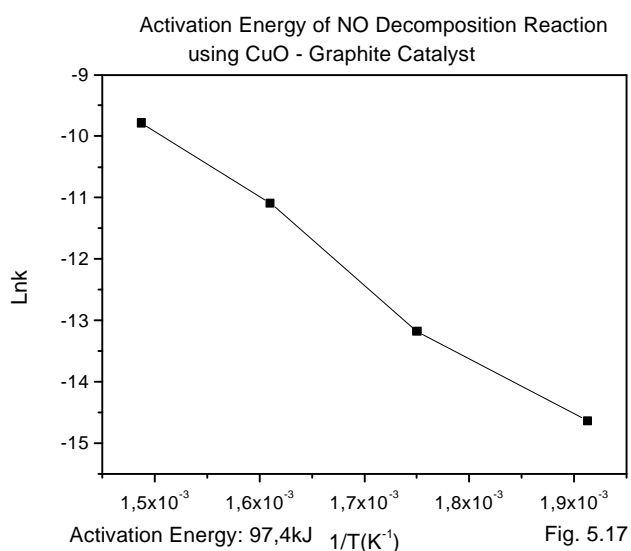


Fig. 5.17: Arrhenius plot for the CuO graphite mixture.

An apparent activation energy of 97.4kJ/mol is determined.

5.2.2 NO Decomposition – using AlCu graphite as catalyst

A plot of NO conversion into N_2 at the measured reaction gas flow rates and the corresponding temperatures are indicated in Fig. 5.18. In the figure S represents the surface area (m^2) of the catalyst used. ω_{NOi} represents nitric oxide molar flow rate (mol/s). In each trial 0.4g of catalyst material is used. The initial NO concentrations were 500ppm in all the trials.

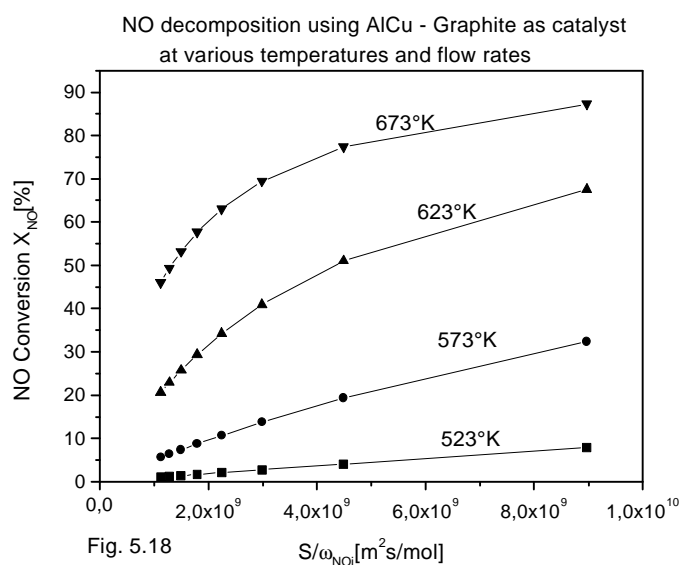
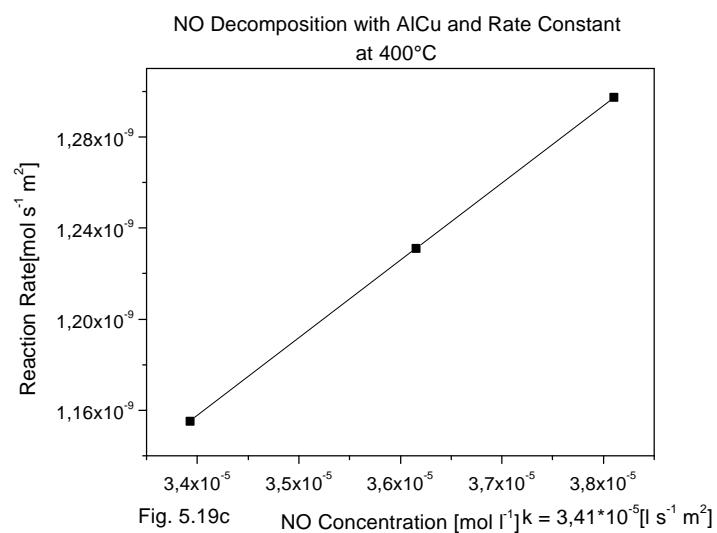
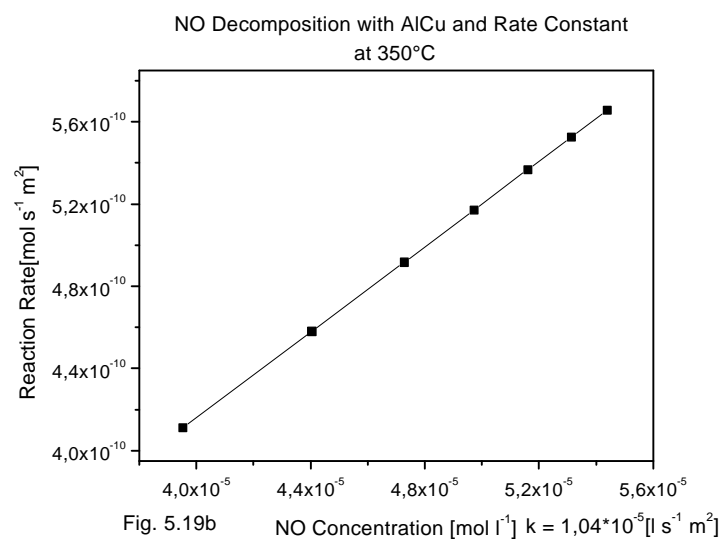
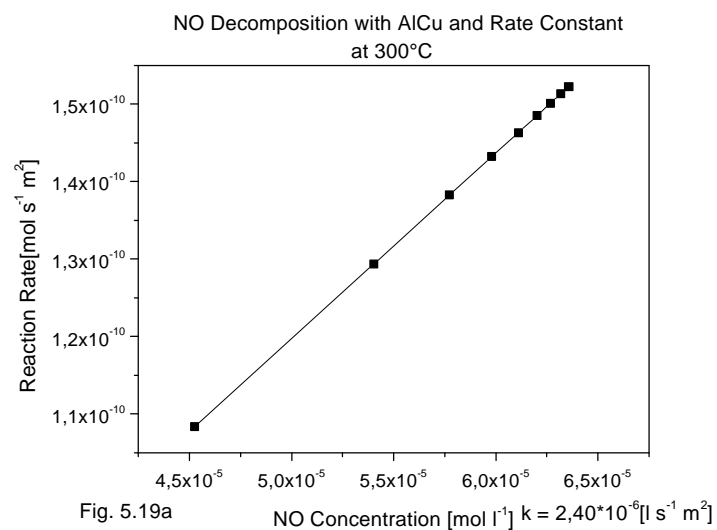


Fig. 5.18 : CO conversion as a function of molar feed rate.
AlCu graphite.

Reaction rate constants – using AlCu graphite as catalyst

Plots of reaction rate versus concentrations at the investigated temperatures are presented for AlCu graphite in Fig. 5.19a to 5.19c. The initial concentrations of NO were 1500ppm in He.



Activation energy – using AlCu graphite as Catalyst

A plot of the Arrhenius function using the rate constants and the corresponding reaction temperatures is shown in Fig. 5.20. The apparent activation energy determined is also indicated in the figure.

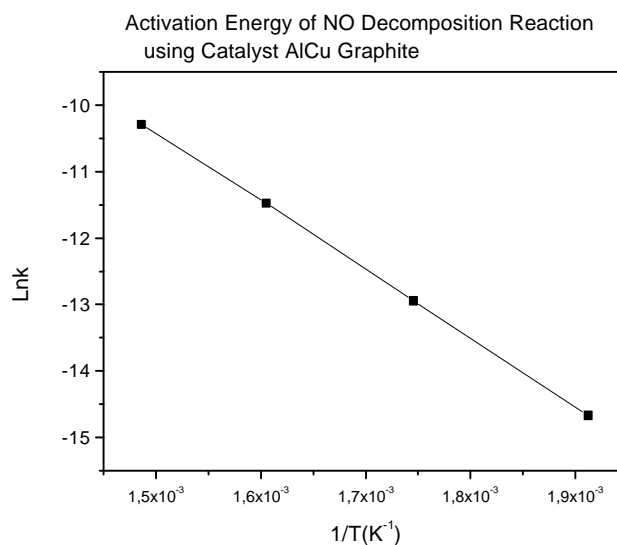


Fig. 5.20: Arrhenius plot for the AlCu graphite. An apparent activation energy of 85.6kJ/mol is determined.

5.2.3 NO Decomposition – using AlMoCu graphite as catalyst

A plot of NO conversion into N_2 at the measured reaction gas flow rates and the corresponding temperatures are indicated in Fig. 5.21. In the figure A represents the surface area (m^2) of the catalyst used. F_{NOi} represents nitric oxide molar flow rate (mol/s). In each trial 0.4g of catalyst material is used. The initial NO concentrations were 500ppm in all the trials.

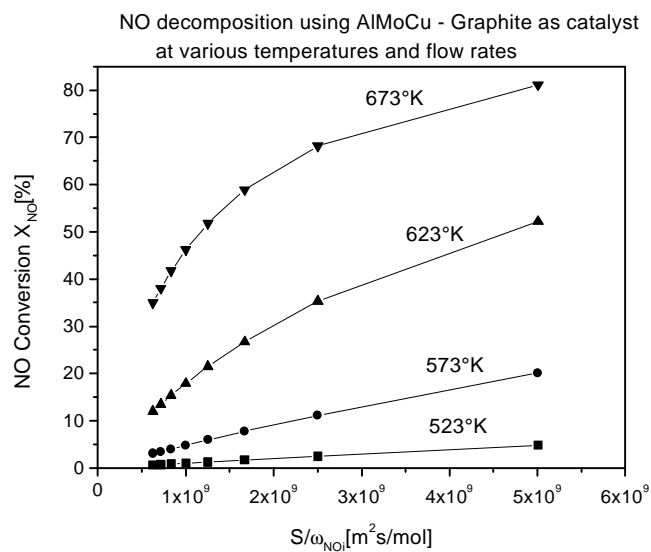
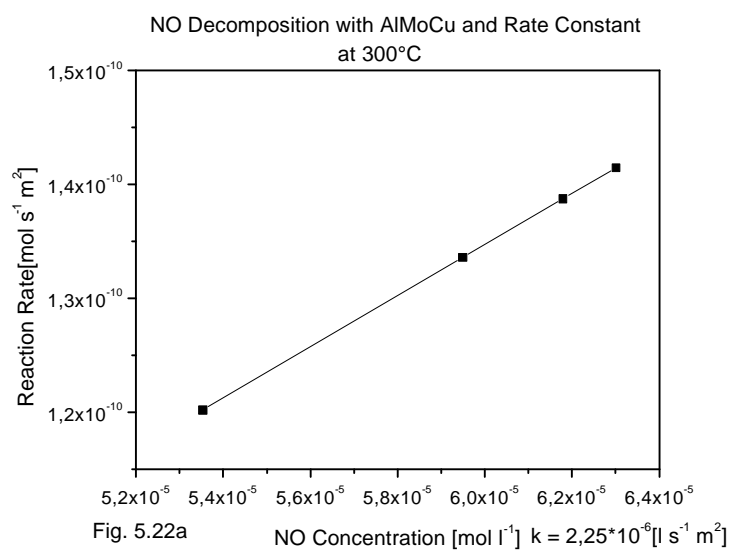
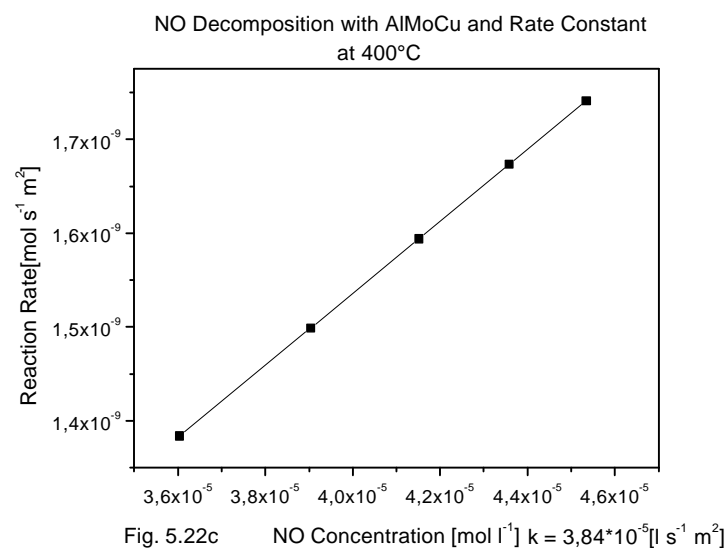
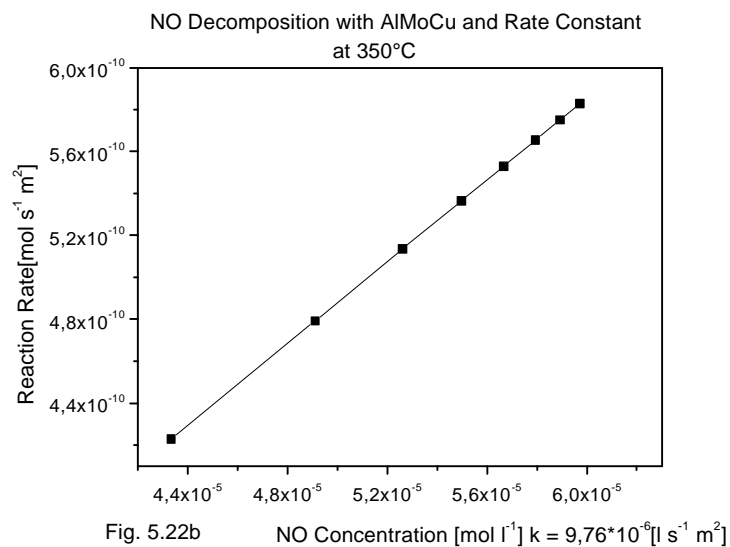


Fig. 5.21 : CO conversion as a function of molar feed rate.
AlMoCu graphite.

Reaction rate constants – using AlMoCu graphite as catalyst

Plots of reaction rate versus concentrations at the investigated temperatures have been presented for AlMoCu graphite in Fig. 5.22a to 5.22c. The initial concentrations of NO were 1500ppm in He.





Activation energy – using AlMoCu graphite as Catalyst

A plot of the Arrhenius function using the rate constants and the corresponding reaction temperatures is shown in Fig. 5.23. The apparent activation energy determined is also indicated in the figure.

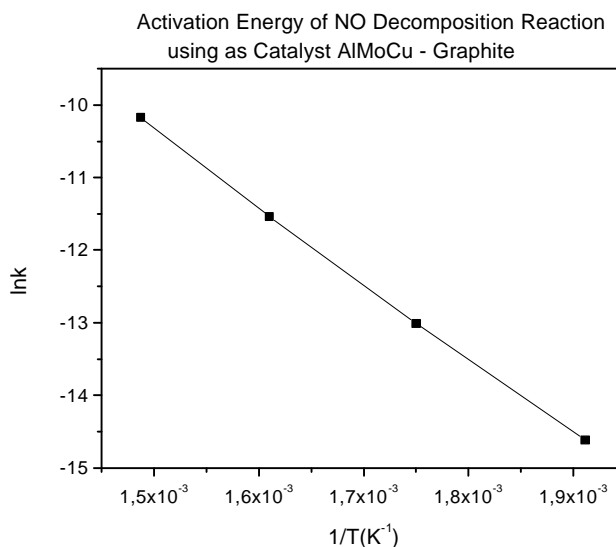


Fig. 5.23: Arrhenius plot for the AlMoCu graphite. An apparent activation energy of 87.0 kJ/mol is determined.

5.2.4 NO Decomposition – using MoCu graphite as catalyst

A plot of NO conversion into N_2 at the measured reaction gas flow rates and the corresponding temperatures are indicated in Fig. 5.24. In the figure S represents the surface area (m^2) of the catalyst used. ω_{NO_i} represents nitric oxide molar flow rate (mol/s). In each trial 0.4g of catalyst material is used. The initial NO concentrations were 500ppm in all the trials.

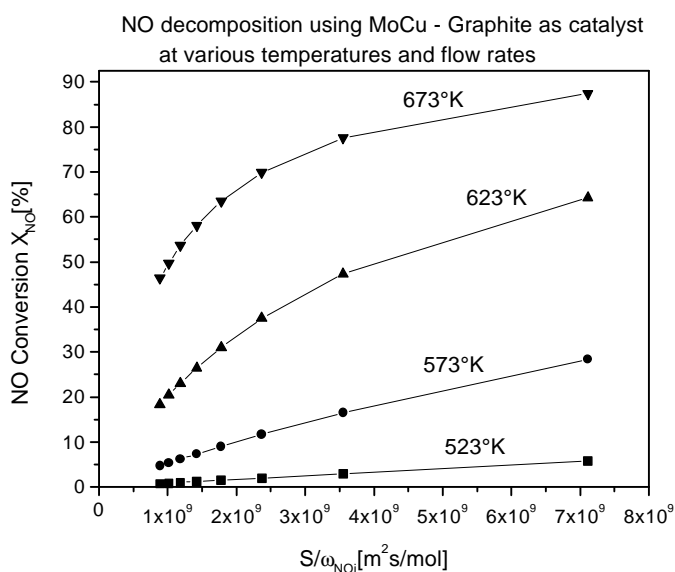
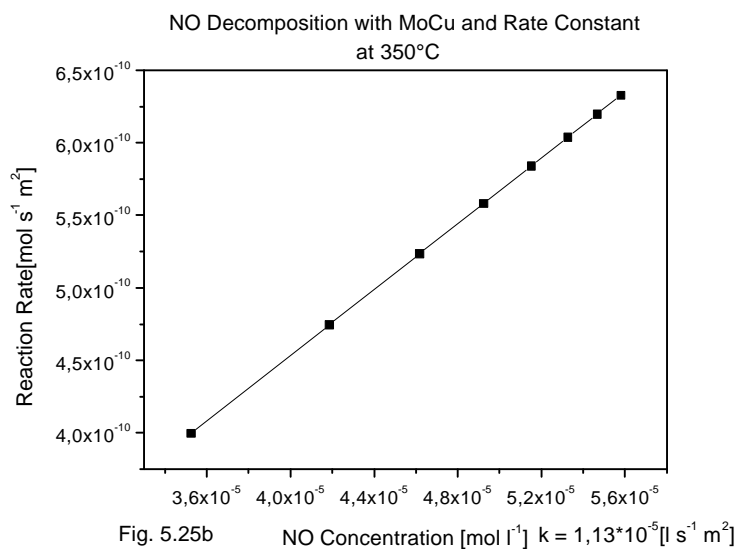
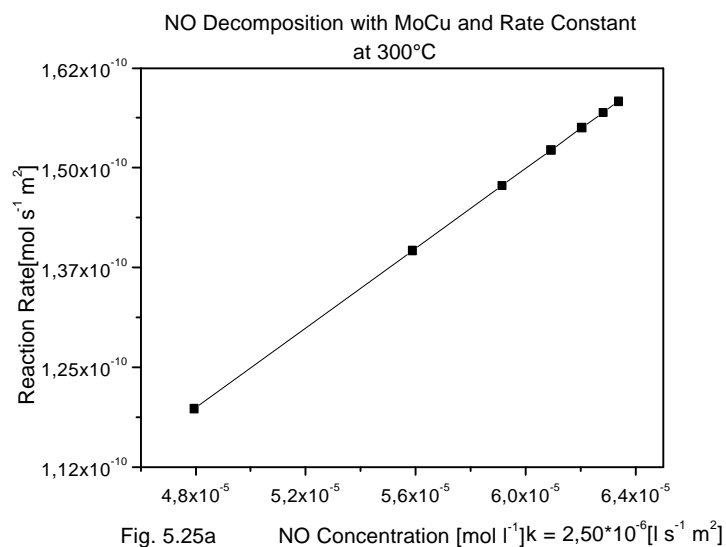
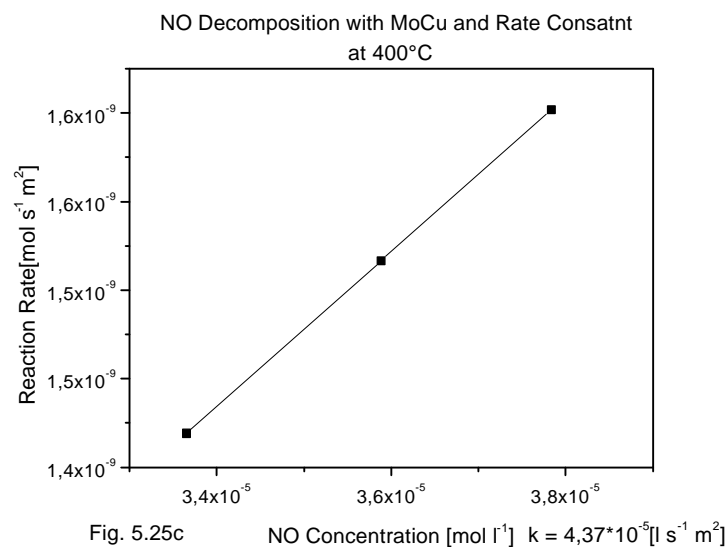


Fig. 5.24 : NO conversion as a molar feed rate. MoCu graphite

Reaction rate constants – using MoCu graphite as catalyst

Plots of reaction rate versus concentrations at the investigated temperatures have been presented for MoCu graphite in Fig. 5.25a to 5.25c. The initial concentrations of NO were 1500ppm in He.





Activation energy – using MoCu graphite as Catalyst

A plot of the Arrhenius function using the rate constants and the corresponding reaction temperatures is shown in Fig. 5.26. The apparent activation energy determined is also indicated in the figure.

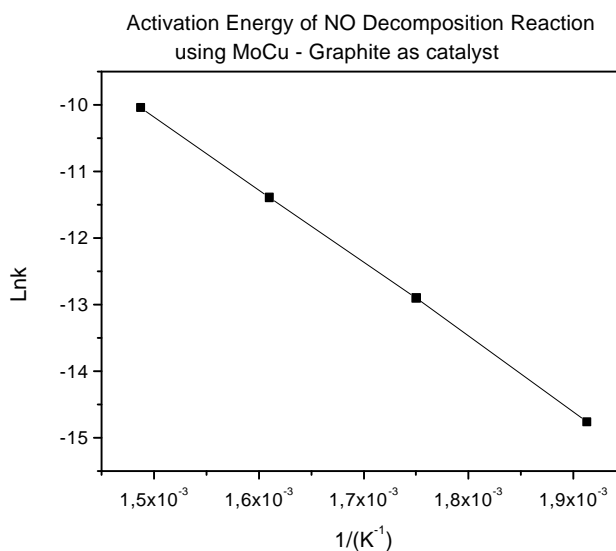


Fig. 5.26: Arrhenius plot for the MoCu graphite. An apparent activation energy of 92.2kJ/mol is determined.

5.2.5 NO Decomposition – using FeCu graphite as catalyst

A plot of NO conversion into N_2 at the measured reaction gas flow rates and the corresponding temperatures are indicated in Fig. 5.27. In the figure S represents the surface area (m^2) of the catalyst used. ω_{NOi} represents nitric oxide molar flow rate (mol/s). In each trial 0.4g of catalyst material is used. The initial NO concentrations were 500ppm in all the trials.

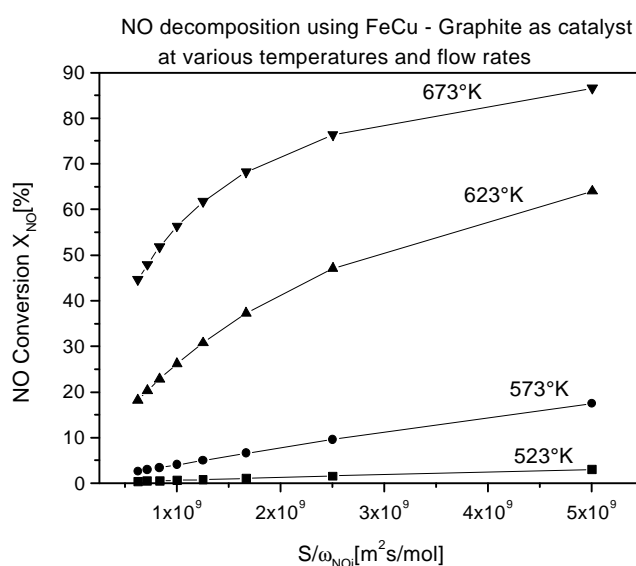
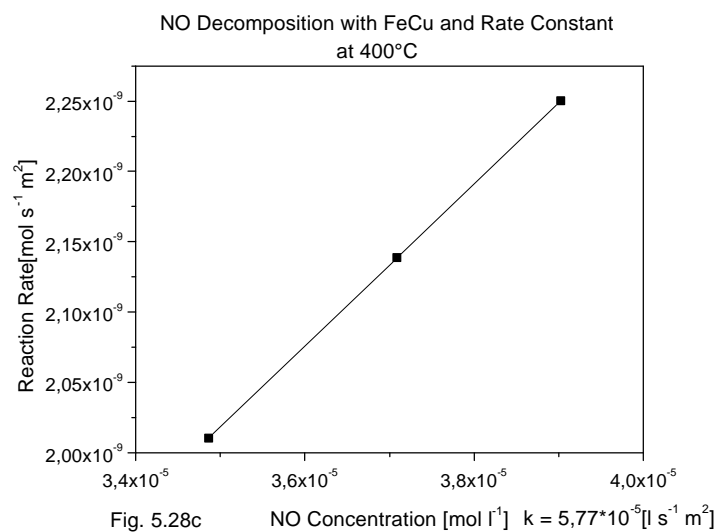
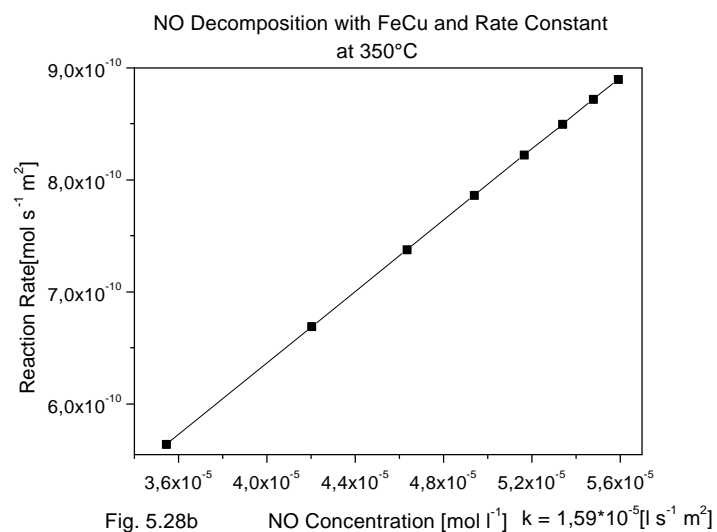
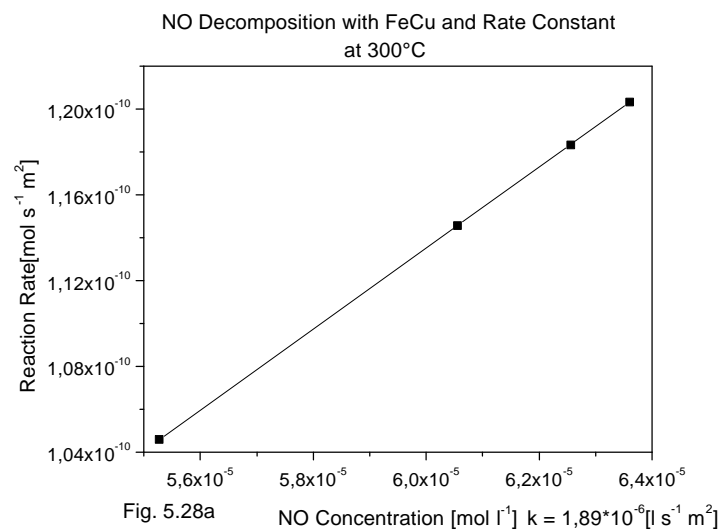


Fig. 5.27 : NO conversion as a function of molar feed rate.
FeCu graphite.

Reaction rate constants – using FeCu graphite as catalyst

Plots of reaction rate versus concentrations at the investigated temperatures have been presented for FeCu graphite in Fig. 5.28a to 5.28c. The initial concentrations of NO were 1500ppm in He.



Activation energy – using FeCu graphite as Catalyst

A plot of the Arrhenius function using the rate constants and the corresponding reaction temperatures is shown in Fig. 5.29. The apparent activation energy determined is also indicated in the figure.

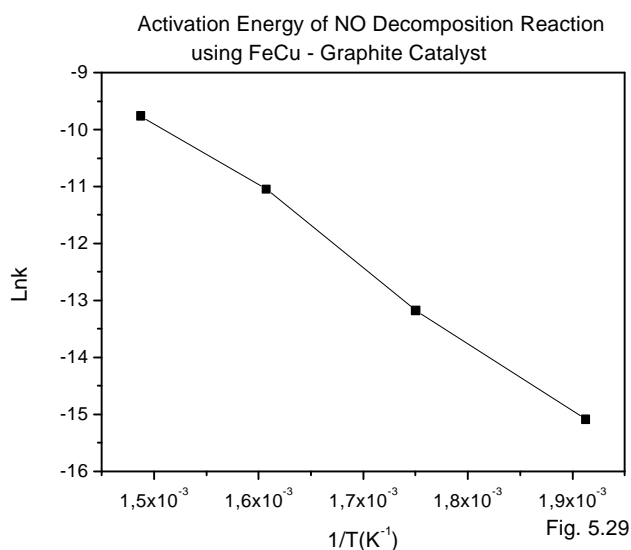


Fig. 5.29: Arrhenius plot for the FeCu graphite. An apparent activation energy of 106.1 kJ/mol is determined.

5.3 Activity Tests of CeO₂ graphite

CO oxidation and NO decomposition were tested using the prepared exfoliated Ce (IV) nitrate graphite compound and a mixture of pulverised CeO₂ and graphite for comparison purposes. Reduction of NO with CO was also tested but will be discussed together with the other catalysts in section 5.4.

The mixture of CeO₂ and graphite applied here is referred further in this work as “free CeO₂”. The free CeO₂ was made up of roughly one part by weight of CeO₂ and four parts by weight of graphite to correspond to the composition of the exfoliated Ce(IV)nitrate graphite compound. 0.6g of each of the catalyst material was used in the following tests.

Of all the catalysts prepared and tested in this work, CeO_2 graphite has the least thermal stability. Under the reaction conditions tested, large quantities of carbon burnt out were observed, even at very low temperatures when oxygen is available. For this reason, several measurements could not be taken for convincing kinetic data to be presented.

The results of the measurements carried out in the tests are presented diagrammatically.

5.3.1 CO – Oxidation using CeO_2 graphite and free CeO_2 .

CO oxidation reactions, using these catalysts were carried out at constant flow rate (2 l/h), which is roughly equal to the average flow of the various flow rates investigated in all the other cases. Temperature of reactions investigated ranged from 80° to 300°C. 0.1% Volume of CO in He and 0.1% Volume of synthetic air (O_2/N_2 ratio 1:4) in He were employed for the CO oxidation reaction tests. A reaction mixture of CO and O_2 – with overwhelming proportion of O_2 – was tested. The CO turnover at the investigated operational temperatures were measured for the prepared CeO_2 graphite and free CeO_2 catalysts.

The results of the tests for CeO_2 graphite and free CeO_2 are presented diagrammatically below. In the figure 5.30 shown below the conversion, x_{CO} , of CO to CO_2 at the tested reaction temperatures and flow rate are presented.

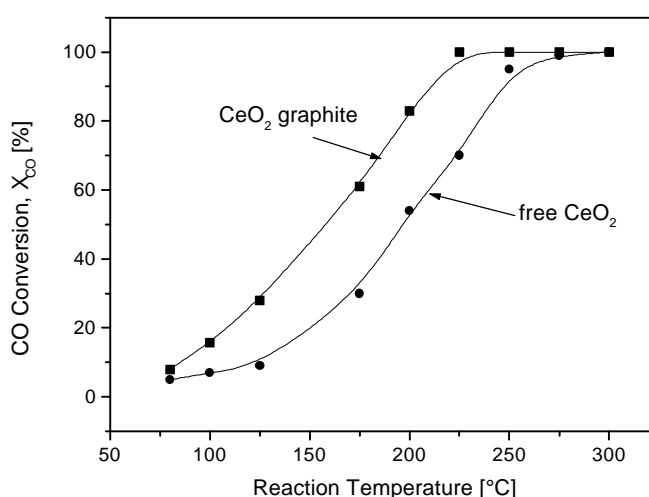


Fig.5.30: CO oxidation using CeO_2 graphite and free CeO_2 as catalyst.
(Other reaction conditions : see text)

5.3.2 NO – decomposition using CeO₂ graphite and free CeO₂.

The decomposition of NO was done in the absence and also in the presence of O₂. Reaction gas mixtures made up of 1000 ppm NO in He and a mixture of 1000 ppm NO in He and 1000 ppm O₂ in He were tested for CeO₂ graphite and free CeO₂. The reaction temperatures were from 80°C to 400°C in all cases. The flow rate investigated was 2l/h. In the absence of oxygen no practicable conversion was realised for NO conversion and the results are therefore not presented here. In figure 5.31 shown below, NO conversions into N₂ as a function of temperature are presented for CeO₂ graphite and free CeO₂ catalysts.

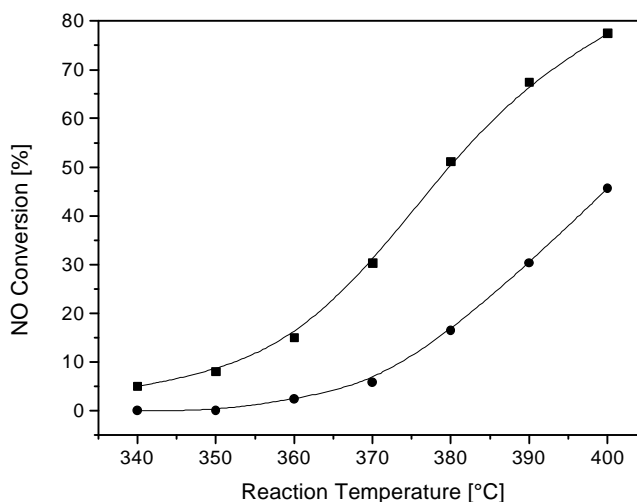


Fig.5.31:NO decomposition using CeO₂ graphite and free CeO₂ as catalyst.

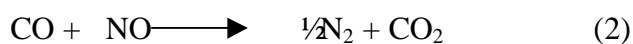
(Other reaction conditions : see text)

5.4 CO - NO Redox Reaction

NO reductions with CO were carried out, applying exfoliated graphite substances, all prepared in this work and containing copper oxide. It is to be noted, that the NO reduction with CO does not run selectively, especially in the presence of O₂ as in automobile exhaust tests. In this case CO oxidation is highly favoured. The portion of NO that gets reduced becomes very small in oxygen environment. The catalytic CO – NO redox reactions are

therefore performed without the addition of O₂ from external source. In these trials, 0.4g of catalyst material and 1000 ppm of NO and CO in He at 2l/h reaction gas flow rates, are tested.

The NO - CO redox reaction is represented as:



The conversion of NO and CO at the investigated temperatures for all the tested catalysts are diagrammatically presented.

5.4.1 NO - CO redox reaction – using CuO / graphite mixture as catalyst

The results obtained are presented as nitric oxide converted into nitrogen and carbon dioxide produced from the inserted carbon monoxide at the investigated temperatures. Figure 5.32 shows the results obtained for CuO / graphite mixture.

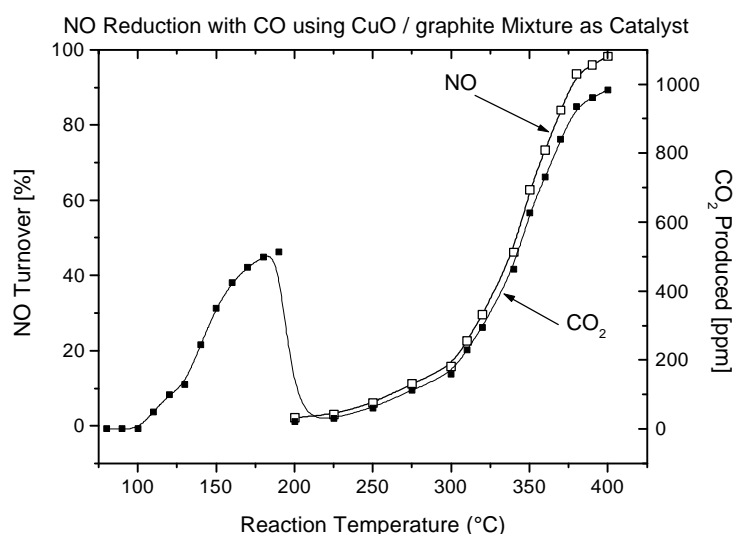


Fig.5.32. : NO reduction with CO using CuO / graphite mixture as Catalyst.

Other reaction conditions : see text

5.4.2 NO - CO redox reaction – using AlCu graphite as catalyst

The results obtained are presented as nitric oxide converted into nitrogen and carbon dioxide produced from the inserted carbon monoxide at the investigated temperatures. Figure 5.33 indicates the results obtained for AlCu graphite.

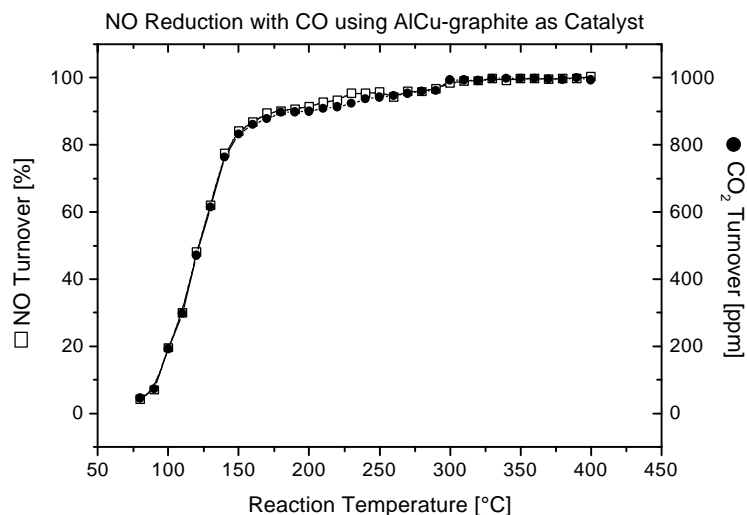


Fig.5.33. : NO reduction with CO using AlCu graphite as Catalyst.
(Other reaction conditions : see text)

5.4.3 NO - CO redox reaction – using FeCu graphite as catalyst

The results obtained are presented as nitric oxide converted into nitrogen and carbon dioxide produced from the inserted carbon monoxide at the investigated temperatures. Figures 5.34 indicates the results obtained for FeCu graphite.

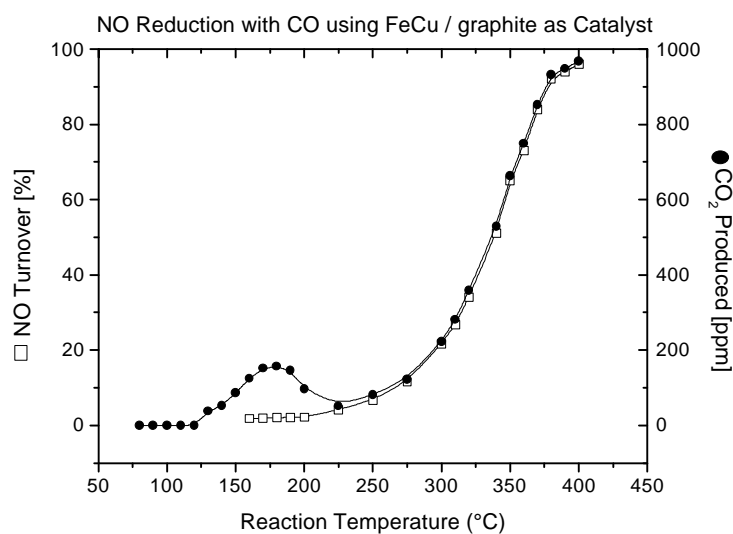


Fig.5.34: NO reduction with CO using FeCu graphite as Catalyst.
(Other reaction conditions : see text)

5.4.4 NO - CO redox reaction – using AlMoCu graphite as catalyst

The results obtained are presented as nitric oxide converted into nitrogen and carbon dioxide produced from the inserted carbon monoxide at the investigated temperatures. Figures 5.35 represents the results obtained for AlMoCu graphite.

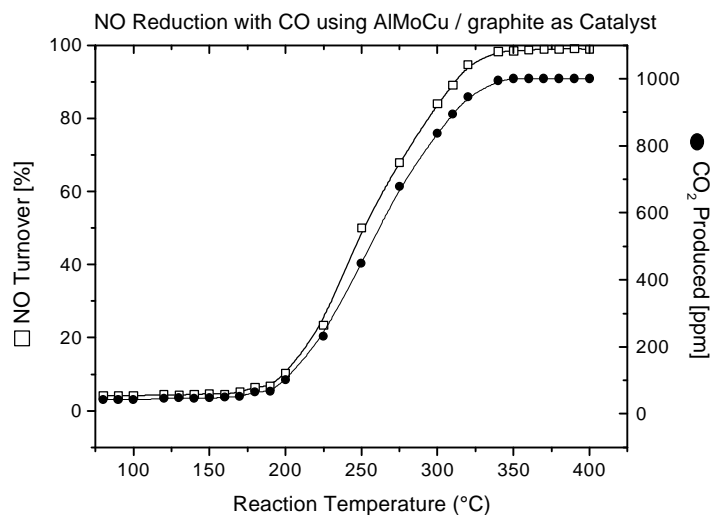


Fig.5.35: NO reduction with CO using AlMoCu / graphite as Catalyst.

(Other reaction conditions : see text)

5.4.5 NO - CO redox reaction – using MoCu graphite as catalyst

The results obtained are presented as nitric oxide converted into nitrogen and carbon dioxide produced from the inserted carbon monoxide at the investigated temperatures. Figures 5.36 represents the results obtained for MoCu.

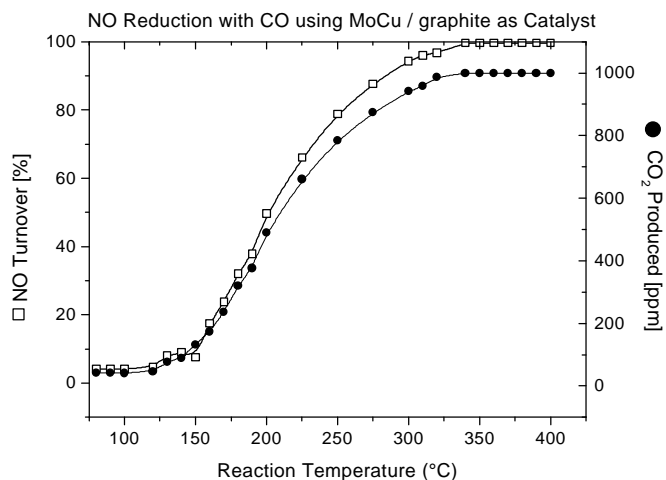


Fig.5.36: NO reduction with CO using MoCu / as Catalyst.

(Other reaction conditions : see text)

5.4.6: NO – CO Redox using CeO₂ graphite and free CeO₂.

In these tests, 1000 ppm NO and 1000 ppm CO in Helium were used. Reaction gas flow rate was kept at 2l/h. The results obtained are presented as nitric oxide converted into nitrogen and carbon dioxide produced from the inserted carbon monoxide at the investigated temperatures. Figures 5.37a and 5.37b represent the results obtained for CeO₂ graphite and free CeO₂ respectively.

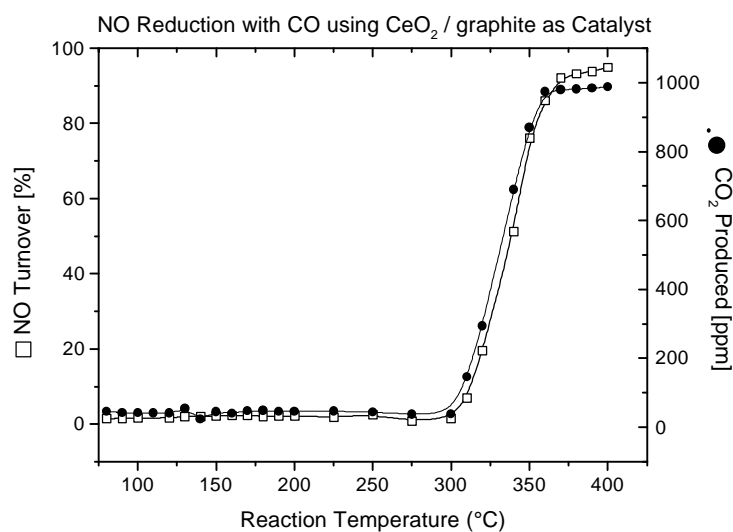


Fig.5.37a: NO reduction with CO using CeO₂ graphite as catalyst
(Other reaction conditions : see text)

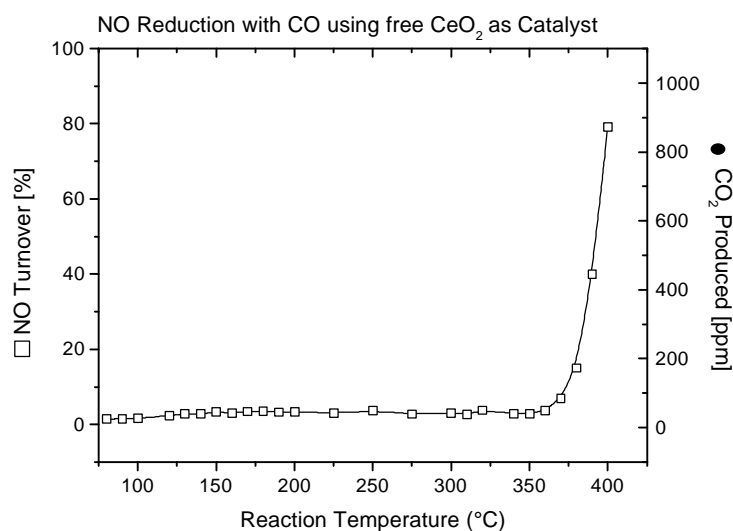


Fig.5.37b: NO reduction with CO using free CeO₂ as Catalyst.
(Other reaction conditions : see text)

6 Discussion of the Results

6.1 CO Oxidation and NO Decomposition

The results obtained in the CO oxidation and NO decomposition for all copper containing substances prepared in this work are summarised in Table 6.1 below.

In Table 6.1 the prepared metal oxide catalysts are listed in order of decreasing rate of CO oxidation reaction per square meter of catalyst material surface area. It will be noticed that in general the surface areas decrease from AlCu graphite to CuO / graphite mixture. The surface

Table 6.1

Rates of CO Oxidation and NO Decomposition per Square Meter of Catalyst, Surface Areas and Activation Energies.

Catalyst and surface area	Temp [°C]	CO Oxidation Rate [moles per m ² of catalyst sec ⁻¹]*10 ⁻⁹	Activation Energy kJmole ⁻¹	Temp [°C]	NO Decomposition Rate [moles per m ² of catalyst sec ⁻¹]*10 ⁻⁹	Activation Energy kJmole ⁻¹
AlCu graphite (69 m ² /g)	100	69.2	59.1	300	2.4	85.6
	120	139.9		350	10.4	
	140	414		400	341	
AlMoCu graph. (65 m ² /g)	100	13	71.9	300	2.25	87.0
	120	34		350	97.6	
	140	115		400	384	
	160	310				
MoCu graphite (65.3 m ² /g)	100	6.2	79.7	300	2.5	92.2
	120	24.2		350	11.3	
	140	74.3		400	437	
	160	221				
FeCu graphite (59 m ² /g)	100	3.6	81.8	300	1.89	106
	120	11		350	15.9	
	140	47.7		400	577	
	160	127				
	180	404				
CuO and Graphite mixt. (21 m ² /g)	120	1.51	74.3			97.4
	140	44.1		300	1.89	
	160	124		350	15.3	
	180	308		400	124	
	200	716				

areas of AlMoCu and MoCu are roughly the same. The activation energies increase from AlCu graphite to FeCu graphite which on the other hand has greater activation energy than CuO / graphite mixture.

In the discussion of the results a look is taken at the mechanisms of the catalytic CO oxidation, NO_x decomposition and CO and NO redox reactions. The rate and order of reaction within the tested temperature range are presented. The activation energies of the above reactions under the application of the prepared catalysts are compared among one another and also compared with the results of other authors. The catalytic activity is defined here as the rate of turnover or conversion of a particular chemical substance under specified experimental conditions upon the application of a unit mass or unit area of the catalyst.

Previous work done in this field using some of the oxides applied in this work are summarised in Table 6.2. Though, the oxides (or reduced form) used by the other authors apart from that of Sirkoman et al. [SMMB90] are not supported on graphite, the results can well be used in assessing the substances prepared and applied in this work. They can be used to judge the effect that the graphite support has on the overall catalytic activities of the substances examined. The effect of the graphite support and the mixed oxides (double oxides) in the samples tested in contrast to other supports such as alumina or silica and mostly single oxides used in previous work shows the specific potential of our substances in catalysis investigation.

Table 6.2 :

Extracts of the results of some previous work in catalysis research

RT reaction temperature, Flr flow rate,

CO Oxidation

Catalyst used	RT	Flr	Quantity and Reaction Rate	Reaction Order	Act. Energy	Lit .
CuO- alumina	100 to 200°C	320l/hr.	200-2000ppm CO in Air	1 st (CO)		[BN66]
Samples			1 Torr CO mol m ⁻² s ⁻¹			
1	120°C		7.4*10 ⁻¹¹		80.2 kJ/mol	
2	"		94.9*10 ⁻¹¹		84.8 "	
3	"		526.5*10 ⁻¹¹		80.6 "	
4	"		31.7*10 ⁻¹¹		104.2 "	

NO Decomposition

Catalyst used	RT	Flr	Quantity and Reaction Rate	Reaction Order	Act. Energy	Lit
<hr/>						
Copper chromite	320°C		1000ppm NO ₂ in He/O ₂ (4:1) mol m ⁻² s ⁻¹ 3.5*10 ⁻¹⁰	1 st (NO)	121 kJ/mol	[L72]
			1000ppm NO in He/O ₂ (4:1) 6.5*10 ⁻¹⁰			
			1000ppm NO in He(no O ₂) Not detectable			
			1000ppm N ₂ O ₄ in He(no O ₂) Not detectable			
Several Catalysts	300 to 600°C	Low	2000ppm NO (extrapolated conc.) in He(no O ₂) values of order 10 ⁻¹⁴	1 st (NO)		[SOG69]
Al ₂ O ₃	700°C		48 Torr in He 8.3*10 ⁻¹⁴			
CuO			similar results as obtained by Shelef et al.			[Ri57]
CuO- alumina	304 to 520°C	36 to 280l/hr.	720 to 2200ppm NO ₂ in N ₂ 1260ppm 55% dissociation to to N ₂ and O ₂ at 520°C for all Flow Rates	0 for NO ₂ (decomposition to NO + ½O ₂) and 0 for NO decomposition to ½N ₂ + ½O ₂)	141 kJ/mol 133 kJ/mol	[WN65]
CeO ₂ - alumina	400 to 520°C	85 to 280l/hr	1120ppm NO ₂ in N ₂	0 for NO ₂ (decomposition to NO + ½O ₂ and to ½N ₂ + ½O ₂)	157kJ/mol 177kJ/mol	[WN65]

Catalyst used	RT	Flr	Quantity and Reaction Rate	Reaction Order	Act. Energy	Lit
Alumina	400 to 520°C	85to 280l/hr.	1120ppm NO ₂ in N ₂ no decomposition up to 500°C			[WN65]
Cu(2+)-exchanged Zeolite Cu-ZSM-5-73	400 to 700°C	0,9l/hr	4vol % NO in 96% He at 400°C ca. 60 % NO conversion and 20 % conversion into N ₂ , 0 % into O ₂ contact time:4 g s cm ⁻³ at 550°C respective NO conversion and conversions into N ₂ and O ₂ 73, 33, and 0 % contact time 0,5g s cm ⁻³ ; 94, 49, and 12 % at 1.0g s cm ⁻³ ; 97, 85 and 70 % at 10.0g s cm ⁻³			[I86]
Transition metal oxides CuO	250 to 750°C 700°C		100% NO mol m ⁻² s ⁻¹ 1.5*10 ⁻¹⁰	2 nd (NO)		[YPB65]
Fe ₂ O ₃	"		9.8*10 ⁻¹¹			
CuO	700°C		100 % NO 2.5*10 ⁻¹⁰	1 st (NO)		[Win71]
Fe ₂ O ₃	"		1.1*10 ⁻¹¹			
Al ₂ O ₃	"		2.8*10 ⁻¹¹			
Al ₂ O ₃	"		10 %NO in He mols m ⁻² s ⁻¹ 9.5*10 ⁻¹²	0 (NO)	Elem. Reactions: 2NO→ N ₂ + O ₂ 2NO + O ₂ → 2NO ₂ Overall Reaction 4NO→ N ₂ + 2NO ₂ Activation Energy: 133 kJ/mol	[FD58]

Catalyst used	RT	Flr	Quantity and Reaction Rate	Reaction Order	Act. Energy	Lit
CuO	700°C		48 Torr NO in He $\text{mols m}^{-2} \text{s}^{-1}$ 1.1×10^{-10}	1 st (NO)	Activation Energy: 34.4(77.7) kJ/mol	[ABB73]
Fe ₂ O ₃	"		2.5×10^{-12}	"		
Al ₂ O ₃	"		9.1×10^{-13}	"		

CO and NO Redox

Catalyst	RT	Flr	Quantity	Reaction Order	Act. Energy	Li t
Copper chromite	115 to 270°C	8*10 ³ l/hr to 36*10 ³ /hr (0.4-1.8*10 ³ l/hr)	NO: 500 to 9000ppm	1 st (NO)	12.6kJ/g mol	[BD65]
	< 220°C	12*10 ³ /hr	1% CO and 1500ppm NO in N ₂	partial NO red. to N ₂ O & N ₂		
	> 220°C	12*10 ³ /hr	1% CO and 1500ppm NO in N ₂	complete NO red.to N ₂		
	270°C	8*10 ³ /hr to 36*10 ³ /hr	1% CO and 1500ppm NO in N ₂	complete NO red. to N ₂		
	> 200°C	16*10 ³ /hr	1% CO and 1500ppm NO in N ₂	NO red N ₂ . > 90%		

The relative activities of catalysts depend on the number of active sites on the surface per unit mass of catalyst and on the relative activities of the sites. The activities of catalysts would not necessarily be proportional to the surfaces determined because the activities of catalysts depend also on the fraction of the surface area, which is active. A catalyst may have a large surface area but only relatively few active sites. However, catalysts, which are similar or differ only in the methods of preparation or activation can at times be compared on the basis of surface area. If one assumes that the fraction of total surface area, which is active, is

approximately the same for two catalysts then a measure of their surface area can be used to predict which catalyst is better for a given reaction.

The activation energy of a surface catalysed reaction as compared to the activation energy of uncatalysed reaction is also a measure of the efficiency of a catalyst. Reactions, catalysed with different substances of the same basic material, can also be measured by comparing their activation energies.

Consideration of the reaction rate constants in both CO oxidation and NO decomposition reactions at equal investigated temperatures and flow rates for all the copper containing catalysts prepared do not differ much from one another. All the catalysts including the CuO and graphite mixture never showed appreciable catalytic activity for CO oxidation below 100°C and NO decomposition below 250°C.

Figures 5.2, 5.4, 5.7, 5.10 and 5.12 give some indications about the relationship of CO conversion into CO₂ at various temperatures with contact time, which is also inversely proportional to flow rate, for the CuO/graphite mixture, AlCu graphite, MoCu graphite, AlMoCu graphite and FeCu graphite respectively. It can be deduced from the diagrams that almost complete conversion of 1000ppm CO is achieved in all cases at temperatures above 120°C depending upon the flow rate. The similarities of the yield at the various temperatures investigated for the copper containing catalysts can be extracted from the diagrams, indicating the reaction rate constants. These are shown in figures 5.2a to 5.2e, 5.5a to 5.5d, 5.8a to 5.8d, 5.10a to 5.10e, and 5.13a to 5.13e for the CuO/graphite mixture, AlCu graphite, MoCu graphite, AlMoCu graphite and FeCu graphite respectively. The reaction rates obtained for these catalysts are again indicated in Table 6.1. The corresponding apparent activation energies calculated from the rate constants are also shown in figures 5.3, 5.6, 5.9, 5.11 and 5.14 and reproduced in Table 6.1.

Figures 5.15, 5.18, 5.21, 5.24 and 5.27 show the functional relationship of NO conversion into N₂, at various temperatures with contact time, for the CuO/graphite mixture, AlCu graphite, AlMoCu graphite, MoCu graphite and FeCu graphite respectively. Complete conversion of 500ppm NO could not be achieved within the investigated temperature and flow rate. The reaction rates obtained from measurements of 1500ppm NO using the same amount of catalyst material as for 500ppm NO is shown in Table 6.1. The substances investigated show similar catalytic characteristics at these temperatures and flow rates. These catalyst activities can be drawn from the diagrams indicating the reaction rate constants. These are shown in

figures 5.16a to 5.16ce, 5.19a to 5.19c, 5.22a to 5.22c, 5.25a to 5.25c, and 5.28a to 5.28c for the CuO/graphite mixture, AlCu graphite, AlMoCu graphite, MoCu graphite and FeCu graphite respectively. The corresponding apparent activation energies calculated from them are also shown in figures 5.17, 5.20, 5.23, 5.26 and 5.29 and reproduced in Table 6.1.

The catalytic activities observed, based on CO oxidation and NO decomposition can be presented as follows:



Under the same experimental conditions – equal reaction temperature, flow rate, concentrations of reacting gases and amount of applied catalyst material – the deciding factor for the catalyst activity is the amount and characteristics of ingredient in the catalyst as well as specific surface area of the material.

The amount of copper in the form of its oxide was practically the same in all the applied catalysts. Eventual traces of $\alpha\text{-Al}_2\text{O}_3$ (formed by calcination above 800°C) in AlCu and AlMoCu would have practically no CO oxidation and NO decomposition catalytic effect. Trace of molybdenum in the form of MoO_3 with a layer structure is present in AlMoCu and MoCu. This oxide has no appreciable oxidising properties. Unlike its counterpart chromium in the sixth group, which forms corresponding oxide CrO_3 of extremely high oxidising characteristics, the oxidation properties of MoO_3 are negligible.

The order of the catalytic activities, keeping all other factors constant, may be attributed to specific catalytic properties of the different oxide species in the substances prepared. Lattice defects, which could form in the aluminium, copper, molybdenum and iron oxides, may effect catalytic activities to different degrees. The different oxides in the different catalyst materials may also not exist separately but in the form of clusters or as mixed oxides. Mixed oxides, such as CuAl_2O_4 spinel may probably occur in AlCu graphite but definitely not in CuO / graphite mixture. It may also occur in FeCu graphite as FeFe_2O_4 or CuFe_2O_4 . In a given catalyst, the existence of different states, such as oxidation state, or their variation may lead to changes in catalytic activity.

Katsumi Sakurai et. al [SOIT76] investigated the surface states of Fe_2O_3 and CuO among other metal oxides and their catalytic activities. His studies by means of ESCA revealed that the

surface states of the metal oxides did not always agree with their bulk constituent and that in the course of reduction with CO at 300°C the oxygen content in surface state of the metal oxide catalyst is richer than in its bulk. He found surface copper oxide to be highly active as oxidising agent. This property was observed to be roughly constant with the increasing reduction of surface copper oxide. They found a sharp and continuous decrease in the oxidising properties of copper oxide after reduction from Cu(II) oxide to Cu(I) oxide and beyond. It could therefore be deduced that Cu(II) oxide possess high oxidising properties and that elemental copper the least oxidising properties. Higher oxidising properties was also proved to lie in the reduced range of Cu(II) oxide to Cu(I) oxide. The activity of copper oxide was found to be the highest among all the oxides examined, and therefore higher than that of Fe₂O₃, in almost all the range of the degree of reduction. The activity of Fe₂O₃ was found to increase as the degree of reduction increases. In the NO – CO reaction, the metal state is most active for iron while the Cu(I) state is more active than the Cu metal state. Even though the oxygen adsorption rate of Fe₂O₃ catalyst is low [Sok90], it is known to be very active in CO oxidation between 150 and 400°C [DL60].

The larger BET surface area of AlCu in comparison to that of MoCu also supports its greater catalytic activity – assuming all other factors such as pore sites, particle size and particle distribution of active substance on the graphite support are constant.

Our EXAFS analyses of AlCu showed the presence of almost only CuO while the analyses of FeCu samples revealed relatively high amounts of both Cu₂O and CuO. FeO and Fe₂O₃ were also determined by EXAFS in FeCu samples. Qualitative analysis by means of magnet attraction measurements showed ferromagnetic effects, which could be attributed to traces of elemental iron or ferric oxide.

The complex formation of Fe with CO and the reduction of iron oxides with CO are well known. The position taken by FeCu in the activity series in the CO oxidation reaction can be partly attributed to iron carbon monoxide complex formation. In this sense Fe acts as inhibitor competing with the active sites. Similar complex formation of Fe with CO may take place in Fe oxides, either in pure oxide or mixed oxide. Iron oxide may also be reduced with CO. These effects can enhance or diminish the catalytic activity of FeCu.

Elemental Fe may on the other hand react with excess oxygen in the reaction mixture to form iron oxides. Depending upon the reaction temperature, pressure, the concentration of CO in the reaction gas mixture and the electronic interaction between the graphite and the iron, the iron carbonyl complex may be stable or not. Unstable complex may give way to the regeneration of elemental iron, which may form a reaction circle with excess oxygen in the reaction mixture just as explained above. In all, the outcome of these reactions can be reasonably considered to have negative effect on the overall catalytic activity.

As explained in section (EXAFS), the occurrence of Cu(I) and Cu(II) oxides as well as FeO and Fe₂O₃ in FeCu can be considered as electronic interaction between Fe₂O₃ and Cu(I). This interaction together with the alternate reduction and oxidation of Fe₂O₃ by CO and O₂ of the reaction gas mixture results in the fluctuation in the amount of effective active sites. This fluctuation was also found to be time dependent. In extreme cases, the FeCu was observed to lose its catalytic activity in CO oxidation after a period of time. This characteristic was observed only for FeCu catalyst.

Of all the catalysts prepared the CuO/graphite mixture showed the least catalytic activity. In comparison to the other catalysts, CuO/graphite mixture is the most tightly packed material tested. This means the active sites are the least accessible to the reacting gas molecules in the reactor. Above this the reaction products CO₂, which must desorb and diffuse from the active sites to pay way for fresh incoming CO, take a long time to leave. The exchange of reaction products and reactants on the catalyst surface consequently takes a long time. This results in lowering the reaction rate and consequently the catalytic activity.

At high temperatures all investigated catalysts delivered 100 % conversion of the reactants. The effectiveness of the catalysts in relation to each other, in both CO oxidation and NO decomposition reactions, can be determined by comparing the temperatures, at which 50% conversions are achieved. These temperatures are given in Tab. 6.3.

Table 6.3 :

Minimum temperatures at which 50% CO oxidation and NO decomposition were obtained.

	<u>CO oxidation</u>	<u>NO decomposition</u>
AlCu oxide-graphite	100°C	250°C
AlMoCu oxide-graphite	100°C	250°C

	<u>CO oxidation</u>	<u>NO decomposition</u>
MoCu oxide graphite	100°C	250°C
FeCu oxide graphite	120°C	250°C
Mixture of CuO and graphite	120°C	300°C
Free CeO ₂	190°C	—
CeO ₂ graphite	170°C	379°C

6.2 NO reduction with CO

With the exception of AlCu graphite (see section 5.4.2) all catalyst substances containing copper oxides exhibit similar characteristics in their NO / CO redox reaction at higher temperatures. At temperatures around 200°C and above, the relations of converted NO and CO are roughly in molar ratio of one to one. This implies that at these high temperatures, the second equation in section 5.4 applies and that complete or total conversion of NO to N₂ occurs. The results obtained in the CO / NO redox reactions on applying the catalysts are presented in Tab. 6.3. The minimum investigated temperatures at which 50% complete NO conversions were obtained for the catalysts are presented.

Table 6.3 :

Minimum temperatures at which 50% complete NO conversions were obtained.

Catalyst	Temperature (°C)
CuO / graphite mixture	350
AlCu graphite	122
MoCu graphite	200
AlCuMo graphite	250
FeCu graphite	335
Free CeO ₂	394
CeO ₂ graphite	338

For the catalyst made up of a mixture of CuO and graphite, and also for FeCu graphite catalyst, at low temperatures bulges are observed in the CO conversion curves. At these temperatures practically no NO conversion into N₂ is to be seen. This could be attributed to

formation of N_2O as stated in equation 1 above. Considerations of thermodynamic data for equation 1 and 2 support the formation of both N_2O and N_2 at the operating reaction temperatures. That almost no NO conversion into N_2 is observed at temperatures below 200°C but above can be attributed to changes in catalytic properties of these samples. In the case of CuO and graphite mixture, intercalation process might occur, reducing the amount of oxide available for reaction. The possibility of having more surface oxygen, which preferentially supports CO_2 formation, at these relatively low temperatures cannot be ruled out. In the case of FeCu graphite, changes in the crystal structures (of the various spinels), variations in the surface and bulk oxygen as well as changes in electronic states of the various iron oxidation states with temperature may explain the seemingly anomaly in catalytic behaviour. The measurement of conversion of NO is based solely on the N_2 produced. This was followed and measured chromatographically. At a temperature indicating no NO conversion, N_2 formation is not observed or the amount formed is below the instrumental measuring area.

Differences in NO and CO conversions (molar ratio 1:1) at the investigated temperatures for AlCu, AlMoCu and MoCu graphite catalysts (Group 1) on one hand and CuO / graphite mixture and FeCu graphite catalyst (Group 2) on the other hand are obvious from the corresponding diagrams above. Group 1 does not show the anomaly characteristic of Group 2. The catalytic effect of Group 1 may be spoken of as specific, the reaction leading to complete conversion of NO into N_2 without any observable intermediate products. The NO conversions are defined by definite minimum reaction temperatures. NO conversions are observed to start around 125°C for both AlCu- and MoCu-graphite and around 150°C for AlMoCu graphite. These differences in temperatures can be attributed to the different properties of the catalyst materials. Differences in chemical composition, oxidation states of transition metal, crystal structure of oxides, presence of mixed oxides among other factors may lead to differences in active sites at different temperatures and therefore differences in initiating temperatures.

The NO conversions for AlMoCu- and MoCu-graphite and for the Group 2 catalysts are spread over large temperature area, the degree of NO conversion rising to a maximum over a wide temperature range. A total NO reduction (equation 2), showing a high degree of NO conversion is observed to take place for AlCu graphite within a narrow temperature range. These differences may be attributed to the degree of adsorption of reacting substances on the catalyst materials at the investigated temperatures and also on the effectiveness of the catalyst

substance. Of all the substances containing copper oxide, AlCu exhibited the best catalytic properties in NO reduction reaction with CO.

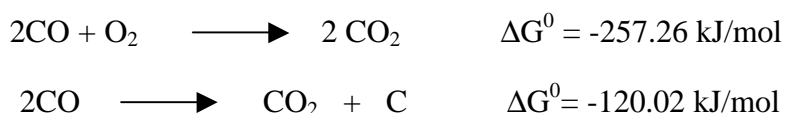
Comparison of Figures 5.4.6a and b shows the difference in NO reduction with CO using free CeO₂ and CeO₂ graphite. The NO conversion into N₂ begins at 300°C and 350°C for CeO₂ graphite and free CeO₂ catalysed reactions respectively. The change in reaction temperature in favour of CeO₂ graphite can be attributed to the electronic interactions between the graphite of the GIC and the CeO₂. Electron shift between CeO₂ and graphite may enhance the adsorption of NO on the CeO₂ active site. This effect may also apply to the CO adsorption.

6.3 Mechanism of the Catalytic Reactions

In the CO oxidation reaction just as in the NO decomposition as well as in the CO – NO redox reaction, the catalytic active component in the prepared samples was found to embody copper oxide in the case of all the mixed oxides supported on graphite. Comparison of the results for the various mixed oxides shown above sheds lights to this conclusion. It is to be noted here that samples containing only molybdenum oxides, or aluminium oxides or a mixture of both never exhibited any remarkable catalytic effect. Only samples with copper oxide component were found to be catalytically active. In the case of the exfoliated cerium oxide or rather cerium nitrate graphite intercalation compound the active component is cerium oxide, because there was not any remarkable catalytic conversion when graphite was used alone under the tested experimental conditions.

First order reaction was observed for the following catalysts: AlCu-, AlMoCu-, MoCu-, FeCu-, and CeO₂-graphite in CO oxidation and NO decomposition.

The CO oxidation can generally be represented as follows:



The simple CO oxidation as well as its disproportionation reaction shown above has both negative standard free enthalpy of reactions. This means that CO reacts in principle according to the equations given above. However, CO is kinetically inactive and its conversion can be achieved only at temperatures above 1500°C. By employing the transition metal oxides as

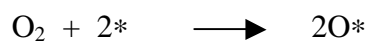
catalysts a new reaction path with low activation energy is created enabling the reaction to take place.

The disproportionation of CO did not take place when the prepared catalysts were used. This was very clear as no conversion of CO was observed when CO is used as the sole reactant. This also rules out the possible donation of bulk oxygen from the copper oxide to the CO in order to form CO₂, although bulk oxygen can not be ruled out since EXAFS investigation of the catalyst showed a mixture of Cu(I)- and Cu(II)-oxide in the catalyst.

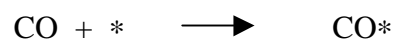
Oxidation of CO on catalysts with surface active copper oxide have been reported by several authors. Schwab G. and Drikos [SD40] working in a temperature range between 300°C and 430°C reported that the rate-determining step of the reaction to be the reduction of copper oxide by carbon monoxide and first order with respect to CO. The catalytic CO oxidation investigated in this work was done in the presence of O₂, and the reduction of copper oxide as reported by Schwab can be ruled out here, even though it was not investigated. The measured amount of O₂ consumed in the oxidation process corresponded to that given by the elementary reaction presented above. Moreover CO oxidation in the absence of oxygen feed from outside was not observed. The discrepancy in the finding of Schwab among others and this work can be attributed to the electronic effect or interference of the graphite, the supporting material. The probability of carbon clinging to the bulk oxygen and therefore making it very difficult for its donation to the CO cannot be ruled out. First order reaction rate found in this investigation is in conformity with Schwab and Drikos and also that of Blumenthal et al [BN66] and the mechanism follows that of Langmuir - Hinshelwood. It can be presented as follows:

1.) Diffusion of the reactants to the catalyst surface

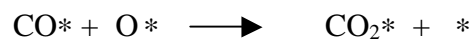
2.) Dissociative adsorption of O₂



3.) Adsorption of CO



4.) Formation of carbon dioxide



6.) Desorption of CO₂



* indicates an adsorption site, O*, CO* and CO₂* representing adsorbed oxygen atom, carbon monoxide and carbon dioxide respectively. CO adsorption is the rate-determining process.

The above mechanism was found to apply in all the cases where copper oxide catalyst was involved. Generally CO₂ was not found as an inhibitor. Keeping the concentration of oxygen constant and varying the concentration of carbon monoxide means difference in turnover of carbon monoxide. Differences in conversion of CO also imply differences in amount of carbon dioxide produced. In the light of this, without even adding external CO₂ to the reaction mixture, it could be proved that CO₂ adsorption has no influence on the reaction rate. CO₂ desorption rate can therefore be considered to be too fast to have any effect on the reaction rate or to be a rate-determining factor. Dissociative adsorption of O₂ is also so fast that there are always adsorbed oxygen atoms available to react with CO. The rate-determining step can then be considered to be the oxidative adsorption of CO on an active site of the catalyst.

Catalytic capabilities of transition metal oxides are among other things attributed to the unoccupied or partially occupied electronic d-energy levels of their central atoms. This permits the promotion of adsorbed molecules into transition by means of electron transfer. The rare earth elements, like the transition elements, also have high energy levels, which will allow freely electron donation and intake. It is therefore not surprising, that CeO₂, a member of the rare earth metal oxide, exhibits catalytic activity. CeO₂ has currently found extensive application as a promotor [GPSD76, SM80, HS85, HDH88, 84T, Ra96 and O90] in a three-way catalyst for the treatment of automobile pollutants. Among other functions attributed to CeO₂ is the oxygen - release and storage capacities due to the redox reaction of Ce⁴⁺/Ce³⁺ oxides as shown immediately below. Formation of Ce³⁺ in the Rh/Ce_{0.6}Zr_{0.4}O₂ sample – containing CeO₂ – is confirmed by magnetic susceptibility measurements [Ra 96]. The oxygen - release and storage of CeO₂ is presented as follows:



Zafiridis and Gorte [ZG 93] have found evidence for an important role of oxygen migration from CeO₂ to Rh in enhancing the catalytic activity of Rh/CeO₂ in CO oxidation. Unlike the catalytic CO oxidation on Rh supported on ceria where ceria serves as an oxygen provider, in the CeO₂-graphite catalysed CO oxidation, oxygen was fed as a reactant in the reaction mixture. CeO₂ served as active site for oxygen absorption and its decomposition prior to reaction with CO in the formation of CO₂. CO adsorption on CeO₂ in CeO₂-graphite within the investigated temperature range can be ruled out as found by Oh [O90] and also by Solymosi et al. [Sol88].

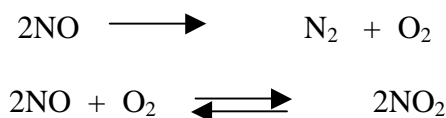
The reaction mechanism takes the pattern of Eley-Rideal and can be presented as follows:

- 1.) Diffusion of reactants to catalyst surface
- 2.) Dissociative adsorption of O₂
$$\text{O}_2 + 2* \longrightarrow 2 \text{O}^*$$
- 3.) Oxidation of CO to CO₂
$$\text{CO} + \text{O}^* \longrightarrow \text{CO}_2^*$$
- 4.) Desorption of CO₂
$$\text{CO}_2^* \longrightarrow \text{CO}_2 + *$$

Here the rate-determining step of the reaction is the diffusion of CO to the catalyst surface which is first order of reaction with respect to CO concentration.

Taking into account the findings of other authors about NO decomposition reactions as presented in Table 6.2 and the common text-book knowledges it can be assumed that within the temperature range of investigation (200 – 400°C) only N₂O, NO₂ and its dimer N₂O₄ are the possible entities involved in the decomposition reaction.

In this work the NO decomposition reaction using copper oxide supported on graphite as catalyst NO₂, O₂ and N₂ were identified as products by the gas-chromatographic method. First order reaction with regard to the measured concentration of N₂ produced was observed and the amount of NO consumed was roughly 2 to 1 in molar relation to N₂ produced. The measured O₂ concentration was less than expected in a direct decomposition of NO to give N₂ and O₂. The observed NO₂ is a product resulting from the reaction of the decomposition product O₂ and the unreacted NO. The observed O₂ is an equilibrium product resulting from the decomposition of NO₂ in the gas-phase. In all the decomposition of NO can be summarised as follows:



The formation of N₂O was not observed as reported to take place in the investigated temperature range by other authors. That N₂O was not formed can be attributed to the reaction conditions under which the experiment was performed. Disproportionation of NO to N₂O is conducive at high pressure but the investigation was done at low pressure. Analogously to the reaction in zeolites, one will expect the formation of N₂O from NO to take place in graphite layers, which are not completely open as it does in zeolites' cavities. That NO was not observed can be attributed to the fact that after exfoliation the graphite structure was

completely decomposed providing a surface-adsorbed graphite supported copper oxide catalyst. This catalyst shows not the completely open cavities of zeolites, which further rules out the possibility of the subsequent disproportionation of NO to N₂O. Much more the gas mixture composed of maximal one percent NO in He was not concentrated enough to promote the conversion of NO to N₂O. The oxygen that reacts with NO to produce NO₂ can also be thought of as a nascent oxygen - being highly reactive and therefore the formation of NO₂ taking place in preference to the disproportionation reaction. The decomposition of NO is in contrast to that suggested by Lawson and supports that found by Wikstrom and Nobe.

The mechanism can therefore be formulated in the following manner:

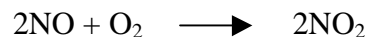
- 1.) Diffusion of the reactant to the catalyst surface
- 2.) Associative adsorption of NO $\text{NO} + * \rightleftharpoons \text{NO}^*$
- 3.) Dissociative adsorption of NO* $\text{NO}^* + * \longrightarrow \text{N}^* + \text{O}^*$
- 4.) Formation of N₂ from adsorbed nitrogen atoms. $2\text{N}^* \longrightarrow \text{N}_2 + 2^*$
- 5.) Formation of O₂ from adsorbed oxygen atoms. $2\text{O}^* \longrightarrow \text{O}_2 + 2^*$

Due to the high energy NO bond its dissociation can be assumed to be the rate – determining step of the decomposition reaction. The mechanism for the decomposition of NO on these surfaces probably involves a surface site reaction with an adsorbed NO molecule. This reaction is “quasi-unimolecular”, because the concentration of the empty surface sites is very high and quasi constant. However, a process involving only one molecule of nitric oxide adsorbed on one surface site would have to desorb nitrogen atoms (rather than molecules), which would require a very high activation energy. That the monomolecular process occurs signifies weak nitrogen atom adsorption properties of the catalyst substances at the investigated reaction conditions.

No significant decomposition or conversion of NO was observed in the absence of O₂ when CeO₂-graphite catalyst was used. Conversion took place only when O₂ was present in the reaction mixture. The reaction products detected under the reaction conditions investigated were NO₂, N₂ and O₂. Second order mechanism with respect to NO consumed was observed. The dimer of NO₂, N₂O₄, normally exists in the gas phase up to a temperature of about 150°C, and it can be assumed that at higher temperatures, NO₂ forms a surface dimer which adsorbs on the catalyst and dissociates to give N₂ and O₂.

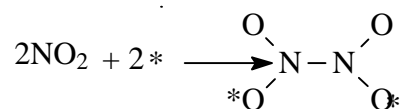
The mechanism of the decomposition reaction can be presented as follows:

1.) Formation of NO₂ in the gas phase

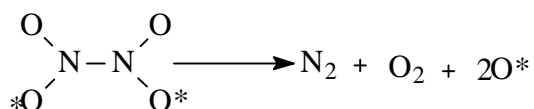


2.) Diffusion of NO₂ to the catalyst surface

3.) Adsorption of 2 NO₂ to form the dimer, N₂O₄



4.) Dissociative desorption of N₂O₄

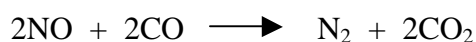


5.) Desorption of O₂



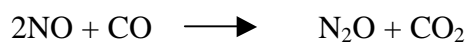
The rate determining-step can be thought of to be the adsorption of N₂O₄, the formation of which involves the proper orientation of two NO₂ molecules to each other. This step is obviously bimolecular, which is in concordance with our observation of a second order reaction.

The kinetics of the reduction of NO by CO on graphite-supported copper oxide, CuO-graphite, was found to follow first order with respect to NO and CO concentrations. N₂ and CO₂ were detected and measured as reaction products. The over-all reduction of NO by CO monitored under the investigation can be represented as follows :



Several investigations have been made in the NO reduction with CO at various reaction temperatures using supported CuO, and other supported transition metal oxides. In their analysis of the reaction products of NO reduction with CO using CuO and Cr₂O₃ as catalyst Baker and Doerr [BD65] identified and measured N₂O, N₂ and CO₂. The partial reduction of NO to N₂O was found to be dependent upon temperature and the space velocity of reacting gas mixture. At a constant space velocity it was observed that at temperatures above 160°C no N₂O peak was observed and that above 270°C almost all NO has been converted to N₂. The finding of Baker et al was confirmed by us. The work presented here was done in the

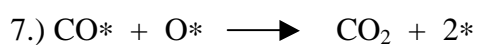
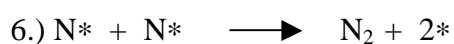
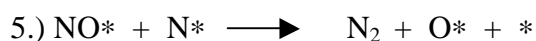
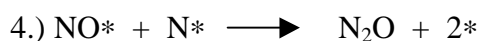
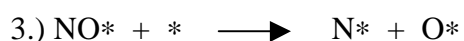
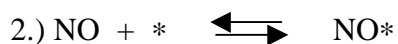
temperature range of 200° to 400°C and the measured N₂ corresponded to that of total reduction of NO. Depending upon the reaction temperature and space velocity of reacting gases, N₂O, N₂ and NO or a combination of these gases can be considered as the reaction products of NO reduction with CO. The overall reaction process presented above can be considered to be made up of the following two reaction processes.:



Within the investigated temperature range the conversion of the N₂O to N₂ can be considered to be so fast that virtually the direct reduction of NO by CO, without the intermediate product N₂O, seems to take place.

Even though N₂O was not identified its production in course of the reaction cannot be ruled out and is therefore considered in the reaction mechanism as shown below.

The mechanism of the CO – NO reaction over CuO-graphite can be represented by the following set of elementary processes :



The rate-determining step can be assumed to be the adsorptive dissociation of NO as represented in equation 3 above, because this step is the only one requiring the input of

dissociation energy without a reaction partner. It was observed that, at higher concentration of NO in the inserted gas mixture, an NO inhibition effect took place. This can be attributed to interactions between neighbouring molecules.

In the case where CeO₂-graphite was used as a catalyst in the NO reduction by CO in the absence of oxygen the reaction mechanism can be postulated as a transfer of oxygen atom from CeO₂ to an adsorbed CO whereby Ce(IV) oxide is reduced to Ce(III) oxide. The Ce(III) oxide on the other hand accepts oxygen atom from an adsorbed NO resulting in the production of Ce(IV) oxide and the reduction of NO to N₂ or its intermediate product N₂O.

7 Summary

This work describes:

- The preparation and characterisation of graphite intercalation compounds (GICs) embodying selected transition metal chlorides. The corresponding metal oxides are known to show catalytic activities. The chlorides were bi- and tri-intercalated in the following combinations: aluminium (III) with copper (II); molybdenum (VI) with copper (II); aluminium (III) with copper (II) and molybdenum (VI); iron (III) with copper (II). In addition to these GICs, Ce(IV) nitrate GICs were prepared and characterised.
- The exfoliation of the prepared graphite intercalation compounds and the characterisation of the products.
- The application of the characterised exfoliation products in catalysis investigation. The catalytic activities of the prepared substances were compared with those obtained from mixture of pristine CuO (for copper containing substances) and graphite, and of pristine CeO₂ (for cerium containing substances) and graphite.

Graphite intercalation compounds are layer compounds. Their structures are described in this work and the experimental methods for structural determination are reported. The general preparation methods of GICs and their application in this work, are treated. The experimental procedures for determining the density and surface area (BET) are presented. Intercalate compositions in GICs are determined. Instrumental methods, namely X – ray diffraction, X – ray fluorescence, X – ray absorption spectroscopy (XANES and EXAFS) used in characterising the GICs and the exfoliation products are presented in detail. The exfoliation process of GICs to obtain the substances applied in the catalysis investigation is treated in this work. The changes in mass, density and surface area GICs, in the course of the exfoliation process, are also presented. The oxidation states of the metal oxides in the exfoliation products, and the coordination numbers of the central metal atoms are determined.

The application of the exfoliation products in :

- CO oxidation reactions
- NO decomposition reactions
- NO / CO redox reactions

and the results obtained are presented. Gas chromatography method used in separating and measuring the reactants and products involved in the catalysis investigation is discussed. Because flow reactor was used in the catalysis investigation, the theory of the plug flow reactor is discussed. In the catalysis tests, activation energies were determined.

In all cases the preparations were geared towards the realisation of first stage intercalation compounds (saturation) and very good results were obtained. X – ray diffraction analyses of

the GICs revealed first and second stage compounds for the Cu containing GICs, second and third stage compounds for the Ce (IV) nitrate GICs. In the case of the tri-intercalated GIC prepared from aluminium (III), copper (II) and molybdenum (VI) chloride mixture, first stage in both copper (II) and molybdenum (VI) chloride was obtained. Co-intercalation products - with the metal chlorides embedded between graphite layers as an entity - were obtained from iron (III) and copper (II) chloride.

The exfoliations of the prepared graphite intercalation compounds were carried out at 700°C, and the density and specific surface area were determined as a function of exfoliation time. The densities and specific surface areas determined for all the different substances were observed to follow the same pattern. Both values were found to increase with time attaining maximum values after a certain time. With the exception of a mixed intercalate prepared from copper (II) and iron (III), the exfoliation products offered relatively high specific surface area to warrant their use as catalyst.

Using X-ray fluorescence method, the relative amounts of the different metallic elements were found. The X-ray absorption spectroscopy enabled the determination of the charge transfer (an index for oxidation state) from or to the central metal atoms and also give insight to the co-ordination of the ligands (oxygen atoms) to the central metal atoms.

The exfoliated substances tested as catalysts contain the metals as oxides. They are indicated as follows:

- a) AlCu oxide-graphite b) AlMoCu oxide-graphite c) MoCu oxide graphite
- d) FeCu oxide graphite e) Mixture of CuO and graphite f) CeO₂ graphite
- g) free CeO₂ (mixture of CeO₂ and graphite)

The catalysts e) and g) were used as control substances.

0.1 vol% CO in He and up to 0.15 vol% NO in He were used for the tests. 1% O₂ in He was used in the CO oxidation. The tested temperatures ranged in most cases from 80°C to 400°C. In the CO oxidation reaction, the results obtained for all copper containing compounds were far better than those obtained using CuO / graphite mixture. The smallest apparent activation energies determined within the measured temperature ranges were found to be 59.1 kJ/mol and 85.6 kJ/mol for the AlCu oxide-graphite catalysed CO oxidation and NO decomposition reactions respectively, meaning AlCu oxide-graphite the best catalyst amongst the all the copper containing catalysts prepared. FeCu oxide graphite delivered apparent activation energies of 81.8 kJ/mol in CO oxidation reaction and 106.1 kJ/mol in NO decomposition reaction and proved to be the least effective catalyst of the copper containing catalysts. Taking into consideration the minimum temperatures at which 50% conversions were obtained in the CO oxidation and NO decomposition reactions, it can be stated that AlCu oxide-graphite is the best catalyst and free CeO₂ the worst. 50% conversions were at 100°C and 250°C

respectively for CO oxidation and NO decomposition reactions catalysed with AlCu oxide-graphite. On the other hand 50% CO conversion was obtained for free CeO₂ at 190°C and 50% conversion could not be obtained for the NO decomposition, even at 400°C.

The order of catalytic activity in the CO oxidation reactions and the NO decomposition reactions were found to follow the following pattern:

AlCu oxide graphite > AlMoCu oxide graphite > MoCu oxide graphite
> CuO / graphite mixture > FeCu oxide graphite > free CeO₂ > CeO₂ graphite

At high temperatures all investigated catalysts delivered 100 % conversion of the reactants.

The trend of the catalytic activity observed in the CO oxidation and NO decomposition reactions was also observed in the CO – NO redox reaction. In this case, the 50% conversion temperatures were 100°C for AlCu oxide graphite and 394°C for free CeO₂. Also in this case AlCu oxide graphite proved to be the best or most effective catalyst and free CeO₂ the least.

Characteristics of the exfoliation products, such as oxidation states of the transition metals, possible spinel formation etc., leading to this order of activity, have been discussed.

The kinetics of the above reactions were examined. First order reaction rate was found for the copper containing substances in their CO oxidation and NO decomposition reactions. First order reaction mechanism was found for CO oxidation and second order in NO decomposition in the case of CeO₂ catalysed reactions. The reaction mechanisms are discussed.

The results obtained, compared with the results obtained by other authors using CuO on other substrate, indicate the effectiveness of the prepared catalysts. The only disadvantage is the oxidation of the substrate in course of the catalysis investigation. It reached a maximum value of 6% for the copper containing exfoliation products, and about 9% for the CeO₂ graphite.

8 Zusammenfassung

Diese Arbeit beschreibt:

- Darstellung und Charakterisierung von Graphit-Intercalationsverbindungen (GICs), die ausgewählte Übergangsmetall-Chloride enthalten. Die entsprechenden Metall-Oxide sind bekannt für ihre katalytische Aktivität. Die Chloride wurden in folgenden Kombinationen bi- und tri-intercaliert: Aluminium (III) mit Kupfer (II); Molybdän (VI) mit Kupfer (II); Aluminium (III) mit Kupfer (II) und Molybdän (VI); Eisen (III) mit Kupfer (II). Zusätzlich zu diesen GICs wurden Ce(IV)-nitrat GICs dargestellt und charakterisiert.
- Die Exfoliation der dargestellten Graphit-Intercalationsverbindungen und die Charakterisierung der Produkte.
- Die Anwendung der charakterisierten Exfoliationsprodukte bei Katalyse-Untersuchungen. Untersuchungen. Die katalytischen Aktivitäten der dargestellten Substanzen wurden verglichen mit denen von Mischungen von reinem CuO (für die Kupfer enthaltenden Substanzen) und Graphit beziehungsweise von CeO₂ (für die Cer enthaltenden Substanzen) und Graphit.

Graphit-Intercalationsverbindungen sind Schichtverbindungen. Ihre Strukturen werden in dieser Arbeit beschrieben, und die experimentellen Methoden zur Strukturbestimmung werden wiedergegeben. Die allgemeinen Methoden zur Darstellung von GICs und ihre Anwendung im Rahmen dieser Arbeit werden behandelt. Die experimentellen Verfahren zur Bestimmung der Dichte und der Oberfläche (BET) werden beschrieben. Die Intercalat-Zusammensetzungen innerhalb der GICs werden ermittelt. Die instrumentellen Methoden, die zur Charakterisierung der GICs und der exfolierten Produkte verwendet werden, nämlich Röntgenbeugung, Röntgenfluoreszenz und Röntgenabsorptionsspektroskopie (XANES und EXAFS), werden detailliert beschrieben. Der Prozess der Exfoliation, mit dem aus den GICs die zu Katalyseuntersuchungen verwendeten Substanzen gewonnen wurden, wird in der Arbeit behandelt. Die Massen- Dichte- und Oberflächenänderungen im Verlauf des Exfoliationsprozesses werden ebenfalls dargelegt. Der Oxidationszustand der Metalloxide in den Exfoliationsprodukten sowie die Koordinationszahl der zentralen Metallatome werden bestimmt.

Die Anwendung der Exfoliationsprodukte in:

- CO-Oxidationsreaktionen
- NO-Zersetzungsreaktionen
- NO / CO Redoxreaktionen

und die erhaltenen Ergebnisse werden wiedergegeben. Die Gaschromatografie-Methode, die zur Trennung und Bestimmung der Reaktanden und Produkte bei den katalytischen Untersuchungen angewendet wurde, wird diskutiert. Weil für die Katalyse-Untersuchungen ein Durchflussreaktor

Verwendung fand, wird die Theorie des *plug flow*-Reaktors diskutiert. Bei den Katalyseversuchen wurden die Aktivierungsenergien bestimmt.

In allen Fällen wurden bei der Darstellungen die Realisierung der ersten Stufe der Einlagerungsverbindung (Sättigung) angestrebt, und es wurden sehr gute Ergebnisse erzielt. Die Röntgenbeugungsanalysen der GICs zeigten das Vorliegen von Verbindungen erster und zweiter Stufe bei den Kupfer enthaltenden GICs, zweiter und dritter Stufe bei den Ce(IV)-nitrat-GICs. Im Falle der tri-intercalierten GIC mit Aluminium(III), Kupfer(II) und Molybdän(VI) wurde die erste Stufe sowohl für Kupfer(II)-chlorid als auch für Molybdän(VI)-chlorid erhalten. Co-Intercalationsprodukte - bei denen die Metallchloride als Einheit zwischen den Graphitschichten liegen - wurden von Eisen(III)- und Kupferchlorid erhalten.

Die Exfoliationen der dargestellten Graphit-Intercalationsverbindungen wurden bei 700°C durchgeführt, und Dichten sowie spezifische Oberflächen wurden als Funktion der Exfoliationszeit bestimmt. Es wurde gefunden, dass Dichten und spezifische Oberflächen für alle Substanzen demselben Muster folgen. Beide Werte stiegen als Funktion der Zeit an und erreichten nach einer bestimmten Zeit ein Maximum. Mit Ausnahme eines Misch-Intercalats aus Kupfer(II) und Eisen(III) bieten alle Exfoliationsprodukte eine relativ große spezifische Oberfläche, was ihren Gebrauch als Katalysatoren rechtfertigt.

Mit Hilfe der Röntgenfluoreszenzmethode wurden die relativen Mengen der verschiedenen Metalle als Elemente bestimmt. Die Röntgenabsorptionsspektroskopie erlaubte eine Bestimmung des *charge transfers* (als Kennzeichnung des Oxidationszustandes) vom oder zum zentralen Metallatom; sie gab auch Aufschluss über die Koordination der Liganden (Sauerstoffatome) zum zentralen Metallatom.

Die als Katalysatoren getesteten exfolierten Substanzen enthalten die Metalle als Oxide. Sie werden folgendermaßen gekennzeichnet:

- a) AlCu-Oxid-Graphit b) AlMoCu-Oxid-Graphit c) MoCu-Oxid-Graphit
- d) FeCu-Oxid-Graphit e) Mischung von CuO und Graphit f) CeO₂-Graphit
- g) (Mischung aus CeO₂ und Graphit).

Die Katalysatoren e) und g) dienten als Vergleichssubstanzen.

0.1 Vol.-% CO in He und bis zu 0.15 Vol.-% NO in He wurden für die Versuche verwendet. 1% O₂ in He wurde für die CO-Oxidation eingesetzt. Die Versuchstemperaturen lagen in den meisten Fällen zwischen 80°C und 400°C. Bei der CO-Oxidation erwiesen sich die Ergebnisse für alle Kupfer enthaltenden Verbindungen deutlich besser als diejenigen, die bei Anwendung der Mischung CuO / Graphit erhalten wurden. Die niedrigsten scheinbaren Aktivierungsenergien innerhalb des vermessenen Temperaturbereichs wurden zu 59.1 kJ/mol und 85.6 kJ/mol für die mit

AlCu-Oxid-Graphit katalysierte CO-Oxidation bzw. NO-Zersetzung bestimmt. Dies bedeutet, dass AlCu-Oxid-Graphit der beste unter den dargestellten Kupfer enthaltenden Katalysatoren ist. FeCu-Oxid-Graphit lieferte scheinbare Aktivierungsenergien von 81.8 kJ/mol bei der CO-Oxidation und 106.1 kJ/mol bei der NO-Zersetzung und erwies sich damit als der am wenigsten effektive unter den Kupfer enthaltenden Katalysatoren. Auch beim Auswerten der tiefsten Temperatur, für die ein Umsatz von 50% erreicht wird, kann für die CO-Oxidation und die NO-Zersetzungsreaktion festgestellt werden, dass AlCu-Oxid-Graphit der beste Katalysator ist und freies CeO₂ der schlechteste. 50% Umsatz wurden bei 100°C bzw. 250°C für die durch AlCu-Oxid-Graphit katalysierte CO-Oxidation bzw. NO-Zersetzung erzielt. Andererseits wurden bei Anwendung von freiem CeO₂ 50% CO-Umsatz erst bei 190°C erreicht, und für die NO-Zersetzung konnten 50% Umsatz auch bei 400°C noch nicht erzielt werden.

Die Reihenfolge der katalytischen Aktivität bei der CO-Oxidation und bei der NO-Zersetzung verliefen nach folgendem Schema:

AlCu-Oxid-Graphit > AlMoCu-Oxid-Graphit > MoCu-Oxid-Graphit > Mischung von
CuO und Graphit > FeCu-Oxid-Graphit > freies CeO₂ > CeO₂-Graphit

Bei hohen Temperaturen lieferten alle untersuchten Katalysatoren einen Umsatz von 100% der Reaktanden.

Der Trend der katalytischen Aktivitäten, wie er bei der CO-Oxidation und der NO-Zersetzung beobachtet wurde, konnte auch bei der CO-NO-Redox-Reaktion festgestellt werden. In diesem Fall lagen die 50%-Umsätze bei 100°C für AlCu-Oxid-Graphit als Katalysator und bei 394°C für das freie CeO₂.

Charakteristika der Exfoliationsprodukte wie Oxidationszustand der Übergangsmetalle, mögliche Spinell-Bildung etc., die zu dieser Reihenfolge der Aktivität führen, wurden diskutiert. Die Kinetik der genannten Reaktionen wurde untersucht. Für die Kupfer enthaltenden Katalysatoren wurde bei der CO-Oxidation und der NO-Zersetzung die erste Reaktionsordnung festgestellt. Im Falle der CeO₂-katalysierten Reaktionen wurde ein Mechanismus erster Ordnung für die CO-Oxidation und zweiter Ordnung für die NO-Zersetzung gefunden. Die Reaktionsmechanismen wurden diskutiert.

Die erhaltenen Resultate zeigen auch im Vergleich mit denjenigen anderer Autoren, die CuO oder CeO₂ auf anderen Substraten eingesetzt haben, die größere Effektivität der von uns dargestellten Katalysatoren. Der einzige Nachteil besteht darin, dass im Verlauf der katalytischen Untersuchungen eine Oxidation des Substrates stattfindet. Diese erreicht ein Maximum von 6% bei den Kupfer enthaltenden Exfoliationsprodukten und etwa 9% bei CeO₂-Graphit.

9 Literature

Text book references are presented with the year of publication preceding the corresponding initial(s) of the author(s) and vice versa for other articles.

- ABB73** Amirnazmi, A., Benson, J. E., and Boudart, M., J. Catal. 30, 55-65 (1973)
- AC84** Anderson, S. H., Chung, D. D. L., Carbon, 22 (1984), 253
- 67B** Beatie, I. R., Nitrous Oxide, Section 24 in Mellor's Comprehensive Treatise on Inorganic and Theoretical Chemistry, Vol. 8 pp. 189-215, Supplement 2, Nitrogen (part 2), Longmans, London, 1967
- B70** A. Boeck, Dissertation, Techn. Universität Clausthal, 1970
- BET38** Brunauer, S., Emmett, P. H., Teller, E., J. Am. Chem. Soc., 80 (1938), 309
- BD65** Robert A. Baker and Robert C. Doerr, Ind. Eng. Chem., Process Des. Develop. 4, 188 (1965)
- BHLRS94** *Neutron and Synchrotron Radiation for Condensed Matter Studies, Vol. II*, edited by J. Baruchel, J. L. Hodeau, M. S. Lehmann, J. R. Regnard, C. Schlenker, Springer Publication (1994)
- BN66** Blumenthal, J. L., and Nobe, K., Ind. Eng. Chem. Process Des. Develop. 4, 177 (1966)
- BW73** A. Boeck, W. Rüdorff, Z. Anorg. Chem. 397 (1973), 179
- CB89** Che, M., Bennet, C. O., Adv. Catal. 36, (1989), 55
- Chu87** Chung, D. D. L., Carbon, 25 (1987), 641
- CI56** J. M. Cowley, J. A. Ibers, Acta Cryst. 9 (1956), 421
- 80CN** F: A: Cotton, G. Wilkinson, Anorganische Chemie, Verlag Chemie, Weinheim, Deerfield, Florida, Basel 1980, pp 295
- Dew70** E. W. Dewing, Metall. Trans. 1 (1970), 2169
- DFZ65** Dmuchovsky, B., Freeks, M. C., Zienty, F. B., J. Catal., 4, (1965), 446
- DH69** N. Daumas, A. Herold, Compt. Rend. C 268(1969), 373
- DL60** Dixon, J. K., Longfield, J. E., Catalysis, 1960, 347
- DMT57** Dowden, D. A., Mackenzie, N., Trapnel, B. M. W., Adv. Catal., 9, (1957), 65
- DS79** L. Dotto and H. Schiff, Chem. Eng. New, July 1979 pp 34 and 43
- E93** Eickhoff, H. K. Ph. D Thesis, 1993 Institute of Physical Chemistry, University of Hamburg

- Fen57** Fensham, P. J., Quart. Revs. (London), 11, (1957), 227
- Fox79** J. L. Fox, Chem. Eng. New, Oct. 1979 pp 25-35
- FD58** Fraser, J. M., and Daniels, F., J. Phys. Chem. **62**, 215 (1958)
- Gai92** Gai-Boyes, P. L., Catl. Rev. – Sci. Eng., 34, (1992), 1
- 86GE** N.N. Greenwood and A. Earnshaw, Chemistry of the Elements, Pergamon Press, Frankfurt FRG. Pp 709
- GPSD76** Ghandi, H. S., Piken, A. G., Shelef, M., Delosh, R. G., SAE-Paper No. 760201, (1976)
- 93HKK** J. E. Huheey, E. A. Keiter, R. L. Keiter., Inorganic Chemistry, Harper Collins College Publishers, 4th. Edition, 1993, London, pp. 750 -752
- Hag91** M. Hagelstein, Ph. D. Thesis, University of Kiel, Germany (19991)
- Hec47** Hecht, H., Z. Anorg. Allg. Chem. 254 (1947), 37
- Hei76 R.** Heinrich, Diplomarbeit, University of Hamburg 1976
- Hoh72 D.** Hohlwein, Dissertation, University of Hamburg 1972
- Hoo72 J.** G. Hooley, Carbon 10 (1972), 155
- HCFNR89** M. Hagelstein, S. Cunis, R. Frahm, W: Niemann, P. Rabe, Physica B 158, 324 (1989)
- HDH88** Harrison, B. , Dieell, A.F. ,and Hallett, C. ,Platinum Met. Rerv. 32, 73(1988)
- HM74** D. Hohlwein, W. Metz, Z. Krist. 139 (1974), 279
- HMP69** Harris, S. W., Morello, E. F., and Peters, G. H. , U. S. Patent No. 3,459,494, Aug. 5th, 1969
- HS85** Herz, R.K. , and Sell, J.A. , J. Catal. **94**, 166(1985)
- I86** Iwamoto, M.et al. J. Chem. Soc. Chem. , Commun. ,1986 1272-1273
- IYSK81** Iwamoto, M., Yokoo, S., Sakai, K., and Kagawa, S., J. Chem. Soc. Faraday Trans. 1, 1981, 77, 1629-1638
- Jag49** H. Jagodzinski, Acta Cryst. 2 , 201 (1949)
- K77** B. Knörr, Diplomarbeit, University of Hamburg 1977
- Kir84** G. Kirczenow, Phys. Rev. Lett. 52, 437 (1984)

- KP88** D. C. Konigsberger, R. Prinz, X-ray Absorption Spectroscopy, 92, Chemical Analysis, Wiley, New York (1988)
- KP93** A. Kuzmin, J. Purans, J. Phys. : Condens. Matter **5**, 267-282 (1993)
- L72** Lawson, A., J. Catal. 24, 297-305 (1972)
- Lal76** J. M. Lalancette et al., Can. J. Chem. 54 (1976), 2505
- LF83** Leong, K., Forsman, W.C., Synth. Met., 6, (1983), 61
- LGMSVS85** F. W. Lytle, R. B. Greegor, E. C. Marques, D: S. Sandstron, G. H. Via, J. H. Sinfelt, J. Catal. 95, 546 (1985)
- LKAF91** Lööf, P., Kasemo, B., Andersson, S., Frestad, A., J. Catal., 130, (1991), 181
- LM62** Linde, V. R., Margolis, L. Ya., Izv. Acad. Nauk SSR, Otd. Khim. Nauk, **1962**, 1723 – Chem. Abstr. 59, (1963), 1132
- LP75** P.A. Lee, J.B. Pendry, Phys.Rev.B**11**, 2795-2811(1975)
- LPK85** Lepperhoff, G., Pischinger, F., Koberstein, E., Ullmann's Encyclopedias of Industrial Chemistry, **Vol. A3**, 189, Weinheim 1985
- LSS89** F. W. Lytle, D. E. Sayers, E. A. Stern, Proc. 5th Int. EXAFS Conf. (XAFS 5), Seattle, WA 1988, Physica B **158**, 701 (1989)
- 70LT** T. A. Littlefield, N. Thorley, Atomic and Nuclear Physics, English Language Book Society and Van Nostrand Reinhold Company Publishers, London, 1970, pp 121-122
- MS78** W. Metz, L. Siemsglüss, Carbon 16 (1978), 225
- M82** W. Metz, G. Schoppen, 6th. Int. London Carbon and Graphite Conf. 1982, Ext. Abstr., 64
- M89** W. Metz, M. Schamsrizi, Synth. Met., 34, (1989), 85
- Met84** W. Metz, Habilitationsschrift, Hamburg 1984
- Met88** W. Metz, in Guerard, D., Lagrange, P., (hrsg.), Int. Colloq. on Layered Comp., Proceedings, Pont-a-Mousson, France, 1988, 107
- Mey87** Meyer, E; c't – Magazin für Computertechnik, 9/1987, 50
- MB64** Martin, W. H., Brocklehurst, J. E., Carbon, 1(1964), 133
- MH75** W. Metz, D. Hohlwein, Carbon 13 (1975), 87
- NRCB92** Nunan, J. G., Robota, H. J., Cohn, M. J., Bradley, S. A., J. Catal. 113, (1992), 309

- O90** Oh, S.H. , J. Catal. 124, 477(1990)
- OE88** Oh, S: H., Eickel, C. C., J. Catal. 112, (1988), 543
- P88** Persson, Ch; c't – Magazin für Computertechnik, 9/1988, 90
- R41** W. Rüdorff, Z. Anorg.Allg.Chem. 245 (1941), 383
- R54** W. Rüdorff, Z. Anorg.Allg.Chem. 277 (1954), 156
- Ra96** Ranga Rao, G. et al J. Catal. 162, 1-9 (1996)
- Re95** T. Ressler, Ph. D. University of Hamburg, Germany (1995)
- Ri57** Riesz, C. H., et al. Armour Reasearch Foundation of Illinois Inst. of Techn. Report No.20, May 1957
- RA90** J. J. Rehr, R. C. Albers, Phys. Rev. B 41, (12), 8139 (1990)
- RAZ92** J. J. Rehr, R.C. Albers, S.I. Zabinsky, Phys. Rev. Lett. 69, 3397-3400) (1992)
- RH38** Rüdorff, W., Hoffmann, U., Z. Anorg. Allg. Chem., 238, (1938), 1
- RL58** Rüdorff, W., Landel, A., Z. Anorg. Allg. Chem., 293, (1958), 327
- RS40** W. Rüdorff, H. Schulz, Z. Anorg.Allg.Chem. 245 (1940), 121
- RZ55** Rüdorff, W., Zeller, R., Z. Anorg. Allg. Chem., 279, (1955), 182
- S73** E. J. Schulze, Diplomarbeit, University of Hamburg 1973
- S92** Schulz, F., PhD. Thesis, forthcoming
- Sc74** Schäfer, H., Angew. Chem. 88 (1976), 775
- Sc76** Schäfer, H., Z. Anorg. Chem. 403 (1974), 116
- Sch75** G. Schoppen, Diplomarbeit, University of Hamburg 1975
- Sch78** G. Schoppen, Dissertation, University of Hamburg 1978
- Sie73** L. Siemsglüss, Diplomarbeit, University of Hamburg 1973
- Sie76** L. Siemsglüss, Dissertation , University of Hamburg 1976
- Sok87** Sokolovskii, V. D., Reakt. Kinet. Catal. Lett., 35 (1987) 337
- Sok90** Sokolovskii, V. D., Catal. Rev. – Sci. Eng., 32 (1990), 1
- Sol88** Solymosi, F., et al. J. Catal. 110, 413 (1988)
- Spa76** H. Meyer-Spasche, Diplomarbeit, University of Hamburg 1976
- Spa78** H. Meyer-Spasche, Dissertation, University of Hamburg, 1978
- Ste74** E. A. Stern Phys. Rev. B 10, 3027(1974)
- Stö92** J. Stöhr, NEXAFS Spectroscopy, Bd. 25, in the Springer Series Surface Sciences, Springer Publishers, Berlin (1992)

- Stu60** E. Stumpp, Dissertation, Tübingen 1960
- Stu67** E. Stumpp, Habilitationsschrift, Tübingen 1967
- Stu77** E. Stumpp, Mater. Sci. Eng., 31, (1977), 53
- Stu77a** E. Stumpp, Mater. Sci. Forum, 91 - 93, (1992), 1
- Stu92** E. Stumpp Mat. Sci. Forum Vol. 93 – 93 1 - 9 (1992)
- SB60** Sourirajan, S and Blumenthal, J. L., 2nd Int. Congr. Catal. (Editions Technip, Paris, 1960), vol. 2, p. 2521
- SD40** Schwab G. and Drikos G.: Z. Physik. Chem. (A) 186 (1940)348
- SFTSHA60** Stein, K. C., Feenan, J. J., Thompson, J. P., Schulz, J. ., Hofer, L. J. E., Anderson, R. B., Ind. Eng. Chem., 52, (1960 671)
- SM80** Schlatter, J.C. and Mitchell, P.J., Ind. Eng. Chem. Prod. Res. Dev. **19**, 288(1980)
- SMMB90** G.Sirkoman, A. Mastalir, A. Molnar, and M. Bartok, Carbon Vol 28 No. 1 pp 35-42 (1990)
- SMSM77** G. Schoppen, H. Meyer-Spasche, L. Siemsglüss, W. Metz, Proc. Franco-American Conf. on Intercalation Compounds, La Napoule, France, Mat. Sci. Eng. 31, 115-117 (1977)
- SOG 69** Shelef, M., Otto, K., and Ghandi, H., Atmos. Environ. 3, 107 (1969)
- SOIT76** Sakurai, K., Okamoto, Y., Imanaka, T., Teranishi, S., Bulletin of Chemical Society of Japan, Vol.47 No.7 (1976) 1732
- SRWC61** Sakada, R. R., Rinker, R. G., Wang, Y. L. and Corcoran, W. H., AIChE J. 658, December 1961
- SW66** E. Stumpp, E. Werner, Carbon 4 (1966), 538
- 84T** Taylor, K. C. , in “Catalysis – Science and Technology” (J. R. Anderson and M.Boudart, Eds.), Vol. 5. Springer-Verlag, Berlin, 1984
- Teo81** B. K. Teo, J. Am Chem. Soc. 103, 3990-4001 (1981)
- Teo86** B. K. Teo, EXAFS : Basic Principles and Data Analysis, Springer Verlag, New York (1986)
- Thi32** Thiele, H., Z. Anorg. Allg. Chem., 207, (1932), 340
- TBDFLT90** H. Tolentino, F. Bandelet, E. Dartge, A. Fontaine, A. Lenn, G. Tourillon, Nucl. Instr. Meth. Phys. Res. A289, 307 (1990)
- TPSK88** Tarasov, A. L., Przheval'skaya, Shvets, V. A.,Kazanskii, V: B., Kinet.,Kataal., 29, (1988) 1181

- V93** M. Vaarkamp, Ph. D. Thesis, University of Eindhoven, Holland, (1993)
- VA67** Voge, H. H., Adams, C. R., Adv. Catal., 17, (1967)
- Wie87** Wiegand, U., Diplomarbeit, Hamburg, 1987
- Win71** Winter, E. R. S., J. Catal. **22**, 158 (1971)
- 65WMD** H. H. Willard, L. L. Merritt, Jr., J. A. Dean., Instrumental methods of Analysis, 4th. Edition, 1965, Publisher: D. Van Nostrand Company Inc. London, pp217
- WN65** Wilkstrom, L. L., and Nobe, K., Ind. Eng. Chem. Process Des. Develop. 4, 191 (1965)
- Y84** Yao, Y. Y. – F., J. Catal., 87, (1984), 152
- YPB65** Yur'eva, T. M., Popovskii, V., and Boreskov, G. K., Kinet. Katal. **6**, 941 (1965)
- YY84** Yao, H. C., Yao, Y. Y. – F., J. Catal., 86, (1984), 254
- ZG93** Zafiris, G., and Gorte, J., J. Catal., 143, 86 (1993)
- ZKBS85** F. B. M.van Zon, D. C. Konigsberger, H. F. J. van't Blik, D. E. Sayers, J: Chem. Phys. 82, 5742 (1985)

Acknowledgements

I direct my sincere gratitude to:

My doctor father, Prof. Dr. Wolfgang Metz, for his professional and scientific advice, his readiness to assist, discuss, and above all the very good working atmosphere in all its aspects he provided in making this project a success. His engagement or support during the composition of this work can barely be overseen.

Prof. Dr. H. Lechert (in addition to my doctor father), for accepting to read my dissertation and for his expertise judgement.

All the hard working persons, both former and current co – workers, for the very good team-work. Professional discussions at our seminars as well as personal exchange of ideas among the following co – workers contributed to a great extent in making this work a success:

Dr. Mehdi Alidoosti, Dr. Hans-Peter Eickhoff, Prof. Dr. Michael Fröba, Dr. Karin Lochte, Dr. Thorsten Ressler, Nina Schober, Dipl.-Chem. Britta Scholze, Dipl.-Chem Frank Schulz, Erdmute Seemann, and Dr. Mojtaba Shamrizi,

All the indispensable persons of the glass blowing unit, the technical and electronic workshops, as well as the chemical supply section whose unflinching support helped making this work a success.

All the other people, who in one way or the other, contributed to make this work a success, that I haven't mentioned, I have definitely not forgotten. You all made this working place a great place to be.

Special thanks and love

To my relatives for their moral support and especially to my dear wife Mary and children Ama and Cecilia who had to offer to some extent their own academic development in making my work a success.

Curriculum Vitae

02.02.1949	born in Nkuntin, Ashanti Region of Ghana as a son of cocoa farmers Kwabena Twumasi, father and Akosua Animah, mother
1955 – 1965	Attendance of Agroyesum Roman Catholic Primary and Middle School, Agroyesum, Ghana
1965 – 1972	Attendance of St. John's Secondary, Sekondi, Western Region of Ghana
1970	General Certificate of Education (G.C.E.), O-Level
1972	G.C.E. A-Level
1972 – 1976	Study of Chemistry at then Kwame Nkrumah University of Science and Technology, Kumasi, Ashanti Region of Ghana
1976	BSc (Chemistry)
1976 – 1977	Chemistry and Mathematics Teacher at Apam Secondary School, Apam
1977 – 1978	Physics Teacher at St. John's Secondary School, Accra
1982 - 1985	<i>Diplomvorprüfung</i> at the University of Hamburg
11. June 1985	<i>Diplomvorprüfung</i> Certificate obtained
1985 – 1988	<i>Diplomhauptprüfung</i> at the University of Hamburg
January 1989	Beginning of Diplomarbeit in Prof. Dr. A. Knöchel's working group at the Institute of Inorganic and Applied Chemistry, University of Hamburg.
20.12.1989	Awarded University of Hamburg's academic degree of Diploma in Chemistry.
1990	Beginning of this work in Prof. Dr. W. Metz's working group at the Institute of Physical Chemistry, University of Hamburg.